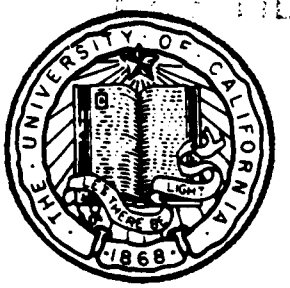

San Diego, California 92152

MARINE PHYSICAL LABORATORY

SCRIPPS INSTITUTION OF OCEANOGRAPHY

HIGH RESOLUTION BEAMFORMING ON VERTICAL ARRAYS IN A REALISTIC OCEANIC ENVIRONMENT

Jean-Marie Q.D. Tran and William S. Hodgkiss

MPL TECHNICAL MEMORANDUM 408

MPL-U-03/89

January 1989

Approved for public release; distribution unlimited.

SECURITY CLASSIFICATION OF THIS PAGE

REPORT DOCUMENTATION PAGE

1a. REPORT SECURITY CLASSIFICATION UNCLASSIFIED	1b. RESTRICTIVE MARKINGS
2a. SECURITY CLASSIFICATION AUTHORITY	3. DISTRIBUTION / AVAILABILITY OF REPORT Approved for public release; distribution unlimited.
2b. DECLASSIFICATION / DOWNGRADING SCHEDULE	
4. PERFORMING ORGANIZATION REPORT NUMBER(S) MPL Technical Memorandum 408 [MPL-U-03/89]	5. MONITORING ORGANIZATION REPORT NUMBER(S)
6a. NAME OF PERFORMING ORGANIZATION Marine Physical Laboratory 6b. OFFICE SYMBOL (If applicable) MPL	7a. NAME OF MONITORING ORGANIZATION Office of Naval Research Department of the Navy
6c. ADDRESS (City, State, and ZIP Code) University of California, San Diego Scripps Institution of Oceanography San Diego, CA 92152	7b. ADDRESS (City, State, and ZIP Code) 800 North Quincy Street Arlington, VA 22217-5000
8a. NAME OF FUNDING / SPONSORING ORGANIZATION Office of Naval Research 8b. OFFICE SYMBOL (If applicable) ONR	9. PROCUREMENT INSTRUMENT IDENTIFICATION NUMBER N00014-87-C-0127
8c. ADDRESS (City, State, and ZIP Code) Department of the Navy 800 North Quincy Street Arlington, VA 22217-5000	10. SOURCE OF FUNDING NUMBERS PROGRAM ELEMENT NO. / PROJECT NO. / TASK NO / WORK UNIT ACCESSION NO.

11. TITLE (Include Security Classification)

HIGH RESOLUTION BEAMFORMING ON VERTICAL ARRAYS IN A REALISTIC OCEANIC ENVIRONMENT

12. PERSONAL AUTHOR(S)

Jean-Marie Q.D. Tran and William S. Hodgkiss

13a. TYPE OF REPORT	13b. TIME COVERED	14. DATE OF REPORT (Year, Month, Day)	15. PAGE COUNT
Technical Memorandum	FROM _____ TO _____	January 1989	100

16. SUPPLEMENTARY NOTATION

17. COSATI CODES			18. SUBJECT TERMS (Continue on reverse if necessary and identify by block number)
FIELD	GROUP	SUB-GROUP	vertical line arrays; signal processing

19. ABSTRACT

This technical memorandum discusses the performance of high resolution methods used to process the data from vertical line arrays in a realistic oceanic sound speed environment. Conventional and high resolution processors (Minimum Variance Distortionless Response (MVDR) beamformer and MUltiple Signal Classification (MUSIC) Direction Of Arrival (DOA) estimator) are described and their implementations are discussed as well. The general beamforming structure is decomposed in two steps. After the estimation of the covariance matrix, a measure of the match or mismatch between the measured field and a replica vector characterizing a particular direction is computed. Using a signal framework, the limitations of the high resolution methods under correlated arrivals then are discussed. Preprocessing methods which limit the almost complete degradation of their performance are considered. These spatial smoothing methods are given several interpretations and their performance characterized. The importance of wavefront curvature is assessed and the influence of curvature on the beamformers is described. The spatial smoothing methods are applied in a curved wavefront environment and the performance of the MVDR beamformer and MUSIC algorithm under correlated and curved wavefront arrivals is described.

20. DISTRIBUTION / AVAILABILITY OF ABSTRACT	21. ABSTRACT SECURITY CLASSIFICATION
☐ UNCLASSIFIED/UNLIMITED ☒ SAME AS RPT. ☐ DTIC USERS	UNCLASSIFIED
22a. NAME OF RESPONSIBLE INDIVIDUAL	22b. TELEPHONE (Include Area Code) / 22c. OFFICE SYMBOL MPL

DD FORM 1473, 84 MAR 83 APR edition may be used until exhausted. All other editions are obsolete

SECURITY CLASSIFICATION OF THIS PAGE

☆ U.S. Government Printing Office: 1986—607-044

High Resolution Beamforming on Vertical Arrays in a Realistic Oceanic Environment

Jean-Marie Q.D. Tran
William S. Hodgkiss

Marine Physical Laboratory
Scripps Institution of Oceanography
San Diego, CA 92152

ABSTRACT

This technical memorandum discusses the performance of high resolution methods used to process the data from vertical line arrays in a realistic oceanic sound speed environment. Conventional and high resolution processors (Minimum Variance Distortionless Response (MVDR) beamformer and MUltiple Signal Classification (MUSIC) Direction Of Arrival (DOA) estimator) are described and their implementations are discussed as well. The general beamforming structure is decomposed in two steps. After the estimation of the covariance matrix, a measure of the match or mismatch between the measured field and a replica vector characterizing a particular direction is computed. Using a signal framework, the limitations of the high resolution methods under correlated arrivals then are discussed. Preprocessing methods which limit the almost complete degradation of their performance are considered. These spatial smoothing methods are given several interpretations and their performance characterized. The importance of wavefront curvature is assessed and the influence of curvature on the beamformers is described. The spatial smoothing methods are applied in a curved wavefront environment and the performance of the MVDR beamformer and MUSIC algorithm under correlated and curved wavefront arrivals is described.

January 2, 1989

Table of Contents

I Introduction

This technical memorandum discusses the performance of high resolution methods used to process the data from vertical line arrays in a realistic oceanic sound speed environment.

Chapter II introduces the array processing structures commonly used to beamform line arrays. After an outline of the frequency wavenumber representation and its associated hypothesis, the conventional beamformer is derived. A signal model that relates the covariance matrix to the power and the directions of the arrivals is introduced, and the beamforming process is decomposed into two steps. First, the covariance matrix is estimated and a measure, based on the covariance matrix, is computed to yield the amount of match or mismatch between the field and a replica vector that characterizes a particular arrival angle. High resolution methods are introduced and a well-known adaptive beamforming technique, the MVDR processor, is described. Some performance and implementation issues are addressed. Finally, superresolution methods are introduced and the MUSIC eigenvector method is presented.

High resolution beamformers are well known to fail under correlated arrivals. In Chapter III, the difference in the structure of the array covariance matrix between a scenario with correlated arrivals and a scenario with only uncorrelated arrivals is presented. The observation of the non-Toeplitz character of the covariance matrix for correlated arrivals leads to the spatial smoothing techniques used to decorrelate correlated arrivals. These preprocessing techniques are described and the reasons how and why they perform are discussed. Then, using simulations as well as analytical derivations, the performance of modified spatial smoothing is compared to the performance of the original spatial smoothing.

The effects of wavefront curvature are studied in Chapter IV in the context of vertical arrays using a geometric ray theory approach. Based on Snell's law, a way to generate curved wavefronts is derived analytically. The importance of wavefront curvature is first evaluated by comparing the phase between curved wavefronts and plane wavefronts, both corresponding to the same arrival angles for a realistic scenario. The behaviour of the conventional, MVDR, and MUSIC beamformers using plane wavefront replica vectors then is studied in a curved wavefront environment. The largest mismatch loss occurs for near horizontal arrivals and the aperture length is not critical for this rather general result. Curved wavefront beamforming then is proposed and the behaviour of the processors is described in terms of bearing responses and beam patterns. The distortion caused by the smoothing transformation is studied in the context of high resolution methods. An approach using the eigenvectors of the smoothed covariance matrix for each replica vector allows the loss due to mismatch to be avoided. Finally, the performance of the MVDR beamformer after spatial smoothing under correlated and curved arrivals is discussed.

II Array Signal Processing

This chapter introduces the array processing structures commonly used to beamform line arrays. After an outline of the frequency wavenumber representation and its associated hypothesis, the conventional beamformer is derived. A signal model that relates the covariance matrix to the power and the directions of the arrivals is introduced and the beamforming process is decomposed into two steps. First, the covariance matrix is estimated and a measure based on the covariance matrix, is computed to yield the amount of match or mismatch between the field and a replica vector that characterizes a particular arrival angle. High resolution methods are introduced and a well-known adaptive beamforming technique, the MVDR processor, is described. Some performance and implementation issues are addressed. Finally, superresolution methods are introduced and the MUSIC eigenvector method is presented. These three processing schemes will be used in the subsequent chapters.

II.1 Basic Assumptions

Array processing methods decompose the pressure field into a directionality representation by assuming homogeneous wavefields [Yen1977]. A homogeneous wavefield is the superposition of uncorrelated elementary waves [Bohme1987]. This mathematical formulation sets a clear analogy between time series spectral estimation and array processing in its frequency-wavenumber representation of the random field [Bohme1987, Capon1969] :

$$p(t,\vec{r}) = \int \exp[\, j\ (\omega t + \vec{k}\,\vec{r}\,)\,]\, dZ(\omega,\vec{k}\,) \qquad (2.1.1)$$

where p denotes the random field at time t and spatial position $\vec{r}$, ω the circular frequency in rad/s and $\vec{k}$ the wavenumber vector. dZ is the spectral increment of the random spectral measure $Z(\omega,\vec{k}\,)$ with covariance

$$COV\left[dZ(\omega,\vec{k}\,)dZ(\omega',\vec{k}'\,)\right] = \frac{1}{(2\pi)^4}\,\delta(\omega-\omega')\,\delta(\vec{k}-\vec{k}'\,)\ S(\omega,\vec{k}\,)\ \partial\omega\,\partial\vec{k} \qquad (2.1.2)$$

where ω and ω' are circular frequencies, $\vec{k}$ and $\vec{k}'$ wavenumber vectors , S the frequency-wavenumber spectrum of the random field $p(t,\vec{r}\,)$ and δ the dirac delta function.

This representation is a generalization of the Cramer spectral representation for stationary time series [Priestley1981]. Its main assumption is that spectral increments dZ at two distinct frequencies or at two distinct wavenumber vectors are uncorrelated. It constitutes the foundation of any array processing method.

Thus, this representation is one where the receiving array measures signals which result from the superposition of uncorrelated elementary waves. These elementary waves generally are assumed planar. Such a homogeneous wavefield representation is restrictive since it excludes correlated arrivals (e.g. multipaths).

II.2 Conventional Beamforming

II.2.1 Lagged Regression Approach

Conventional beamforming with a line array made of uniformely spaced sensors is a simple illustration of the already mentioned analogy with classic time series spectral estimation [Kay1988]. The conventional beamformer is the simplest processing structure since it implements a linear regression on the sensor outputs either in the time domain or in the frequency domain [Shumway1988].

The time domain implementation is known as delay-and-sum beamforming. A beam is formed in the time domain by summing up the lagged (delayed) outputs of the array sensors [Johnson1982, De Fatta1988]

$$y(t,\theta) = \sum_{m=0}^{M-1} a_m \, x_m(t-\tau_m) \tag{2.2.1}$$

where t denotes time, $x(t)$ is the output of the m^{th} sensor, M the number of sensors, $(a_m)_{m=0,M-1}$ the shading coefficients and $(\tau_m)_{m=0,M-1}$ the delays associated with each sensor corresponding to a particular look direction, θ. The time delays τ_m are determined by making additional assumptions on the propagating signals. If one considers plane waves impinging on a line array with equally spaced sensors, the delays τ_m are given by

$$\tau_m = \frac{m\, d\, \sin\theta}{c} \tag{2.2.2}$$

where d is the interelement spacing, c the sound velocity and θ the look direction [DeFatta1988]. The delay-and-sum beamformer is summarized in Figure II.1.

The frequency domain regression can be derived by taking the Fourier transform of the output $y(t)$

$$Y(f,\theta) = \sum_{m=0}^{M-1} a_m e^{-j2\pi f \tau_m} \, X_m(f) \tag{2.2.3}$$

where f is the carrier frequency, $Y(f,\theta)$ and $X_m(f)$ the Fourier transforms of $y(t)$ and $x(t)$ respectively. In essence, Equation (2.2.3) is the narrow-band implementation of Equation

(2.2.1) at frequency f. Equation (2.2.3) can also be expressed as an inner product :

$$Y(f,k) = \mathbf{A}^H \mathbf{X} \tag{2.2.4}$$

$$\mathbf{X}^T = \left[X_o(f)\ X_1(f)\ \cdots\ X_{M-1}(f) \right] \tag{2.2.5}$$

$$\mathbf{A}^T = \left[a_o e^{j2\pi f \tau_o}\ a_1 e^{j2\pi f \tau_1}\ \cdots\ a_{M-1} e^{j2\pi f \tau_{M-1}} \right] \tag{2.2.6}$$

the superscript H denotes the Hermitian operation (complex conjugate transpose operation), and the superscript T denotes the transpose operation. Assuming plane waves, that is using Equation (2.2.2) and letting

$$k = \frac{f\ d\ \sin\theta}{c} \tag{2.2.7}$$

Equation (2.2.3) is in the form of a spatially windowed Discrete Fourier Transform [Oppenheim1975] :

$$Y(f,k) = \sum_{m=0}^{M-1} a_m\ e^{-j2\pi k m}\ X_m(f) \tag{2.2.8}$$

where k is a normalized wavenumber.

The frequency-wavenumber power spectral density is estimated by the periodogram

$$I_P(f,k) = \frac{1}{M\left(\frac{1}{M}\sum_{i=0}^{M-1} a_i^2\right)} \left| Y(f,k) \right|^2 \tag{2.2.9}$$

where M is the number of sensors. $I_p(f,k)$ can be converted into a power spectral density parametrized by the arrival angle θ by the nonlinear mapping given in Equation (2.2.7) [De Fatta1988]. The narrow-band conventional beamformer often is implemented as a FFT beamformer [Williams1968]. The FFT beamformer is summarized in FIgure II.2. Since it is well known that the periodogram gives an inconsistent estimate of the power spectral density [Priestley1981], additional incoherent averaging over successive time snapshots is typically performed. The estimate then becomes

$$P(f,k) = \frac{1}{M\left(\frac{1}{M}\sum_{i=0}^{M-1} a_i^2\right)} \frac{1}{K} \sum_{i=0}^{K-1} \left| Y_i(f,k) \right|^2 \tag{2.2.10}$$

where $Y_i(f,k)$ is FFT beamformer output from from the i^{th} time snapshot.

II.2.2 Formulation in Terms of the Covariance Matrix

When the window applied is the rectangular window, the a_i's are taken equal to unity and the spectral density can then be expressed in a simplified matrix form as :

$$I_P(f,k) = \frac{1}{M} (\mathbf{E}^H \mathbf{X}) (\mathbf{E}^H \mathbf{X})^H \tag{2.2.11}$$

$$= \frac{1}{M} \mathbf{E}^H \mathbf{X} \mathbf{X}^H \mathbf{E} \tag{2.2.12}$$

where $\mathbf{E}$ is the plane wave steering vector,

$$\mathbf{E}^T = \left[1 \;\; e^{j\,2\pi k} \;\; \cdots \;\; e^{j\,2\pi k\,(M-1)} \right] \tag{2.2.13}$$

and $\mathbf{X}\,\mathbf{X}^H$ is an estimate at the frequency f of the cross spectral density matrix based on the data, or covariance matrix. With additional averaging over time snapshots, the conventional beamformer, also called the Bartlett beamformer, is given by

$$P_B(f,k) = \frac{1}{M} \mathbf{E}^H \mathbf{R} \mathbf{E} \tag{2.2.14}$$

with

$$\mathbf{R} = \frac{1}{K} \sum_{i=0}^{K-1} \mathbf{X}_i \mathbf{X}_i^H \tag{2.2.15}$$

where $\mathbf{X}_i$ is the vector of Fourier coefficients corresponding to the time snapshot i. $\mathbf{R}$ is an estimate of the array covariance matrix. When a weighting window is appplied, one gets

$$P_B(f,k) = \frac{1}{M} \mathbf{E}^H \mathbf{W} \mathbf{R} \mathbf{W}^H \mathbf{E} \tag{2.2.16}$$

where the (M,M) diagonal matrix $\mathbf{W}$ is

$$\mathbf{W}^T = \frac{1}{\sqrt{\sum_{i=0}^{M-1} a_i^2}} [a_0\, a_1 \cdots a_{M-1}] \tag{2.2.17}$$

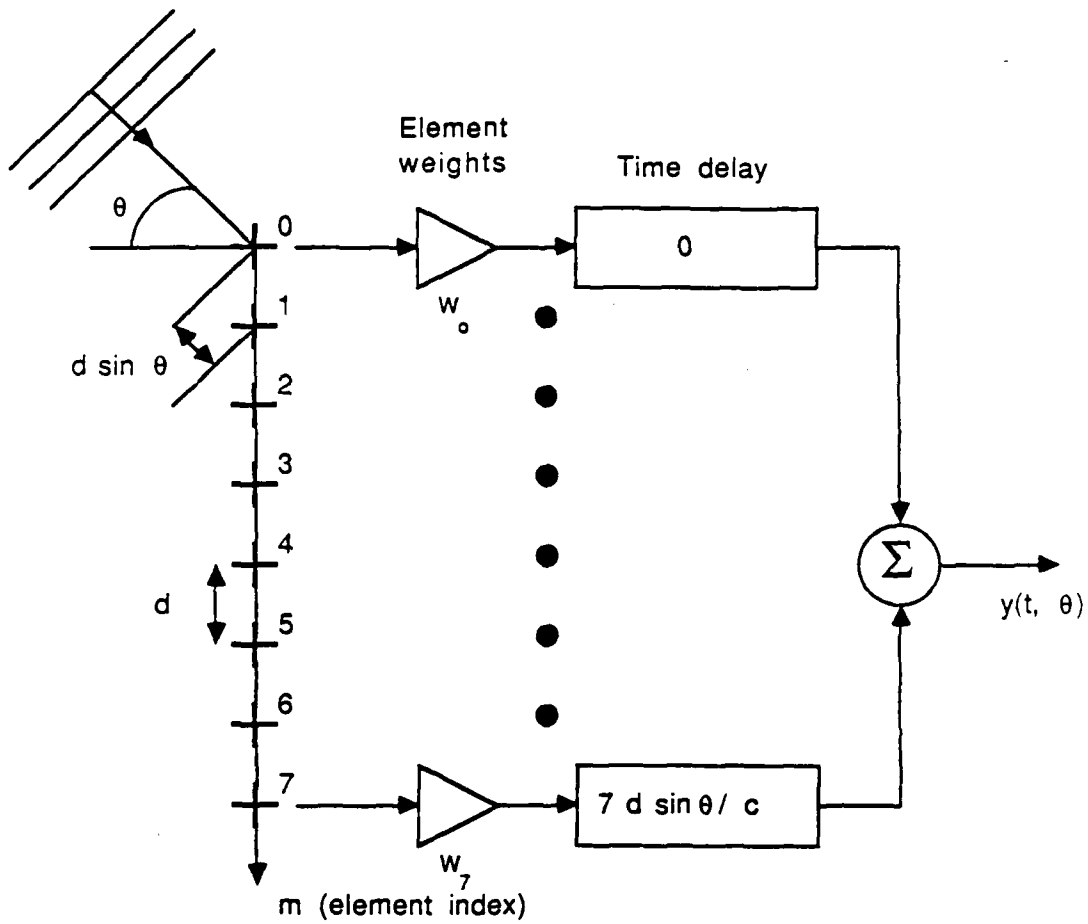

Figure II.1: Delay-and-sum beamformer.

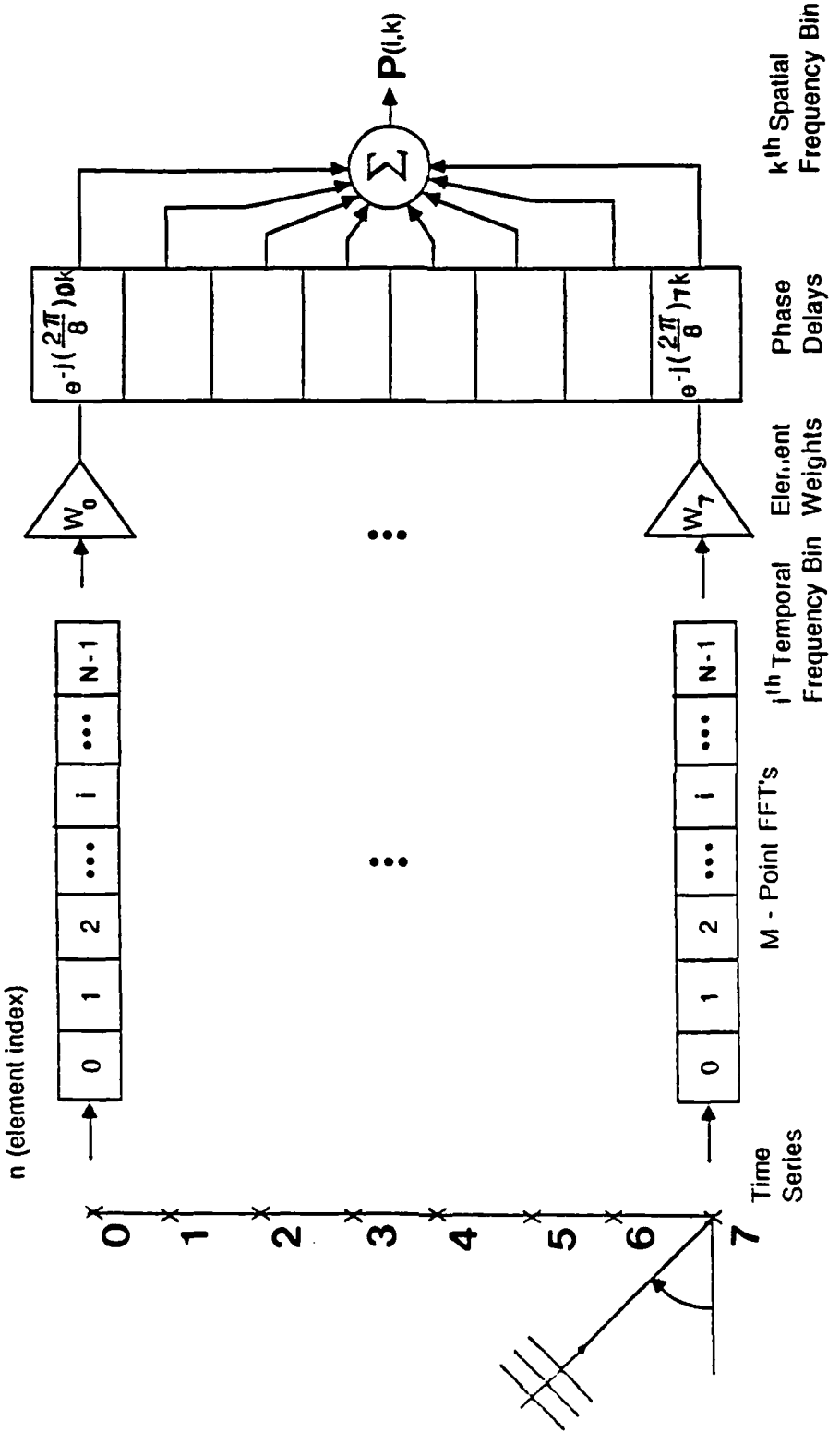

Figure II.2: FFT beamformer.

II.2.3 Matched Filter Interpretation

Expressed as a function of the array covariance matrix, the conventional or Bartlett beamformer allows the decomposition of the processing structure into two components: the processor itself and the set of steering vectors.

Using a given set of replica vectors, finding directions of arrival corresponds to finding the angles of maximum power at the output of the processor. Therefore, the beamforming operation can be interpreted as a spatial matched filtering operation. Considering Equation (2.2.12), the quantity to be maximized is

$$\mathbf{A}^H \mathbf{X}\,\mathbf{X}^H \mathbf{A} = |\mathbf{A}^H \mathbf{X}|^2 \qquad (2.2.16)$$

where $\mathbf{A}$ is a direction vector given by Equation (2.2.6) corresponding to an arrival angle θ. $\mathbf{A}$ belongs to a set of steering vectors or replica vectors which often is called the array manifold [Schmidt1981, Clarke1988]. The choice of an array manifold is equivalent to the choice of a wavefront model. Such a choice is guided by the underlying assumptions about the signal propagation and wavefront shape. Generally, the plane wave array manifold is selected.

If a single signal impinges on the array at a given but unknown angle of arrival, the measured array signal vector $\mathbf{X}$ given by Equation (2.2.5) will be an amplitude weighted plane wavefront vector. From the Schwartz inequality the output of the beamformer will be maximum if the replica vector $\mathbf{A}$ and the array signal vector $\mathbf{X}$ are colinear. The beamformer provides a measure of the mismatch between the observed field and a replica vector or steering vector. A match implies a high output and indicates an arrival direction [Cox1973].

II.3 Covariance Matrix Representation

In the previous section, it was shown that the conventional processor operates on the array covariance matrix. In general, any beamformer will operate on the array covariance matrix since it contains information on directionality. Therefore, it is of interest to discuss the covariance matrix representation.

If p narrowband signals at the carrier frequency f impinge on the array, the time domain array signal vector at the input of the beamformer is given by [Cox1973, De Graaf1985]

$$\mathbf{r}(t) = \mathbf{B}\,\mathbf{s}(t) + \mathbf{n}(t) \tag{2.3.1}$$

where $\mathbf{s}(t)$ is the $(p,1)$ signal vector, sometimes called the envelope vector [Cadzow1988], $\mathbf{n}(t)$ is the $(M,1)$ vector of additive noise and $\mathbf{B}$ the matrix of stacked directions with columns equal to

$$\mathbf{B} = \left[\mathbf{A}_o \;\; \mathbf{A}_1 \;\; \cdots \;\; \mathbf{A}_{p-1}\right] \tag{2.3.2}$$

each $(M,1)$ column vector $\mathbf{A}_j$ corresponds to an arrival angle θ_j. The equivalent narrowband frequency domain representation is, at the signal carrier frequency f,

$$\mathbf{r} = \mathbf{B}\,\mathbf{s} + \mathbf{n} \tag{2.3.3}$$

where $\mathbf{s}$ is the $(p,1)$ signal vector, $\mathbf{n}$ is the additive noise $(M,1)$ vector, and $\mathbf{B}$ the matrix of stacked directions. The corresponding model covariance matrix $\mathbf{R}_{model} = \mathbf{r}\;\mathbf{r}^H$ is thus

$$\mathbf{R}_{model} = \mathbf{B}\,\mathbf{S}\,\mathbf{B}^H + \mathbf{Q} \tag{2.3.4}$$

where $\mathbf{S}$ is the (p,p) signal covariance matrix given by $E(\mathbf{s}\,\mathbf{s}^H)$ and $\mathbf{Q}$ is the noise covariance matrix given by $E(\mathbf{n}\,\mathbf{n}^H)$ with E denoting the expectation.

Under the assumption of a homogeneous wavefield, the signals are uncorrelated, and one can show that the (p,p) signal matrix $\mathbf{S}$ is of full rank p. Recalling that $\mathbf{S} = E(\mathbf{s}\,\mathbf{s}^H)$ with $\mathbf{s}^T = [s_0\, s_1 \cdots s_{p-1}]$, uncorrelated arrivals means that the signal envelopes are such that for $i \neq j$,

$$E(s_i\ s_j^*) = 0 \tag{2.3.5}$$

where * denotes the complex conjugate operation. If s_i and s_j are correlated, then

$$E(s_i\ s_j^*) \neq 0 \tag{2.3.6}$$

Restricting the discussion to two arrivals, the signal covariance matrix is

$$\mathbf{S} = \begin{bmatrix} E(s_0\, s_0^*) & E(s_0\, s_1^*) \\ E(s_0^*\, s_1) & E(s_1\, s_1^*) \end{bmatrix} \tag{2.3.7}$$

with $E(s_i s_i^*) = \sigma_i^2$, the power of the i^{th} signal, and for $i \neq j$, $E(s_i\ s_j^*) = \sigma_i \sigma_j \rho_{i,j}$, where $\rho_{i,j} = \rho_{j,i}^*$ is the complex correlation given by

$$\rho_{i,j} = \frac{E(s_i\ s_j^*)}{E(|s_i|^2)E(|s_j|^2)} \tag{2.3.8}$$

Then, the signal covariance matrix **S** can be written [Reddy1987]

$$\mathbf{S} = \begin{bmatrix} \sigma_0^2 & \sigma_0\, \sigma_1 \rho \\ \sigma_0\, \sigma_1 \rho^* & \sigma_1^2 \end{bmatrix} \tag{2.3.9}$$

For fully coherent arrivals $|\rho| = 1$, hence $\det \mathbf{S} = \sigma_0^2\, \sigma_1^2\, (1 - |\rho|^2) = 0$.

The standard model for the noise covariance **Q** is a sensor noise uncorrelated from sensor to sensor [Nickel1988, Schmidt1986]. Under this assumption, the noise covariance matrix is $\mathbf{Q} = \sigma^2 \mathbf{I}$, where σ^2 is the noise power and **I** the identity matrix. It follows that the (M, M) covariance matrix $\mathbf{R}_{model}$ is of full rank.

Furthermore, if one assumes the elementary waves of the field to be planar, the covariance matrix $\mathbf{R}_{model}$, which is Hermitian by construction (i.e. $\mathbf{R}^H{}_{model} = \mathbf{R}_{model}$), also is Toeplitz (constant along the diagonals).

$$\mathbf{R}_{model} = \sigma_0{}^2\, \mathbf{A}_0\, \mathbf{A}_0{}^H + \sigma_1{}^2\, \mathbf{A}_1\, \mathbf{A}_1{}^H + \cdots + \sigma_{p-1}{}^2\, \mathbf{A}_{p-1}\, \mathbf{A}_{p-1}{}^H \tag{2.3.10}$$

Since $\mathbf{A}_i = \left[1\ e^{j2\pi k_i}\ e^{j2\pi 2k_i}\ \cdots e^{j2\pi(M-1)k_i} \right]$, each outer product in the sum given by Equation (2.3.9) is Toeplitz :

$$\mathbf{A}_i\ \mathbf{A}_i{}^H = \begin{bmatrix} 1 & e^{-j2\pi k_i} & e^{-j2\pi 2k_i} & \cdots & e^{-j2\pi(M-1)k_i} \\ e^{j2\pi k_i} & 1 & e^{-j2\pi k_i} & \cdots & . \\ . & . & 1 & \cdots & . \\ . & . & . & \cdots & . \\ . & . & . & \cdots & . \\ e^{j2\pi(M-1)k_i} & e^{j2\pi(M-2)k_i} & . & \cdots & 1 \end{bmatrix} \tag{2.3.11}$$

so that $\mathbf{R}_{model}$ is both Toeplitz and Hermitian. The Toeplitz character of the array covariance matrix is a result of the duality between homogeneous plane wavefields and wide sense stationary time series.

II.4 Adaptive Beamforming

II.4.1 Derivation of the MVDR beamformer

The narrow-band beamforming problem can be viewed as finding a set of complex weights or, equivalently, a steering vector given by Equation (2.2.6) [De Graaf1985] corresponding to the signal direction of arrival. The plane wave assumption only corresponds to a particular signal model. The conventional technique is the most widely used, the best known and the most robust, but it has the least resolution. In an effort to improve the resolution, data adaptive techniques can be used. The increase in resolution results from the full use of the information summarized in the covariance matrix, along with specific assumptions about the signal model

An adaptive beamformer determines a data dependent set of weights as the solution of a constrained optimization problem [Griffiths1977, Monzingo1985, Van Veen1988]. Thus, it is referred to as an optimum beamformer in the literature [Cox1973, Reddy1987].

The classical optimization criterion is to minimize the output power or variance under the constraint of passing the look direction signal undistorted [Cox1973, Kanasewich1975, Marple1987, Lacoss1971] :

$$MIN \left[\mathbf{W}^H \mathbf{R} \mathbf{W} \right]_{\mathbf{A}^H\mathbf{W}=1} \tag{2.4.1}$$

where $\mathbf{W}$ is the unknown weight vector, $\mathbf{A}$ the look of direction vector or replica vector from the array manifold, as in Equation (2.2.6), and $\mathbf{R}$ the cross-spectral density matrix

estimated from the data given by Equation (2.2.5). As before, one asssumes that the data have been Fourier analysed and one considers a single frequency f. Using the Lagrange's multiplier method [Lacoss1971, Kanasewitch1975, Marple1987], the weight vector W is given by

$$\mathbf{W} = \frac{\mathbf{R}^{-1}\mathbf{A}}{\mathbf{A}^H \mathbf{R}^{-1} \mathbf{A}} \tag{2.4.2}$$

and the wavenumber spectrum is

$$P_{MVDR}(f, k) = \frac{M}{\mathbf{A}^H \mathbf{R}^{-1} \mathbf{A}} \tag{2.4.3}$$

where M is the number of sensors. This is the so-called Maximum Likelihood method of Capon [Capon1969], which is the maximum likelihood estimator in the case of Gaussian noise (i.e. it minimizes the log-likelihood under the assumption of Gaussian statistics). This beamformer also is called the Minimum Energy [De Graaf1985] or Minimum Variance Distortionless Response (MVDR) beamformer [Zoltowski1988]. The MVDR beamformer stands as a high resolution method compared to the conventional beamforming. For this reason, it is used in various areas such as the seismic field [Capon1969, Baggeroer1974, Baggeroer1982, Hsu1986], the oceanographic field [Oltman-shay1984] as well as the underwater acoustics arena [Owsley1985].

II.4.2 Performance of the MVDR Beamformer

The performance of the MVDR beamformer has been studied rather extensively [Cox1973, De Graaf1985]. The main results are presented here succintly. In the context of matched filtering, the MVDR processor is such that a slight mismatch in the replica vector results in serious signal reduction at its output [Cox1973]. For the adaptive array pointing in a given direction, the signal arriving in another bearing is an interference to be cancelled. The stronger the interference, the more suppression the designed filter is able to put on it. This suppression is based on the covariance structure across the array

that samples the field. Depending on the signal-to-noise ratio SNR, the resolution varies. For a line array and two signals 30 dB above the noise level, the resolution of the MVDR beamformer [Cox1973] is slightly over three times the Rayleigh resolution of conventional processing [Burdic1984] which is given in radians by

$$\theta = \frac{\lambda}{L} \tag{2.4.4}$$

where λ is the acoustic wavelength and L is the length of the array. When $SNR \rightarrow 0$, the resolution of the MVDR processor decreases and becomes comparable to the conventional processor one [Cox1973, Kanasewich1975, Zoltowski1988]. This improved resolution results in a higher sensitivity to mismatch. Some cost may thus be associated to this higher sensitivity to mismatch in terms of signal to noise ratio improvement or processing gain. If the array manifold is chosen with improper assumptions about the true underlying wavefronts, the resolving capability of the MVDR beamformer can be less than that of the conventional processor [Seglison1970, McDonough1972].

II.4.3 Implementation Issues

The MVDR beamformer is implemented by

(1) performing the Fourier analysis at the output of each sensor using conventional FFT based techniques on time subsegments

(2) computing the cross-spectral matrix based on the data, using Equation (2.2.5)

(3) inverting the cross-spectral matrix

(4) computing the angular wavenumber spectrum given by Equation (2.4.3).

It is assumed that the signals are superimposed on an incoherent noise. A nonnegative definite cross-spectral matrix is ensured theoretically by averaging at least M dyad products $\mathbf{X}_i \mathbf{X}_i^H$, each dyad product corresponds to a dimension. Averaging K cross-spectral matrices as in Equation (2.2.15), corresponds to averaging across K time seg-

ments, each $\mathbf{X}_i$ results from a time subsegment. Even when $K \geq M$, the matrix inversion requires special attention, that is double precision arithmetic and an additional check for matrix ill-conditioning. A cross-spectral matrix based on the data often is numerically noninvertible ; this situation is characterized by the ratio of its smallest to its largest eigenvalue with a practical criterion being a ratio below 10^{-6}. The solution [Capon1969] then is to add a small amount of incoherent noise to the cross-spectral matrix $\mathbf{R}$, that is to add to the main diagonal of $\mathbf{R}$:

$$\varepsilon = \gamma \frac{tr(\mathbf{R})}{M} \tag{2.4.5}$$

where tr denotes the trace operation, and γ the fraction of noise, and $\frac{tr(\mathbf{R})}{M}$ represents the mean power across the sensor array. Typical values for γ are in the range of 10^{-4} to 10^{-2}. Taking $\gamma = 10^{-4}$ corresponds to introducing an uncorrelated sensor noise 40 dB below the average sensor power level.

This stabilization procedure is equivalent to increasing the incoherent sensor noise and thus produces a small bias in the power spectral density estimate, in addition to the one due to the data sequence length limitation which is given by [Capon1970]

$$bias(dB) = 10 \log \frac{K - M + 1}{K} \tag{2.4.6}$$

The asymptotic distributions (i.e. for very long data sequences) of the MVDR spectrum, $P_{MVDR}(f, k)$, is a Wishart distribution, or a multidimensional chi-square [Capon1970] with a number of degrees of freedom given by

$$d.o.f. = 2(K-M+1) \tag{2.4.7}$$

II.5 Eigenvector Beamforming

The direction of arrival estimation problem can be solved using spectral estimation techniques. However, sufficient angular resolution may not be achieved with conventional or adaptive techniques. Direction of arrival or frequency estimators have been developed to yield maximum resolution based on the covariance matrix eigenstructure. These alternative methods provide super resolution but not an estimation of the power spectral density.

The eigenvector beamformer has the same assumptions as the adaptive beamformer, the covariance matrix is the superposition of a signal covariance matrix and a noise covariance matrix, as in Equation (2.3.4). There are p signals impinging on the array and the noise is a sensor noise uncorrelated from sensor to sensor. The p largest eigenvalues of the covariance matrix allow the separation of the p signals from the noise, the corresponding eigenvectors span the signal subspace. The other $M - p$ eigenvectors corresponding to the lowest eigenvalues span the noise subspace which is orthogonal to the signal subspace [Schmidt1981]. This geometrical formulation leads to two classes of estimators, one based on the signal subspace and the other based on the noise subspace [Kay1988, Marple1987].

The MUSIC (MUltiple Signal Classification) algorithm [Clarke1988, Cantoni1980] is a principal candidate among the various spectral eigenvector estimators, and is widely referenced in the literature. MUSIC is a noise subspace estimator where the orthogonality of the noise and signal subspaces plays a major role. This estimator is given by

$$P_{MUSIC} = \frac{1}{\mathbf{A}^H \mathbf{R}_N \mathbf{A}} \tag{2.5.1}$$

where $\mathbf{A}$ is the steering vector as in Equation (2.1.5) and $\mathbf{R}_N$ the noise only covariance matrix, given by

$$\mathbf{R}_N = \sum_{k=0}^{M-p-1} \mathbf{V}_k \mathbf{V}_k^H \tag{2.5.2}$$

where $\mathbf{V}_k$ is the k^{th} noise eigenvector of the data covariance matrix given by Equation (2.2.15). $\mathbf{V}_k$ is such that $\mathbf{V}_k^H \mathbf{V}_k = 1$.

MUSIC is implemented by

(1) the eigenvalue and eigenvector decomposition of the covariance matrix

(2) the selection of the number of signals p

(3) the computation of the noise only covariance matrix given by Equation (2.5.2)

(4) the computation of the MUSIC spectrum given by Equation (2.5.1) using the plane wave array manifold

The MUSIC spectrum is the inverse of the squared distance of the projection of $\mathbf{A}$ on the noise subspace. When scanning all the possible replica vectors of the array manifold, global minima occur if this distance is zero, or equivalently, when $\mathbf{A}$ belongs to the signal subspace. Then, the MUSIC spectrum theoretically will show a peak to infinity. In practice, the peaks are finite because one has only an estimate of the covariance matrix.

The noise only covariance matrix $\mathbf{R}_N$ is of rank $M-p$, thus rank deficient. The quadratic form $\mathbf{A}^H \mathbf{R}_N \mathbf{A}$ in Equation (2.5.1) is positive semi-definite. The noise covariance matrix has $M-p$ eigenvalues equal or close to unity, and p eigenvalues close to zero. To avoid numerical problems when computing the quadratic form in Equation (2.5.1), (i.e., small negative values), a small fraction of noise can be added to the main diagonal of $\mathbf{R}_N$, typical fractions of noise are between 10^{-8} and 10^{-6}. A fraction of noise equal to 10^{-7} corresponds to clipping the direction of arrival peaks to approximately 70 dB.

The angular resolution enhancement of the eigenanalysis based methods [Kay1988, Marple1987] and more precisely of MUSIC [Schmidt86, Nickel1987] is recognized widely. An explicit relationship between the MVDR beamformer and the MUSIC algorithm is derived in [Nickel1988] where the MVDR beamformer is shown to

be a weighted projection on the noise subspace, like MUSIC, when the signal to noise ratio goes to infinity. This explains the superior resolution of MUSIC with respect to the MVDR beamformer.

One of the major tasks in practice is to determine the number of signals impinging on the array [Schmidt1981, Wax1984]. Three methods can be used

(1) the number of signals is determined by observing the spread of the eigenvalues of the covariance matrix and using a threshold level to seperate high/signals from low/noise eigenvalues [Wax1984, Oswley1988]

(2) the number of signals is determined using hypothesis testing on the multiplicity of the smallest eigenvalues [Schmidt1980, Wax1984]

(3) information theoretic criteria of model selection allow the determination of the number of signals without any subjective judgement as in (1) and (2) [Wax1985]

III. Processing Correlated Arrivals

High resolution beamformers are well known to fail under correlated arrivals [White1979, Cantoni1980]. Here, the difference in the structure of the array covariance matrix between a scenario with correlated arrivals and a scenario with only uncorrelated arrivals is presented. The observation of the non-Toeplitz character of the covariance matrix for correlated arrivals leads to the smoothing techniques [Shan1985, Williams1988] used to decorrelate correlated arrivals. These preprocessing techniques are described and the reasons how and why they perform are discussed. Then, the performance of modified spatial smoothing is compared to the performance of the original spatial smoothing [Reddy1987], using simulations as well as analytical derivations.

III.1 Limitation of the High Resolution Methods

The analogy between time series analysis and spatial array processing leads to the formulation of directionality in the framework of homogeneous wavefields. Nevertheless, array processing is not identical to time series power spectral density estimation. An oceanic environment is bounded at the surface and the bottom and these boundaries are known to have a major impact on the pressure field [Yen1977]. Multipath propagation produces correlated arrivals at the receiving line array [Urick1983].

Techniques such as the adaptive and eigenvector methods are high resolution and lack robustness as soon as the structure of the array covariance matrix significantly departs from the assumed signal model. Under such conditions, they generally report improper arrival directions or incorrect power levels.

The severe limitation of the performance of the MVDR beamformer under correlated arrivals are well known [White1979, Cantoni1980]. The adaptive filter uses the non-look direction signals to minimize its output power and since the signals are correlated with the look direction signals, the latter is suppressed. This process is the so-called signal cancellation phenomena in adaptive antennas [Widrow1982]. On an algorithmic level, the adaptive technique fails because the model signal covariance is singular [Gabriel1980].

The MUSIC algorithm also does suffer from arrival intercorrelation [Schmidt1981]. If there are two correlated arrivals on the array, the signal subspace is degenerate of rank one: the direction of arrivals are associated to the same single waveform corresponding to a single emitter [Gabriel1980].

From a practical standpoint, the high resolution MVDR and MUSIC methods are unable to resolve correlated arrivals as indicated by the results in [White1979] and [Williams1988]. This point is further illustrated by Figure III.1 and III.2.

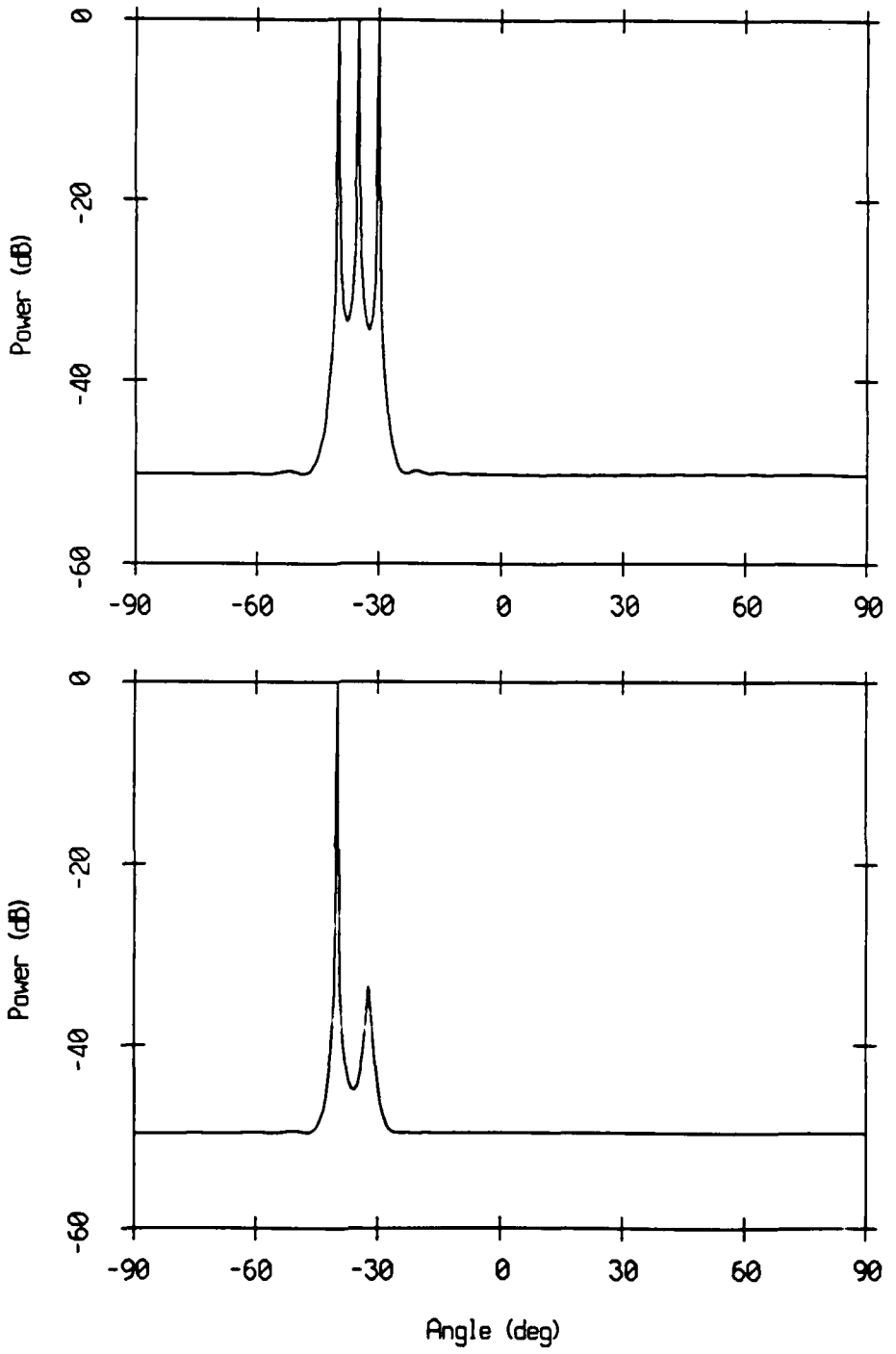

Figure III.1: MVDR beamforming on 3 plane wave arrivals at $-40°$, $-35°$ and $-30°$. Panel A: the arrivals are uncorrelated, Panel B: the arrivals at $-35°$ and $-30°$ are fully correlated ($\rho = 1$). The array has 32 sensors with 25 m spacing and operates at 20 Hz in an isovelocity medium of sound speed 1498 m/s.

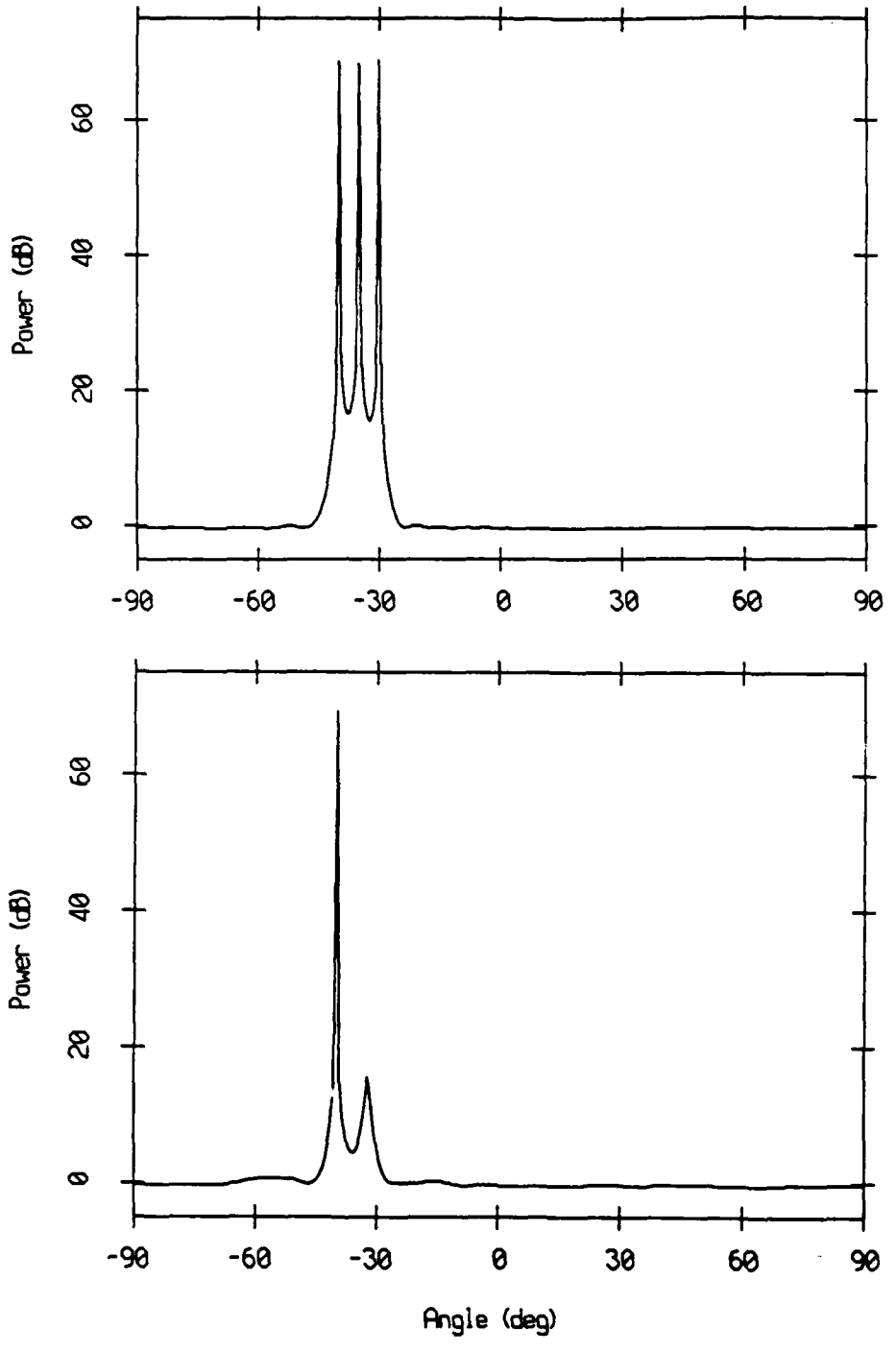

Figure III.2: MUSIC beamforming on 3 plane wave arrivals at $-40°$, $-35°$ and $-30°$. Panel A: the arrivals are uncorrelated, Panel B: the arrivals at $-35°$ and $-30°$ are fully correlated ($\rho = 1$). The array has 32 sensors with 25 m spacing and operates at 20 Hz in an isovelocity medium of sound speed 1498 m/s.

III.2 Structure of the Covariance Matrix Under Correlated Arrivals

It was shown earlier that full coherence among arrivals is equivalent to a rank deficiency in the signal covariance matrix. This explains why the adaptive and eigenvector methods fail under correlated arrivals. Since the available data is the array covariance matrix, the structure of the covariance matrix for an inhomogeneous field is now investigated.

It was shown earlier that the array covariance matrix of a homogeneous field using the plane wave array manifold is both Toeplitz and Hermitian. In a realistic environment, arrivals such as multipaths are correlated so that the field is not homogeneous (i.e. not stationnary in space). Thus, although it is Hermitian by construction, the covariance matrix of a line array is not Toeplitz with the plane wave array manifold [Gabriel1980]. The model covariance matrix for two correlated arrivals can be expressed as [Reddy1987]

$$\mathbf{R}_{model} = [\mathbf{A}_0\, \mathbf{A}_1] \begin{bmatrix} \sigma_0^2 & \sigma_0\sigma_1\rho \\ \sigma_o\sigma_1\rho^* & \sigma_1^2 \end{bmatrix} \begin{bmatrix} \mathbf{A}_0^H \\ \mathbf{A}_1^H \end{bmatrix} + \sigma^2\,\mathbf{I} \tag{3.2.1}$$

where $\mathbf{A}_i$ is the direction of the i^{th} arrival, σ_i^2 the power of the i^{th} arrival, and ρ the complex correlation between the two arrivals, $|\rho| \le 1$, and σ^2 the uncorrelated sensor noise power. Using the plane wave array manifold, one has with a M element array

$$\mathbf{A}_i = \left[1\; e^{j2\pi k_i} \;\cdots\; e^{j2\pi(M-1)k_i} \right]^T \tag{3.2.2}$$

where k_i is the normalized wavenumber of the i^{th} arrival.

The upper diagonal terms are given by

$$\mathbf{R}_{model}(i,i+1) = \sigma_0^2\, e^{-j2\pi k_0} + \sigma_1^2\, e^{-j2\pi k_1} + \sigma_0\sigma_1 \left\{ [\rho\, e^{j2\pi i(k_0 - k_1)}]\, e^{-j2\pi k_0} + [\rho^*\, e^{j2\pi i(k_1 - k_0)}]\, e^{-j2\pi k_1} \right\} \tag{3.2.3}$$

for $i = 1, M-1$. Inspecting these terms, one concludes that the matrix is not Toeplitz. The last term due to correlation ($\rho \neq 0$) is responsible for that character. Correlation can be

thought of as introducing a modulation term in the diagonals of the array covariance matrix.

The effects of correlation on the covariance matrix can be observed on Figure III.3 and Figure III.4 by comparing the magnitude and phase of the upper diagonals of the array covariance matrix for a field corresponding to two uncorrelated and two fully correlated arrivals ($\rho = 1$). The order of the diagonals can be identified by their length. The arrivals are unit power plane waves impinging on a $10\frac{1}{3}$ wavelength line array of 32 sensors, at -10° and -20° incidence angles. The interelement spacing is 25 m, the operating frequency is 20 Hz and the sound speed is 1498 m/s. The magnitude and phase in the uncorrelated case of Figure III.3 are constant on each diagonal, while they both significantly vary in the correlated case on Figure III.4.

This observation of this non-Toeplitz character is important since it points out the difference in nature between uncorrelated arrivals and correlated arrivals, and leads to the processing methods designed to limit the negative effects of correlation.

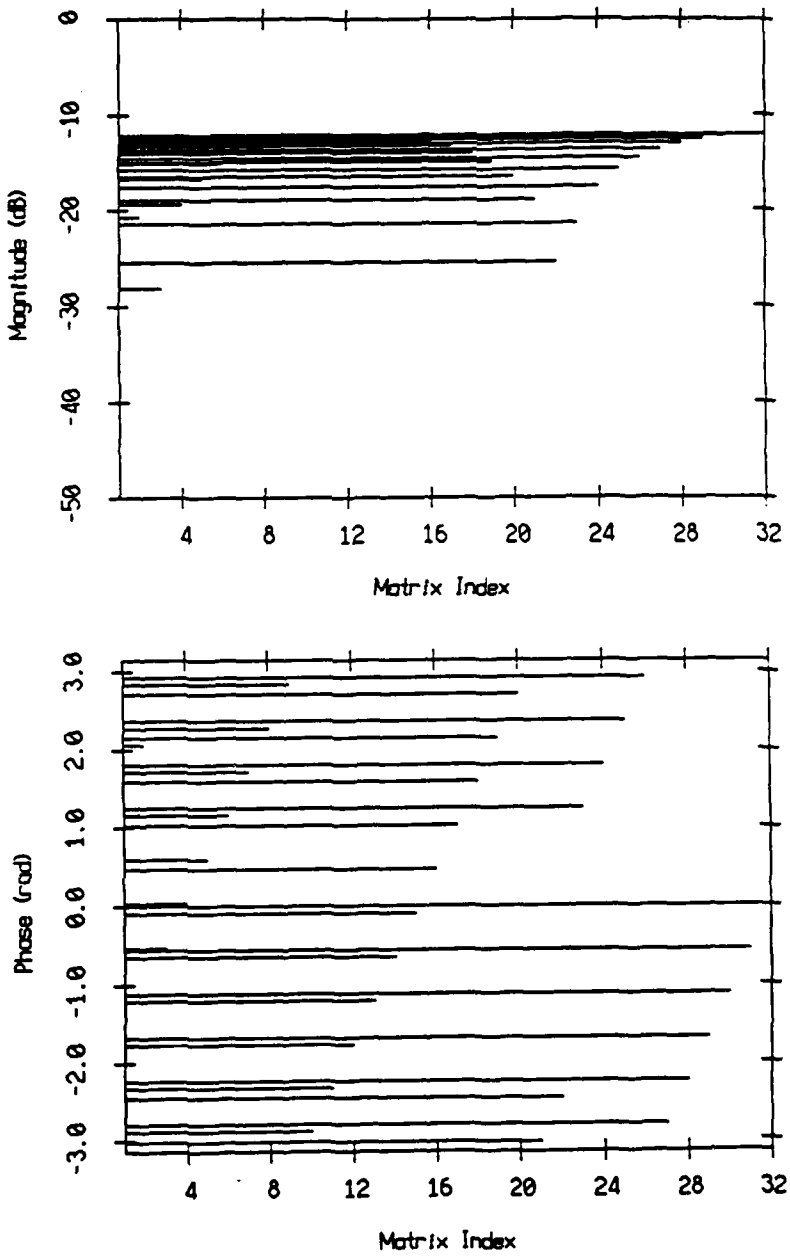

Figure III.3: Magnitude and phase of the upper diagonals of the 32 by 32 covariance matrix. Diagonals are identified by looking at their length. Matrix index corresponds to element index along the diagonal. The 32 sensor line array (25 m interelement spacing) receives two uncorrelated arrivals at -10° and -20° incidence angles at 20 Hz. The sound speed is 1498 m/s.

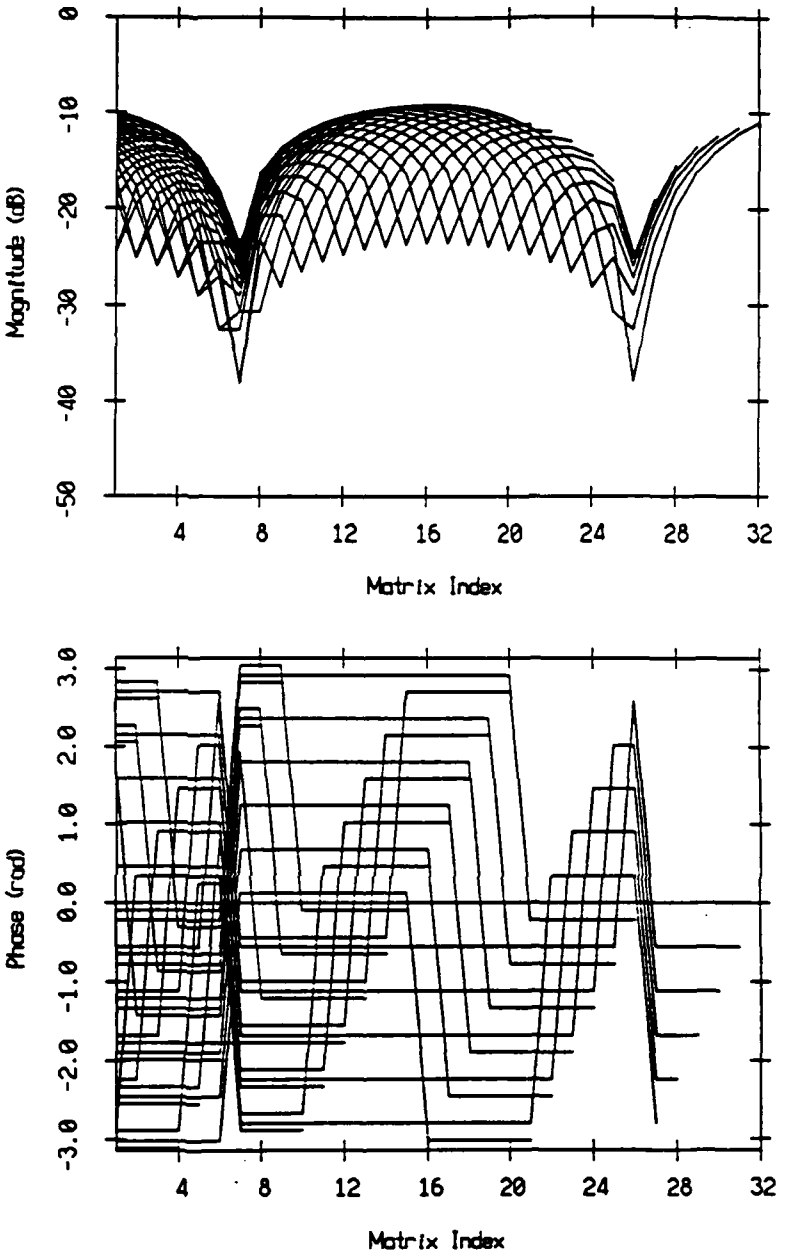

Figure III.4: Magnitude and phase of the upper diagonals of the 32 by 32 covariance matrix. Diagonals are identified by looking at their length. Matrix index corresponds to element index along the diagonal. The 32 sensor line array (25 m interelement spacing) receives two correlated arrivals ($\rho = 1$) at $-10°$ and $-20°$ incidence angles at 20 Hz. The sound speed is 1498 m/s.

III.3 Processing Methods

The methods which limit the effects of spatial correlation operate on the covariance matrix to make it "more Toeplitz" by performing some kind of averaging [Linebarger1988]. The straight arithmetic and geometric averaging of the covariance matrix diagonals, based on the concept of redudancy [Linebarger1988], have been proposed in the literature [Naidu1988, Hsu1986]. However, forcing a Toeplitz structure does not systematically result in a non negative definite cross-spectral matrix and is considered not viable [Linebarger1988]. The major averaging techniques proposed in the literature are

(1) Frequency averaging which is averaging covariance matrices at different frequencies [Wang1985, Zhu1988]. This method is relevant only to broadband situations.

(2) Spatial Averaging or Spatial Smoothing, developed for narrowband problems (and for a plane wavefront array manifold) [Gabriel1980, Shan1985, Su1986, Reddy1987, Takao1987, Linebarger1988]. This method is particularly relevant to the problems discussed here.

III.4 Spatial Smoothing

III.4.1 Description and Interpretation

The concept of spatial smoothing comes form the idea that the relative phase between two correlated arrivals changes in space [Gabriel1980, Widrow1982]. In practice, moving the array spatial position is out of question. Spatial smoothing implements this idea by averaging covariance matrices estimated on subarrays extracted from the full aperture and corresponding to slightly different spatial position. This averaging induces a reduction of the terms due to correlation [Linebarger1988] because the phase variations are eventually averaged to zero.

The technique uses the special geometry of line arrays with equi-spaced sensors

[Linebarger1988] and computes the average of the covariance matrix estimated on subarrays, where each subarray shares all but one of its sensors with an adjacent subarray [Shan1985]. If the full aperture array has M sensors, and the subarrays have s sensors, this is equivalent to averaging $M - s + 1$ blocks of s by s element extracted from the full array M by M covariance matrix along the main diagonal [Takao1987]. This procedure is summarized in Figure III.5. It can also be viewed as a low-pass filtering operation [Linebarger1988]. Furthermore averaging decreases the variance of the estimate of the cross-spectral matrix.

Spatial smoothing is implemented as follows [Shan1985]. If $\mathbf{X}$ if the full aperture $(M, 1)$ array vector, and $\mathbf{X}_i$ the i^{th} $(s,1)$ subaperture signal vector

$$\mathbf{X}_i^T = \left[X_i(f)\ X_{i+1}(f)\ \cdots\ X_{i+s}(f) \right] \tag{3.4.1}$$

the spatially smoothed covariance matrix is

$$\mathbf{R}_{smoothed} = \frac{1}{M - s + 1} \sum_{i=0}^{M-s} \mathbf{X}_i\ \mathbf{X}_i^H \tag{3.4.2}$$

III.4.2 Effects of Spatial Smoothing

It is shown in [Shan1985] that if p correlated signals impinge on the array, at least p averages over subarrays of p elements must be performed in order to recover the rank of the signal covariance matrix, that is to have $\det \mathbf{S} \neq 0$ (i.e. $\mathbf{S}$ is a p by p matrix of rank p). This result is of great importance because it indicates the number of averages necessary to allow the determination of the direction of arrivals with high resolution methods such as the MVDR beamformer or the MUSIC algorithm. It leads to the rule of thumb for spatial smoothing that a M sensor array is able to detect at most $\frac{M}{2}$ correlated arrivals [Shan1985].

In addition to their direction of arrival, it often is of interest to estimate the power of the arrivals. The rule of thumb described earlier is of little value with respect to

this problem since a full rank matrix does not ensure total decorrelation of the arrivals, that is a diagonal signal covariance matrix. Partial correlation among the arrivals leads to partial signal cancellation for the adaptive beamformers.

The spatial smoothing decorrelation rate for two correlated arrivals is studied in [Reddy1987]. It is shown that the model covariance matrix corresponding to the k^{th} subarray can be expressed as

$$\mathbf{R}_k = \mathbf{B}\,\Phi^{k-1}\,\mathbf{S}\,(\Phi^{k-1})^H\,\mathbf{B}^H + \sigma^2\,\mathbf{I} \tag{3.4.3}$$

where $\mathbf{R}_k$ is the subarray covariance matrix and corresponds to $\mathbf{X}_k\,\mathbf{X}_k^H$, $\mathbf{B}$ is the stacked plane wave direction matrix (a s by d matrix, where d is the number of signals), $\mathbf{S}$ is the d by d signal covariance matrix and Φ the diagonal matrix given by

$$\Phi = \begin{bmatrix} e^{-j\omega\tau_1} & 0 & 0 & \cdots & 0 \\ 0 & e^{-j\omega\tau_2} & 0 & \cdots & 0 \\ 0 & 0 & e^{-j\omega\tau_3} & \cdots & 0 \\ . & . & . & \cdots & . \\ . & . & . & \cdots & . \\ . & . & . & \cdots & . \\ 0 & 0 & 0 & \cdots & e^{-j\omega\tau_d} \end{bmatrix} \tag{3.4.4}$$

where τ_i represents the elementary time delay between two consecutive sensors for the i^{th} arrival.

This formulation shows that the effects of spatial smoothing can be interpreted in a useful way in terms of a modified signal covariance matrix, the smoothed covariance matrix:

$$\bar{\mathbf{S}} = \frac{1}{K}\sum_{k=1}^{K} \Phi^{k-1}\,\mathbf{S}\,(\Phi^{k-1})^H \tag{3.4.5}$$

where K is the number of averages, also called smoothing index. Restricting the discussion to two correlated arrivals, [Reddy1987] indicates that perfect decorrelation is achieved when the (1,2) term of $\bar{\mathbf{S}}$ is equal to zero. This term is given by

$$\bar{\mathbf{S}}(1,2) = \frac{\sigma_0\sigma_1\rho}{K}\sum_{k=1}^{K} \exp\left[-j(k-1)2\pi\frac{\Delta}{\lambda}(\sin\theta_0 - \sin\theta_1)\right] \tag{3.4.6}$$

$$\bar{S}(1,2) = \frac{\sigma_1\sigma_2\rho}{K} \frac{1 - \exp\left[\frac{2\pi K\Delta}{\lambda}(\sin\theta_0 - \sin\theta_1)\right]}{1 - \exp\left[\frac{2\pi\Delta}{\lambda}(\sin\theta_0 - \sin\theta_1)\right]} \tag{3.4.7}$$

where ρ is complex correlation between the two arrivals of power σ_0^2, σ_1^2 and physical arrival angles θ_0 and θ_1, Δ is the array interelement spacing, λ the acoustic wavelength.

The minimum value of the smoothing index necessary to completely decorrelate the two arrivals is

$$K = \frac{\lambda}{\Delta\,|\sin\theta_0 - \sin\theta_1|} \tag{3.4.8}$$

The values of the smoothing index K are tabulated, for an array with half wavelength element spacing, as a function of the angular pair separation $|\theta_0 - \theta_1|$ and the position of the pair referenced by $|\theta_0|$ (with $|\theta_0| < |\theta_1|$) in Table III.1. An arrival pair with 5^o separation arriving at 10^o requires at least 12 averages to achieve total decorrelation or, equivalently, allow the MVDR beamformer to yield the proper powers.

Equation (3.4.8) shows that the number of averages necessary to decorrelate two close arrivals greatly depends on the pair angular spacing. Two closely spaced arrival are very difficult to decorrelate [Reddy1987]. In practice, full decorrelation of the arrivals may not be possible if the array has a limited number of sensors. The effective aperture is reduced from M to s which results in lower resolution. Although decorrelation is achieved at the cost of resolution and numerical processing burden, spatial smoothing is necessary to use with high resolution beamformers.

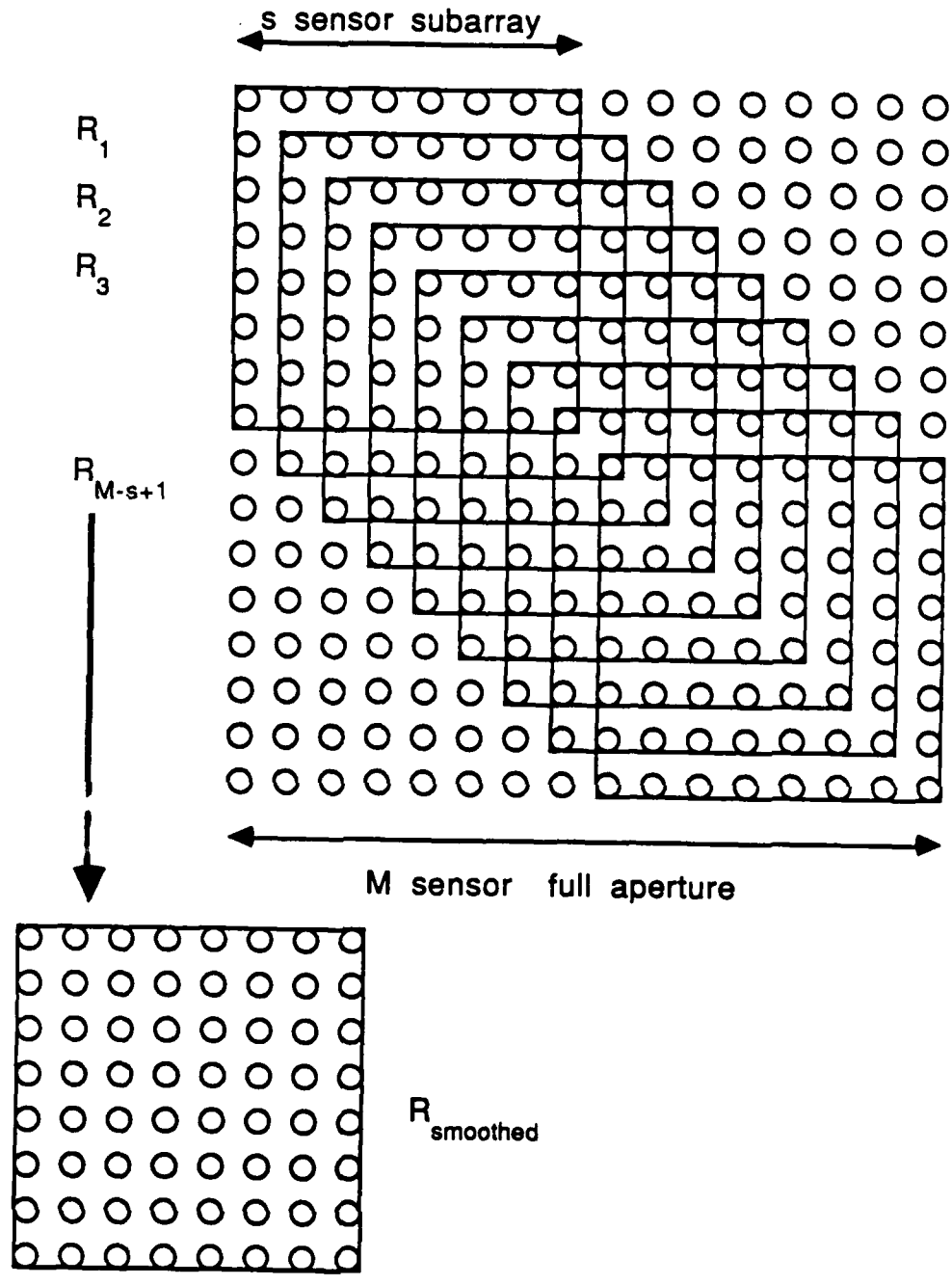

Figure III.5: Summary of spatial smoothing [Takao1987].

	1	2	3	4	5	6	7	8	9	10	11	12	13	14	15	16	17	18	19	20	21	22	23	24	25	26	27	28	29	30	31	32	33	34	35
0	115	58	39	29	23	20	17	15	13	12	11	10	9	9	8	8	7	7	7	6	6	6	6	5	5	5	5	5	5	5	4	4	4	4	4
1	115	58	39	29	23	20	17	15	13	12	11	10	9	9	8	8	7	7	7	6	6	6	6	5	5	5	5	5	5	5	4	4	4	4	4
2	115	58	39	29	23	20	17	15	13	12	11	10	9	9	8	8	7	7	7	6	6	6	6	5	5	5	5	5	5	5	4	4	4	4	4
3	115	58	39	29	24	20	17	15	13	12	11	10	9	9	8	8	7	7	7	6	6	6	6	5	5	5	5	5	5	5	4	4	4	4	4
4	115	58	39	29	24	20	17	15	13	12	11	10	9	9	8	8	7	7	7	6	6	6	6	6	5	5	5	5	5	5	4	4	4	4	4
5	116	58	39	29	24	20	17	15	13	12	11	10	10	9	8	8	7	7	7	6	6	6	6	6	5	5	5	5	5	5	4	4	4	4	4
6	116	58	39	29	24	20	17	15	13	12	11	10	10	9	8	8	7	7	7	6	6	6	6	6	5	5	5	5	5	5	4	4	4	4	4
7	116	58	39	30	24	20	17	15	14	12	11	10	10	9	8	8	8	7	7	7	6	6	6	6	5	5	5	5	5	5	4	4	4	4	4
8	116	59	39	30	24	20	17	15	14	12	11	10	10	9	8	8	8	7	7	7	6	6	6	6	5	5	5	5	5	5	4	4	4	4	4
9	117	59	39	30	24	20	17	15	14	12	11	10	10	9	8	8	8	7	7	7	6	6	6	6	5	5	5	5	5	5	5	4	4	4	4
10	117	59	39	30	24	20	17	15	14	12	11	10	10	9	9	8	8	7	7	7	6	6	6	6	6	5	5	5	5	5	5	4	4	4	4
11	117	59	40	30	24	20	17	15	14	12	11	11	10	9	9	8	8	7	7	7	6	6	6	6	6	5	5	5	5	5	5	4	4	4	4
12	118	59	40	30	24	20	17	15	14	12	11	11	10	9	9	8	8	7	7	7	6	6	6	6	6	5	5	5	5	5	5	5	4	4	4
13	118	60	40	30	24	20	18	15	14	13	12	11	10	9	9	8	8	7	7	7	6	6	6	6	6	5	5	5	5	5	5	5	4	4	4
14	119	60	40	30	24	20	18	16	14	13	12	11	10	9	9	8	8	7	7	7	7	6	6	6	6	5	5	5	5	5	5	5	5	4	4
15	119	60	40	30	25	21	18	16	14	13	12	11	10	9	9	8	8	7	7	7	7	6	6	6	6	6	5	5	5	5	5	5	5	5	4
16	120	60	41	31	25	21	18	16	14	13	12	11	10	9	9	8	8	8	7	7	7	6	6	6	6	6	5	5	5	5	5	5	5	5	5
17	121	61	41	31	25	21	18	16	14	13	12	11	10	9	9	8	8	8	7	7	7	6	6	6	6	6	5	5	5	5	5	5	5	5	5
18	121	61	41	31	25	21	18	16	14	13	12	11	10	10	9	8	8	8	7	7	7	6	6	6	6	6	6	5	5	5	5	5	5	5	5
19	122	61	41	31	25	21	18	16	14	13	12	11	10	10	9	9	8	8	7	7	7	7	6	6	6	6	6	5	5	5	5	5	5	5	5
20	123	62	42	31	25	21	18	16	15	13	12	11	10	10	9	9	8	8	7	7	7	7	6	6	6	6	6	5	5	5	5	5	5	5	5
21	124	62	42	32	25	21	19	16	15	13	12	11	10	10	9	9	8	8	8	7	7	7	6	6	6	6	6	6	5	5	5	5	5	5	5
22	125	63	42	32	26	22	19	16	15	13	12	11	11	10	9	9	8	8	8	7	7	7	7	6	6	6	6	6	6	5	5	5	5	5	5
23	125	63	42	32	26	22	19	17	15	13	12	11	11	10	9	9	8	8	8	7	7	7	7	6	6	6	6	6	6	6	5	5	5	5	5
24	126	64	43	32	26	22	19	17	15	14	12	12	11	10	9	9	9	8	8	7	7	7	7	6	6	6	6	6	6	6	5	5	5	5	5
25	127	64	43	33	26	22	19	17	15	14	13	12	11	10	10	9	9	8	8	8	7	7	7	7	6	6	6	6	6	6	6	5	5	5	5
26	129	65	44	33	27	22	19	17	15	14	13	12	11	10	10	9	9	8	8	8	7	7	7	7	6	6	6	6	6	6	5	5	5	5	5
27	130	65	44	33	27	23	20	17	15	14	13	12	11	10	10	9	9	8	8	8	7	7	7	7	6	6	6	6	6	6	6	5	5	5	5
28	131	66	44	34	27	23	20	17	16	14	13	12	11	11	10	9	9	9	8	8	8	7	7	7	7	6	6	6	6	6	6	6	5	5	5
29	132	67	45	34	27	23	20	18	16	14	13	12	11	11	10	9	9	9	8	8	8	7	7	7	7	6	6	6	6	6	6	6	6	5	5
30	133	67	45	34	28	23	20	18	16	15	13	12	11	11	10	10	9	9	8	8	8	7	7	7	7	7	6	6	6	6	6	6	6	6	5
31	135	68	46	35	28	24	20	18	16	15	13	12	12	11	10	10	9	9	8	8	8	8	7	7	7	7	7	6	6	6	6	6	6	6	6
32	136	69	46	35	28	24	21	18	16	15	14	13	12	11	10	10	9	9	9	8	8	8	8	7	7	7	7	7	6	6	6	6	6	6	6
33	138	70	47	35	29	24	21	18	17	15	14	13	12	11	11	10	10	9	9	8	8	8	8	8	7	7	7	7	7	6	6	6	6	6	6
34	140	70	47	36	29	24	21	19	17	15	14	13	12	11	11	10	10	9	9	9	8	8	8	8	7	7	7	7	7	7	6	6	6	6	6
35	141	71	48	36	29	25	21	19	17	15	14	13	12	12	11	10	10	9	9	9	8	8	8	8	8	7	7	7	7	7	7	6	6	6	6
36	143	72	49	37	30	25	22	19	17	16	14	13	12	12	11	10	10	10	9	9	8	8	8	8	8	7	7	7	7	7	7	7	6	6	6
37	145	73	49	37	30	25	22	19	18	16	15	14	13	12	11	11	10	10	9	9	9	8	8	8	8	8	7	7	7	7	7	7	7	6	6
38	147	74	50	38	31	26	22	20	18	16	15	14	13	12	11	11	10	10	9	9	9	8	8	8	8	8	8	7	7	7	7	7	7	7	6
39	149	75	51	38	31	26	23	20	18	16	15	14	13	12	12	11	11	10	10	9	9	9	9	8	8	8	8	8	8	7	7	7	7	7	7
40	151	76	52	39	32	27	23	20	18	17	15	14	13	13	12	11	11	10	10	9	9	9	9	8	8	8	8	8	8	8	7	7	7	7	7

Table III.1: Smoothing index as a function of arrival pair spacing (lines in Table) and position from broadside (0°). The array has a ½ wavelength interelement spacing.

III.4.3 Simulation Results

III.4.3.1 Effects on the Array Covariance Matrix

Spatial smoothing is a preprocessing technique that operates on the full array covariance matrix to obtain a "more Toeplitz" matrix. This preprocessing controls the performance of the high resolution techniques by its ability to decorrelate the arrivals.

To illustrate the process of decorrelation achieved by spatial smoothing, the diagonals of the array covariance of a field composed of two correlated arrivals are inspected under several smoothing scenarios. As in Section III.2, the two unit power plane wave arrivals impinging on the array have incidence angles of -10^{o} and -20^{o}. The array is $10\frac{1}{3}$ wavelength long and has 32 sensors, $\frac{\lambda}{\Delta}=3$. Five different subarray lengths are selected: 28, 24, 20, 16, 14 so that the number of averages in the smoothing increases from 5 to 19.

As the number of average increases or subarray length decreases, the covariance matrix becomes more and more Toeplitz, as can be seen on Figures III.6 to III.10. Using Equation (3.4.8) with $\frac{\lambda}{\Delta}=3$, $\theta_0=-10$, and $\theta_1=-20$, the number of averages necessary to decorrelate the two arrivals is $K \approx 18$ which corresponds to a subarray length of 15. One checks that for subarray lengths equal to 14 and 16, the spatially smoothed matrix is almost Toeplitz, with constant phase and contant magnitude on the upper diagonals.

III.4.3.2 Effects on the Output of the MVDR Beamformer

Theoretical results [Shan1985] provide the criteria for the detection of correlated arrivals using spatial smoothing and high resolution processors. When a good estimate of the power is required, adaptive beamforming must be used, such as the MVDR beamformer. It thus is of interest to study the amount of loss due to correlation at the output of

the MVDR beamformer after spatial smoothing. The simulation described hereafter completes the already known qualitative information about the general behaviour of the angular spectrum estimate [Reddy1987] by providing, in a particular case, quantitative information on the loss due to correlation.

As before, a $10\frac{1}{3}$ wavelength array with 32 sensors receives a pair of correlated ($\rho = 1$) unit power plane wave arrivals in the set with incidence angles {0^o, 5^o, 10^o, 15^o, 20^o, 25^o, 30^o, 35^o, 40^o}. A background sensor noise of – 20 dB is also included. The possible angular spacings are multiple of 5^o which is close to the Rayleigh resolution of the array. For each pair of arrival combinations, spatial smoothing followed by the MVDR beamforming is performed and the loss corresponding to the arrivals measured. The loss is the difference in dB between the true power (in this case 0 dB) and the power of the arrivals at the output of the beamformer.

Figure III.11 shows the influence of the arrival pair angular spacing on the loss due to correlation. Panel A indicates that without any smoothing the MVDR beamformer suffers almost complete signal cancellation. The other panels correspond to different subsegment lengths from 30 to 14, the number of averages varying from 3 to 19. Each panel indicates the amount of loss due to correlation that can be expected from a given number of averages and a given pair angular seperation. Each angular seperation corresponds to a number of combinaison of arrivals, e.g. there is a 10^o seperation for the following pairs: (0^o , 10^o), (5^o , 15^o), (10^o , 20^o), (15^o , 25^o), (20^o , 30^o), (25^o , 35^o), (30^o , 40^o). A small subarray with 14 sensors allows perfect decorrelation of arrivals as close as 10^o and limits the correlation loss to a few dB for 5^o spacing. A subarray of 24 elements does a good job at decorrelating arrivals seperated by at least 10^o.

Figure III.12 shows the same results of loss due to correlation as a function of the number of averages. For a given scenario, it allows one to study the impact of the number of averages on the final angular spectrum and to select a subarray length for each case. It

indicates that considerable smoothing must be performed when the two arrivals are close together. A 5^o seperation requires at least 16 averages for the MVDR beamformer to yield a minimum amount of loss.

In the case of a 10^o seperated pair, Figure III.13 studies the impact under several smoothing conditions of the pair location with respect to the broadside direction. The effect of moving an arrival pair from broadside (0^o , 10^o), toward endfire (30^o , 40^o) is small since the variations of loss are at most of the order of 2 dB, as the pair direction arrives at steeper and steeper angles.

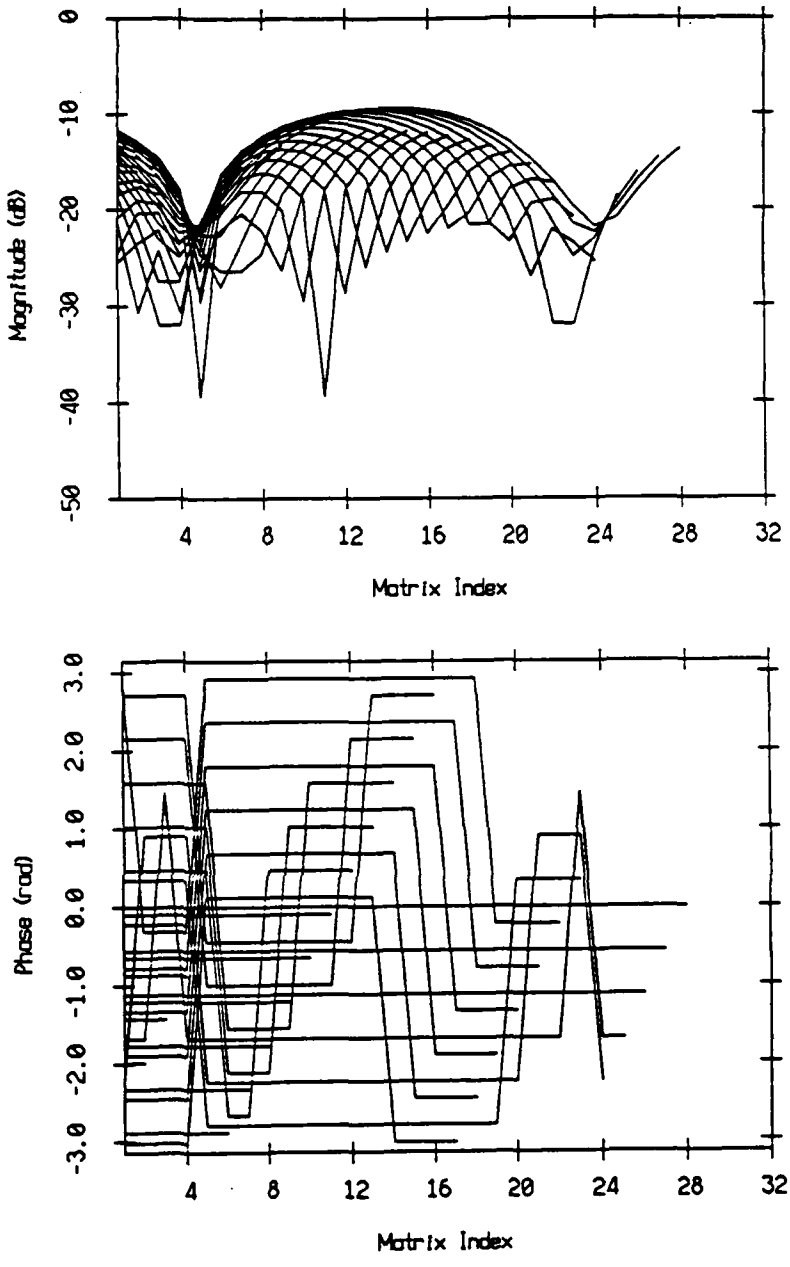

Figure III.6: Magnitude and phase of the upper diagonals of the 28 by 28 spatially smoothed covariance matrix. Diagonals are identified by looking at their length. Matrix index corresponds to element index along the diagonal.The 32 sensor line array (25 m interelement spacing) receives two correlated arrivals ($\rho = 1$) at $-10°$ and $-20°$ incidence angles at 20 Hz. The sound speed is 1498 m/s.

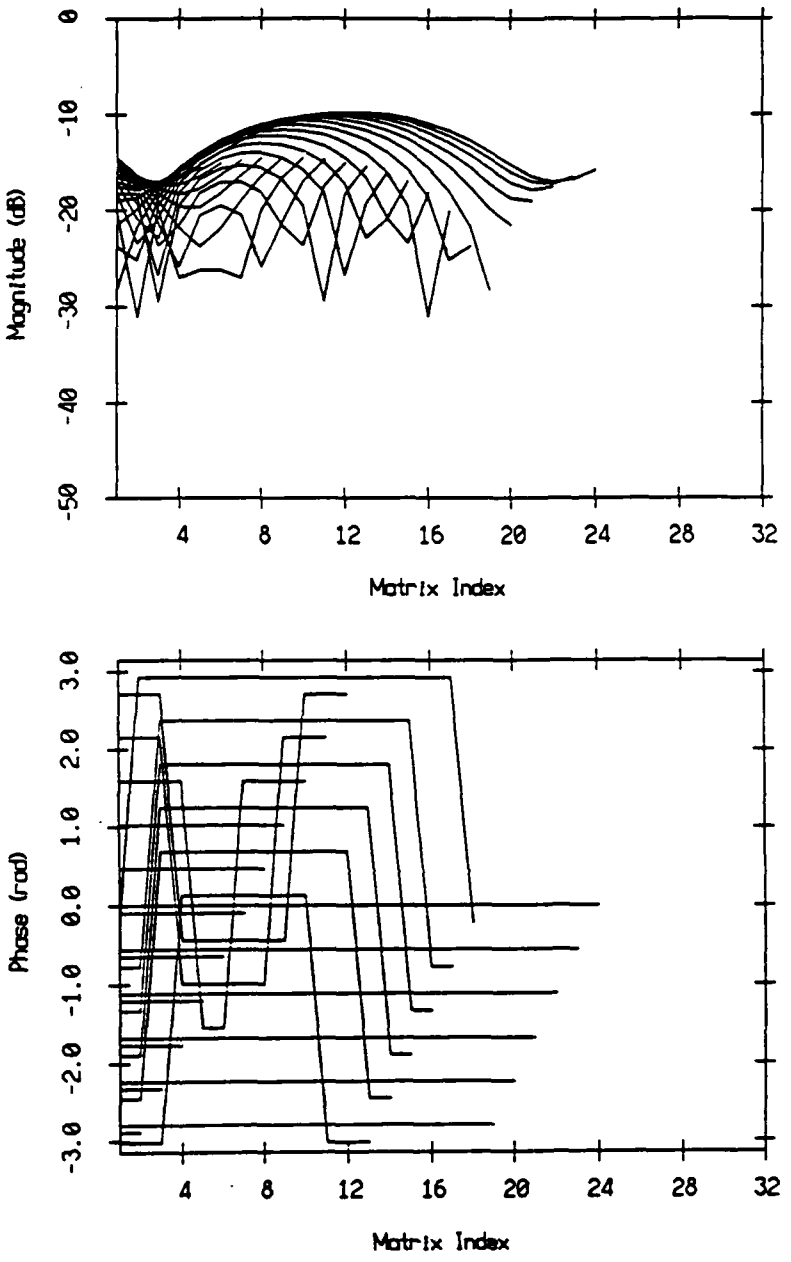

Figure III.7: Magnitude and phase of the upper diagonals of the 24 by 24 spatially smoothed covariance matrix. Diagonals are identified by looking at their length. Matrix index corresponds to element index along the diagonal.The 32 sensor line array (25 m interelement spacing) receives two correlated arrivals ($\rho = 1$) at -10° and -20° incidence angles at 20 Hz. The sound speed is 1498 m/s.

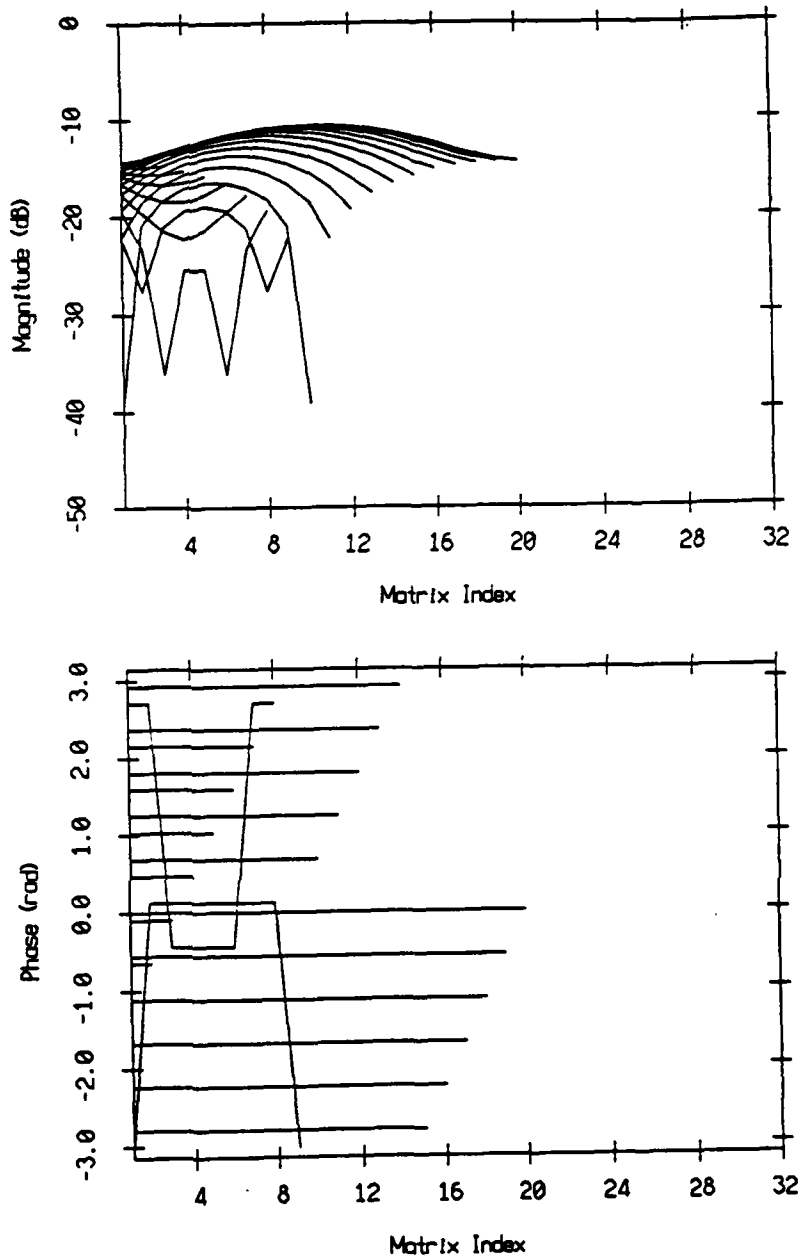

Figure III.8: Magnitude and phase of the upper diagonals of the 20 by 20 spatially smoothed covariance matrix. Diagonals are identified by looking at their length. Matrix index corresponds to element index along the diagonal.The 32 sensor line array (25 m interelement spacing) receives two correlated arrivals ($\rho = 1$) at $-10°$ and $-20°$ incidence angles at 20 Hz. The sound speed is 1498 m/s.

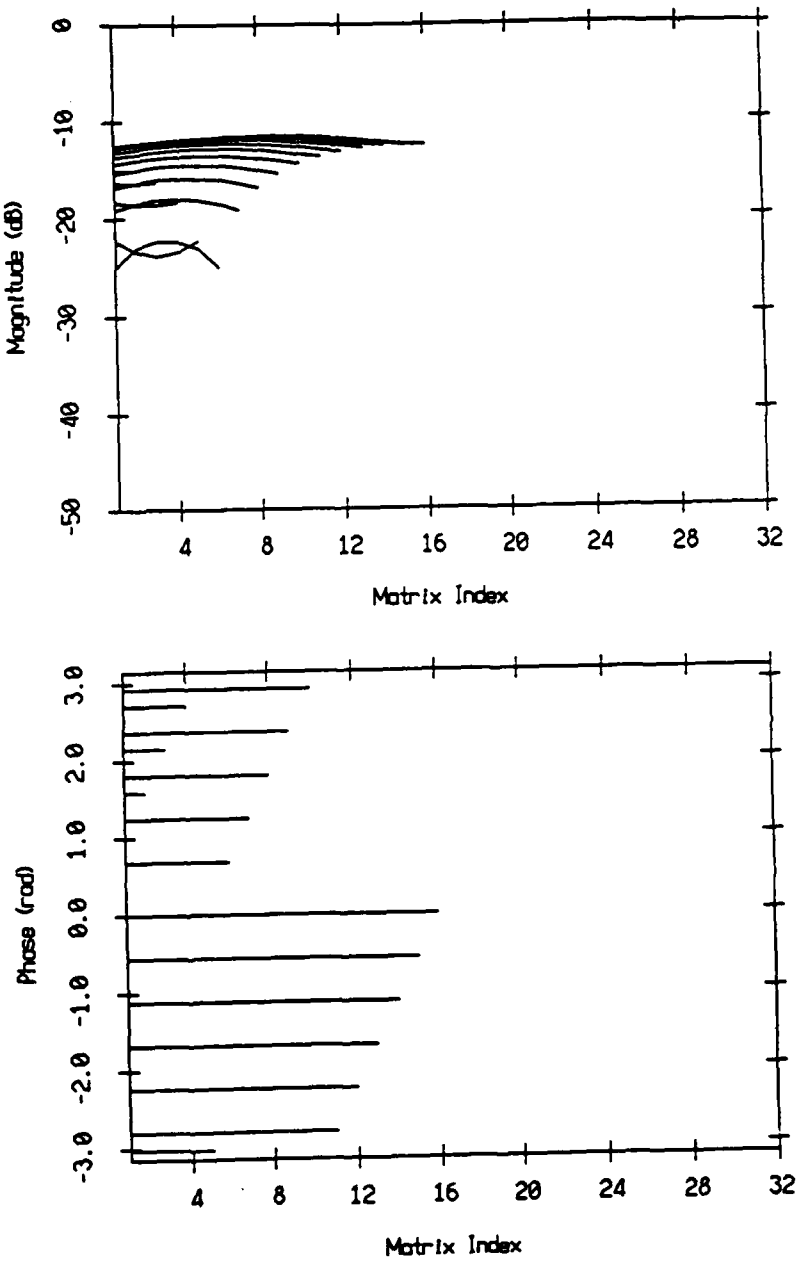

Figure III.9: Magnitude and phase of the upper diagonals of the 16 by 16 spatially smoothed covariance matrix. Diagonals are identified by looking at their length. Matrix index corresponds to element index along the diagonal.The 32 sensor line array (25 m interelement spacing) receives two correlated arrivals ($\rho = 1$) at $-10°$ and $-20°$ incidence angles at 20 Hz. The sound speed is 1498 m/s.

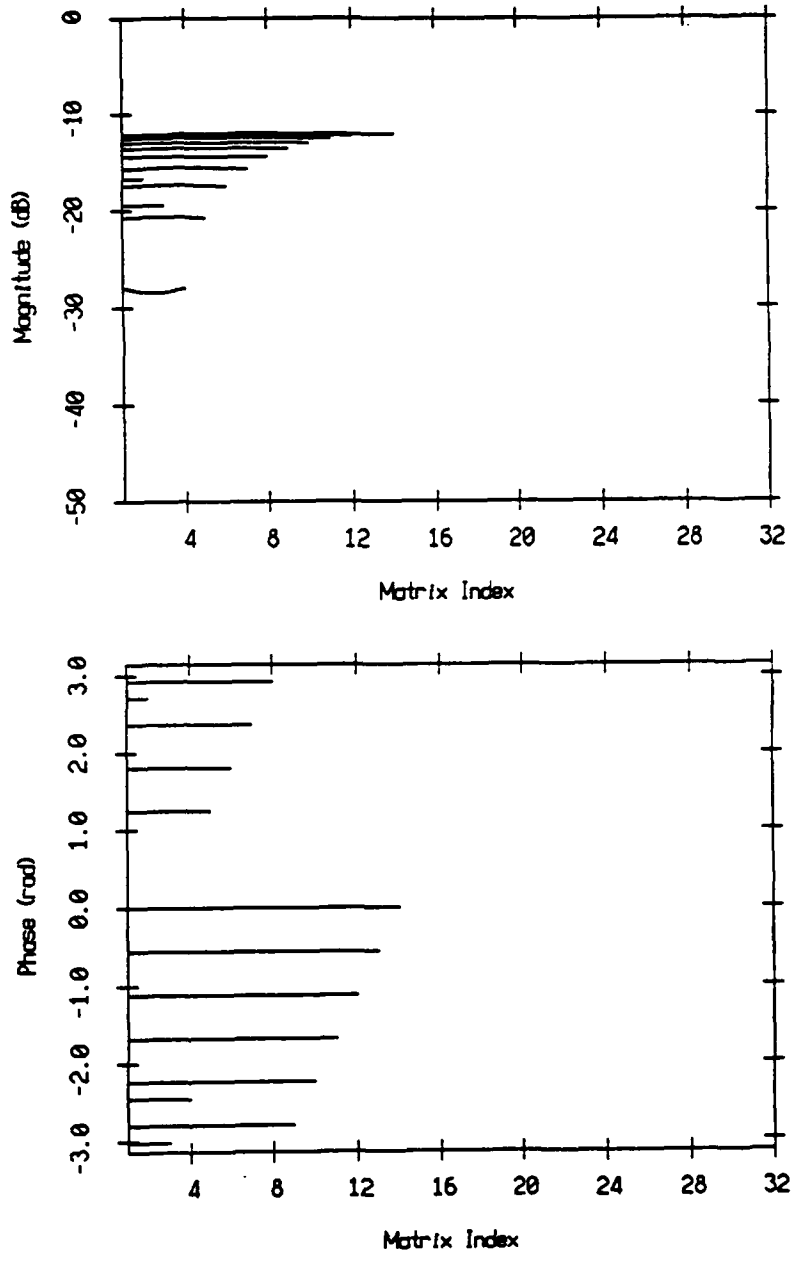

Figure III.10: Magnitude and phase of the upper diagonals of the 14 by 14 spatially smoothed covariance matrix. Diagonals are identified by looking at their length. Matrix index corresponds to element index along the diagonal.The 32 sensor line array (25 m interelement spacing) receives two correlated arrivals ($\rho = 1$) at -10° and -20° incidence angles at 20 Hz. The sound speed is 1498 m/s.

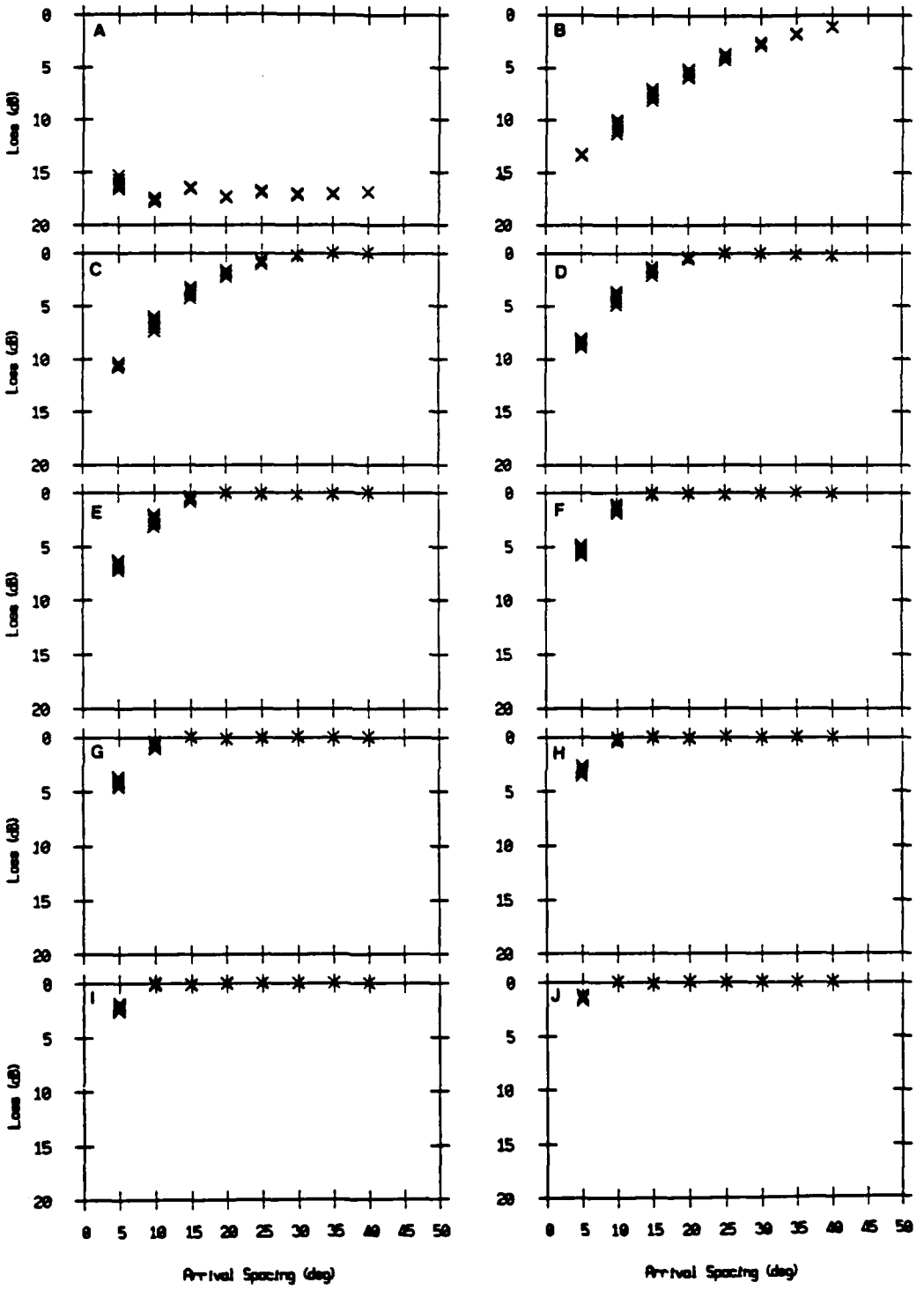

Figure III.11: Loss at the output of the MVDR beamformer after spatial smoothing for a correlated arrival pair. The pair angular spacing varies from 5° to 40°. A given spacing corresponds to several combinations of arrivals at {0°, 5°, 10°, ... , 40°}. Panel A corresponds to no smoothing, Panels B, C, D, E, F, G, H, I, J correspond to smoothing subsegment lengths {30, 28, 26, 24, 22, 20, 18, 16, 14}.

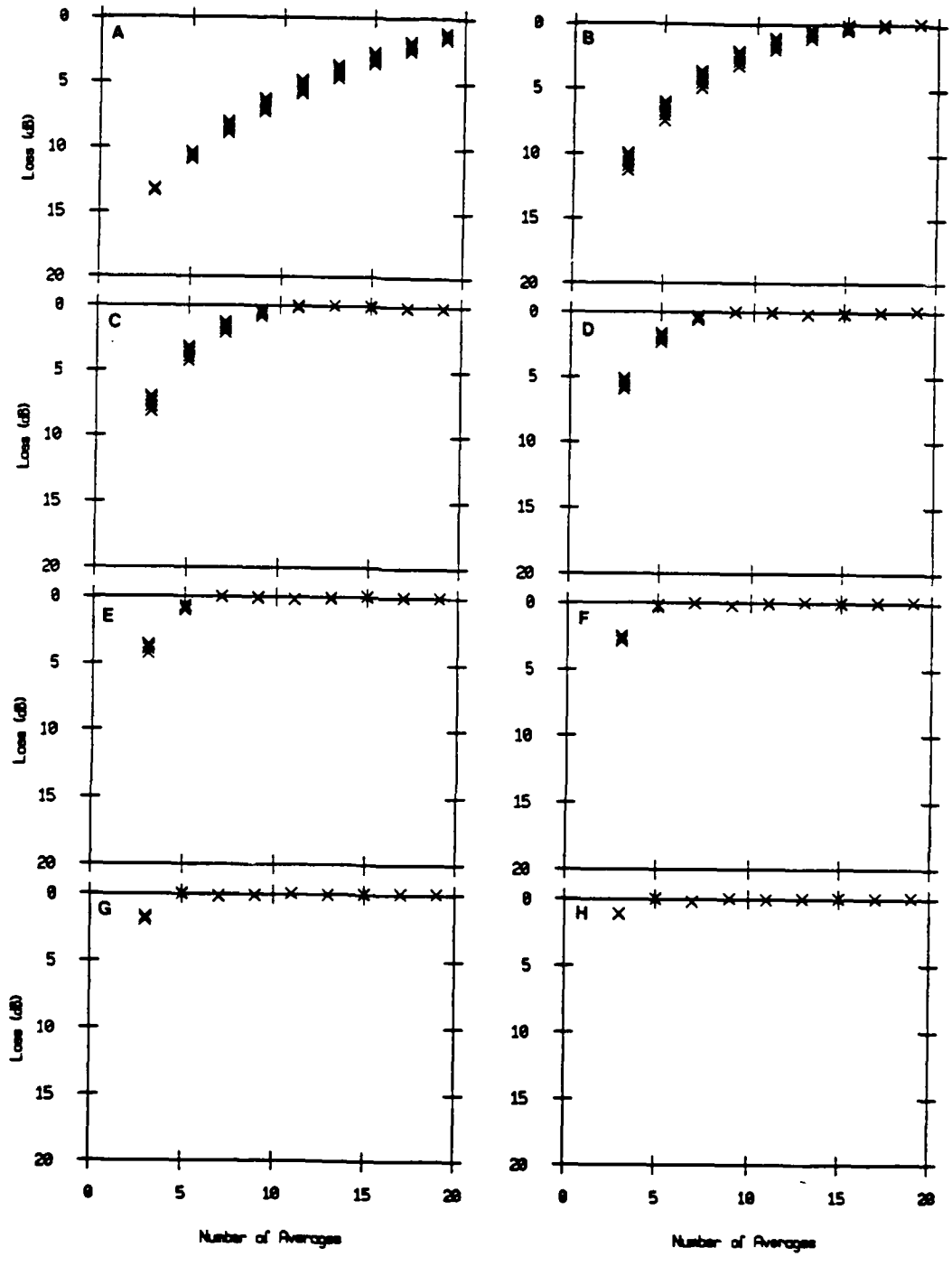

Figure III.12: Loss at the output of the MVDR beamformer as a function of the number of averages performed by spatial smoothing. Panels A, B, C, D, E, F, G, H correspond to correlated ($\rho = 1$) arrival pairs with angular separations {5°, 10°, 15°, 20°, 25°, 30°, 35°, 40°}.

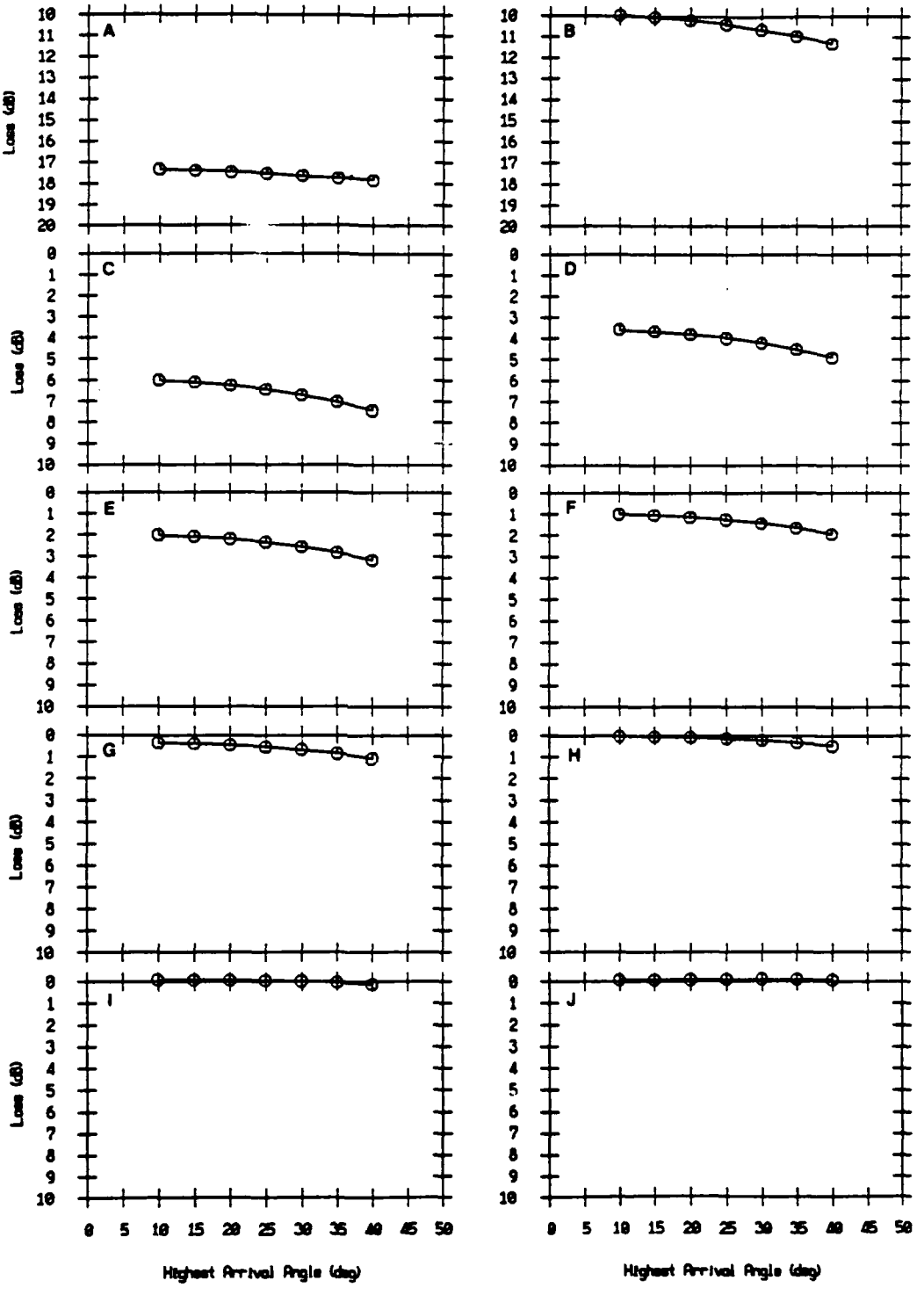

Figure III.13: Impact on the loss at the output of the MVDR beamformer due the location from broadside of a 10° separated pair. Panel A corresponds to no smoothing and Panels B, C, D, E, F, G, H, I, J correspond to smoothing subsegment lengths {30, 28, 26, 24, 22, 20, 18, 16, 14}.

III.5 Modified Spatial Smoothing

III.5.1 Description and Interpretation

A second version of spatial smoothing has been proposed [Williams1988] and uses an estimate of the covariance matrix which is the modified covariance matrix of the combined forward/backward linear prediction algorithm for autoregressive spectral estimation [Burg1967]. The modified covariance method is known to perform better in time series autoregressive spectral estimation in producing less spurious peaks [Marple1987]. The modified covariance matrix also is used in the maximum entropy wavenumber processing for linear arrays [Barnard1982] and in the Kumaresan-Tufts high resolution method of direction of arrival estimation [Kumaresan1983].

Im modified spatial smoothing, the covariance matrix of the array data $\mathbf{x}_f$ and of the reversed data $\mathbf{x}_b$ is estimated. Defining

$$\mathbf{x}_f^T = \begin{bmatrix} x_0 & x_1 & \cdots & x_n \end{bmatrix} \tag{3.5.1}$$

$$\mathbf{x}_b^T = \begin{bmatrix} x_n & x_{n-1} & \cdots & x_0 \end{bmatrix} \tag{3.5.2}$$

then, the modified covariance matrix is

$$\tfrac{1}{2}\left[\mathbf{x}_f \, \mathbf{x}_f^H + \mathbf{x}_b \, \mathbf{x}_b^H \right] \tag{3.5.3}$$

This is made possible by the special geometry of equispaced line arrays. As in the original spatial smoothing, the modified spatial smoothing does the average of the modified covariance matrices estimated on overlapping subarrays. Modified spatial smoothing can be formulated as [Williams1988]

$$\mathbf{R}_{smoothed} = \frac{1}{M - s + 1} \sum_{i=0}^{M-s} \tfrac{1}{2}\left(\mathbf{X}_i \, \mathbf{X}_i^H + \mathbf{J} \, (\mathbf{X}_i \, \mathbf{X}_i^H)^* \, \mathbf{J} \right) \tag{3.5.4}$$

where * is the complex conjugate operation and $\mathbf{J}$ is the reflection matrix or reverse matrix given by

$$\mathbf{J}=\begin{bmatrix} 0 & 0 & 0 & \cdots & 1 \\ 0 & 0 & 0 & \cdots & 0 \\ \cdot & \cdot & \cdot & \cdots & \cdot \\ \cdot & \cdot & \cdot & \cdots & \cdot \\ \cdot & \cdot & 1 & \cdots & \cdot \\ 0 & 1 & 0 & \cdots & 0 \\ 1 & 0 & 0 & \cdots & 0 \end{bmatrix} \tag{3.5.5}$$

III.5.2 Performance of the Modified Spatial Smoothing

It is shown in [Williams1988] that if p correlated arrivals impinge on the array, it is sufficient to average $\frac{p}{2}$ subarrays of p sensors to recover the rank of the signal covariance matrix, that is to have $\det \mathbf{S} \neq 0$. This result holds under some specific constraints detailed in [Williams1988]. With modified spatial smoothing, a M sensor array is able to detect at most $\frac{2M}{3}$ correlated arrivals [Williams1988]. This result is of great interest because it indicates that the number of averages necessary to allow the determination of the direction of arrivals with high resolution methods is half what the original spatial smoothing requires and allows the so-called increase in efficient array aperture.

As with spatial smoothing, an estimate of the power for each arrival often is of interest. Then, one can ask what decorrelation rate modified spatial smoothing achieves compared to the original spatial smoothing.

The study outlined in Section III.4.3 and detailed in [Reddy1987] is repeated here for the modified spatial smoothing. One considers two correlated arrivals impinging on a M sensor array referenced to its center as in [Takao1987]. The full aperture plane wave steering vectors are given by

$$\mathbf{A}_i^T = \left[\exp(j\frac{2\pi\Delta}{\lambda}(k - \frac{M+1}{2})\sin\theta_i \right]_{k=1,M} \tag{3.5.6}$$

The array covariance matrix can be seperated into a part that corresponds to the original spatial smoothing and a part that corresponds to the modified spatial smoothing. The spatially smoothed part of the signal covariance matrix is given by

$$\bar{\mathbf{S}}_1 = \frac{1}{2(M-s+1)} \sum_{k=-\frac{M-1}{2}}^{\frac{M-1}{2}} \mathbf{D}^k \, \mathbf{S} \, (\mathbf{D}^k)^H \tag{3.5.7}$$

where

$$\mathbf{D} = \begin{bmatrix} e^{j2\pi\frac{\Delta}{\lambda}\sin\theta_0} & 0 \\ 0 & e^{j2\pi\frac{\Delta}{\lambda}\sin\theta_1} \end{bmatrix} \tag{3.5.8}$$

and S is given by Equation (3.3.8). The spatially smoothed array covariance matrix is given by

$$\mathbf{R}_1 = \mathbf{B} \, \bar{\mathbf{S}}_1 \, \mathbf{B}^H \tag{3.5.9}$$

where B is the stacked direction matrix over a subarray. Carrying out the algebra,

$$\bar{\mathbf{S}}_1(1,2) = \frac{1}{2(M-s+1)} \sigma_1 \sigma_2 \rho \, \frac{\sin\frac{\pi\Delta K}{\lambda}(\sin\theta_0 - \sin\theta_1)}{\sin\frac{\pi\Delta}{\lambda}(\sin\theta_0 - \sin\theta_1)} \tag{3.5.10}$$

The second part of the array covariance matrix is given by

$$\mathbf{R}_2 = \mathbf{J} \, \mathbf{R}_1^* \, \mathbf{J} \tag{3.5.11}$$

or

$$\mathbf{R}_2 = \mathbf{J} \, \mathbf{B}^* \bar{\mathbf{S}}_1^* \, \mathbf{B}^T \, \mathbf{J} \tag{3.5.12}$$

Since it is shown in [Williams1988] that $\mathbf{J}\,\mathbf{B}^* = \mathbf{B}$, then $\mathbf{R}_2 = \mathbf{B}\,\bar{\mathbf{S}}_1^*\,\mathbf{B}^H$ and the equivalent modified part of the signal covariance matrix is given by $\bar{\mathbf{S}}_2 = \bar{\mathbf{S}}_1^*$. Then the (1,2) term of $\bar{\mathbf{S}}$ is

$$\bar{\mathbf{S}}(1,2) = \frac{\sigma_1\sigma_2 \, |\rho|}{M-s+1} \, \frac{\sin\pi\frac{\Delta}{\lambda}K(\sin\theta_o - \sin\theta_1)}{\sin\pi\frac{\Delta}{\lambda}(\sin\theta_o - \sin\theta_1)} \cos\phi \tag{3.5.13}$$

where ϕ and $|\rho|$ are given by the correlation between the two arrivals $\rho = |\rho| \, e^{j\phi}$.

This result shows a peculiarity of the modified spatial smoothing: when ϕ, the electrical phase between the two arrivals at the center of the array (the reference) is $\frac{\pi}{2}$, perfect decorrelation is achieved. The array covariance matrix is Toeplitz and there is no

loss due to correlation at the output of the MVDR beamformer, even if $s = M$. When the electrical phase is zero, the decorrelation rate is identical to that of spatial smoothing. These results that strongly depend on the electrical phase ϕ are similar to what was observed in [Gabriel1986] for adaptive antennas and in [White1979] for the minimum entropy method operating on fully correlated arrivals in quadrature.

The chances of having two signals in quadrature at the center of the array are slim. Thus, all one can state is that the modified spatial smoothing works as well or better than the original spatial smoothing in decorrelating a pair of correlated arrivals.

If the reference is taken at another spatial position along the array, the dependence of the modified spatial smoothing performance on the electrical phase ϕ still exists. The precise phase relationship between the two signals for which decorrelation is achieved is not $\frac{\pi}{2}$ and depends on the reference point, the interelement spacing, the wavelength, and the arrival angles.

III.5.3 Simulation Results

To illustrate the theoretical developments of the previous sections, the effects of modified spatial smoothing with two signals with a varying electrical phase at the center of a 32 element array now is studied. As before, the array is $10\frac{1}{3}$ wavelength long and receives unit power plane wave arrivals at -5^{o} and 0^{o} incidence angle. The subarray length is 32 so that only two covariance matrix averages are performed. The maximum loss due to correlation for the two arrivals at the output of the MVDR beamformer is plotted on Figure III.14. When the two signals are in quadrature, there is no loss since the modified covariance matrix is Toeplitz. The loss due to correlation increases as the electrical phase decreases, and the loss reduces to that given by the original spatial smoothing, on the order of 50 dB. Then, the behaviour of the modified spatial smoothing is identical to that of the original spatial smoothing.

The angular spectra given by the MVDR beamformer for an electrical phase of 0 and $\frac{\pi}{2}$ radians are plotted on Figure III.15. Perfect resolution is achieved when the two signals are in phase quadrature, while the method fails when the two signals are in phase.

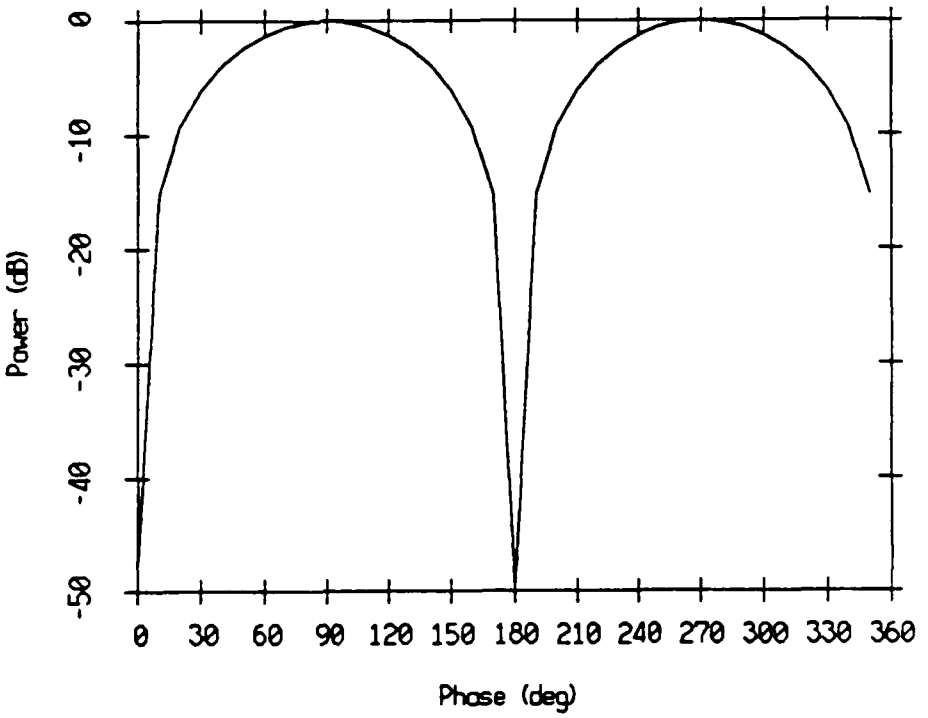

Figure III.14: Variations of the loss at the output of the MVDR beamformer after modified spatial smoothing as a function of the electrical phase between two correlated arrivals ($|\rho| = 1$) with $-5°$ and $0°$ incidence angles. Phase and arrival angles are relative to the aperture center. The array has 32 sensors (25 m spacing) and operates at 20 Hz.

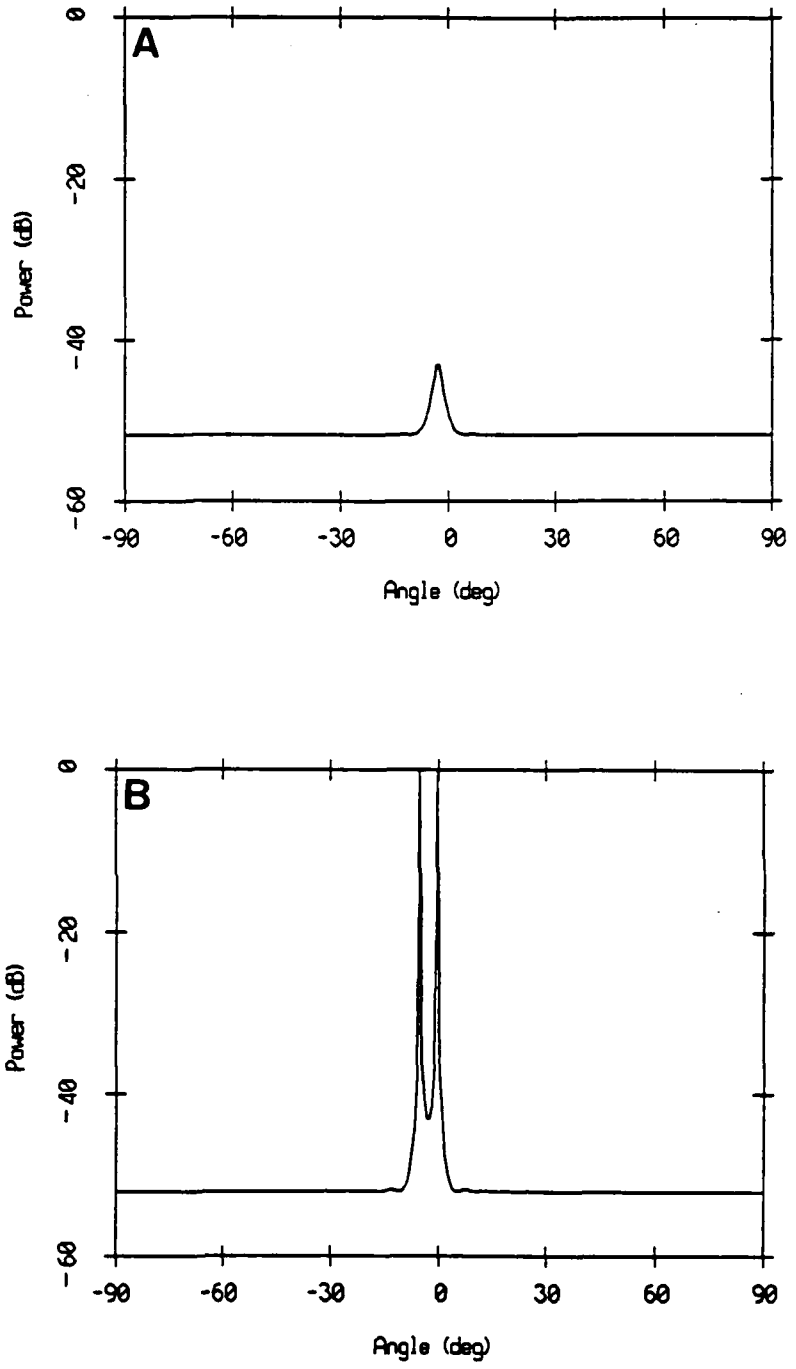

Figure III.15: MVDR Angular Spectra using the full array modified covariance matrix of two correlated arrivals with $-5°$ and $0°$ incidence angles. In Panel A, the two arrivals are in phase ($\rho = 1$) while in Panel B the two arrivals are in quadrature ($\rho = \exp j\pi/2$) with respect to the array center.

III.6 Conclusions

This chapter illustrates the effects of correlation on high and super resolution techniques and explains how the spatial smoothing preprocessing techniques work. The smoothing techniques attempt to reduce the modulations of the diagonals of the covariance matrix which should be Toeplitz according to the signal model. The various interpretations of smoothing were summarized and their performances outlined.

Guidelines were given to use smoothing with the MUSIC algorithm and the MVDR beamformer. Spatial smoothing requires d averages of d sensor subarrays for the MUSIC DOA estimator to detect d correlated signals, while the modified spatial smoothing generally requires $\frac{d}{2}$ averages. The different nature of the problem that the MVDR beamformer attempts to solve was pointed out. In addition to the direction of arrivals, it estimates the power. Signal cancellation occurs as soon as there is some correlation between arrivals. The difficulty of decorrelating two closely spaced arrivals clearly appears in the simulations presented. Some substantial loss due to correlation may still occur even after heavy spatial smoothing.

Differences between the original spatial smoothing and the modified spatial smoothing were outlined. As observed in the simulations, the variations of the decorrelation rate achieved by modified spatial smoothing as a function of the electrical phase between two correlated arrivals, was explained analytically.

Smoothing reduces the effective aperture of the array, and therefore the resolution. In addition, it increases in a significant way the computational burden. Nevertheless, it is a necessary preprocessing step before using the high or super resolution techniques.

IV Processing Curved Wavefronts

The effects of wavefront curvature are studied in the context of vertical arrays using a geometric ray theory approach. Based on Snell's law, a way to generate curved wavefront is derived analytically. The importance of wavefront curvature first is evaluated by comparing the phase between curved wavefronts and plane wavefronts, both corresponding to the same arrival angles for a realistic scenario. The behaviour of the conventional, MVDR, and MUSIC beamformers using plane wavefront replica vectors then is studied in a curved wavefront environment. The largest mismatch loss occurs for near horizontal arrivals and the aperture length is not critical for this rather general result. Curved wavefront beamforming then is proposed and the behaviour of the processors is described in terms of bearing responses and beam patterns. The distortion caused by the smoothing transformation is studied in the context of high resolution methods. A method using the eigenvectors of the smoothed covariance matrix for each replica vector allows the loss due to mismatch to be avoided. Finally, the performance of the MVDR beamformer after spatial smoothing under correlated and curved arrivals is discussed.

IV.1 Introduction

The previous chapter began a realistic description of the oceanic environment. The importance of the ocean surface and bottom was noted and the effects of multipath propagation on the high resolution beamforming methods were studied.

Another important aspect of the underwater medium is its highly refractive character which is variable in the vertical as well as the horizontal. Propagation over long range is controlled by the sound velocity profile and its variations in range [Murphy1987]. The vertical directionality of the wavefield is a natural way to study the complex propagation mechanisms due to the environment, and vertical line arrays are major experimental tools used to measure ambient noise as well as long range propagation signals. At first with lengths of only a few hundred meters [Anderson1974, Anderson1979, Kewley1984, Dosso1987, Sen1988], array apertures have been increased in recent years to provide a better coverage of the water column and enable work at lower frequency [Sotirin1988]. In this framework, it is of interest to study the wavefront curvature due to refraction.

In ray theory, the variation of sound speed with depth causes ray bending and can be summarized by the Snell's law [Brekhovskikh1982] :

$$\frac{c}{\cos\theta} = constant \qquad (4.1.1)$$

where c is the local sound speed and θ the ray angle with respect to the horizontal. Ray bending can be large. A ray with angle with respect to the horizontal of 10^{o} at great depth with sound velocity of 1500 m/s has an angle with respect to the horizontal of 13.8^{o} shallower in the water column where the sound velocity is 1480 m/s. This is depicted on Figure III.1

Since ray bending is large, wavefront curvature is likely to have a large impact on the outputs of the beamforming structures. Processing a field with varying arrival angle across the array aperture is similar to the case of processing nonstationary random

processes in time series analysis. The selection of the plane wave array manifold that corresponds to a medium with a constant sound velocity, may not be appropriate, especially for a very long vertical line array.

Although the effects of index of refraction variations may be negligible for the conventional processor due to its lack of sensitivity or its robustness, there are some indications that they can be large for high resolution processors [Seglison1970, MacDonough1971].

IV.2 Generating Curved Wavefronts

IV.2.1 Derivation of the Phase Relationships in the Vertical

In order to understand the impact of curved wavefronts on the processing structures described in the previous chapters, a model of the wavefront curvature needs to be derived. The simple geometric approach of ray theory is selected. Since the sound velocity continuously varies with depth, the phase variations from a point M_o in space to a point M_1 can be expressed by the integral relationship

$$\phi = \int_{M_o}^{M_1} \vec{k}\, d\vec{r} \tag{4.2.1}$$

where ϕ is the phase of the propagating wavefront, $\vec{k}$ the wavenumber vector varying over space, and position in the two dimensional space sampled by the vertical array is defined by the coordinate system (r, z), with $\vec{r} = r\,\vec{e_r} + z\,\vec{e_z}$. $(\vec{e_r}, \vec{e_z})$ spans the space as defined by Figure IV.2. $\vec{k}$ can be expressed as

$$\vec{k}(r, z) = \frac{2\pi f}{c(r, z)}\left[\cos\theta(r, z)\ \vec{e_r} + \sin\theta(r, z)\ \vec{e_z}\right] \tag{4.2.2}$$

where (r, z) are the coordinates of the point in space where the observation is made, f is the acoustic frequency, $c(r, z)$ the sound velocity at the point (r, z) and $\theta(r, z)$ the ray angle with respect to the horizontal at (r, z).

The receiving array has its sensors numbered from top to bottom and negative angles of arrival corresponds to downgoing sound or uplooking beams.

In the context of vertical line arrays, one is interested in the phase variations due to the sound speed variations in the vertical so that

$$d\vec{r} = dz\ \vec{e_z} \tag{4.2.3}$$

and, assuming a stratified ocean (range independant), Equation (4.2.1) becomes

$$\phi = 2\pi f \int_{z_0}^{z_1} \frac{\sin\theta(z)}{c(z)} dz \tag{4.2.4}$$

Using the Snell's law, one gets

$$\phi = 2\pi f \int_{z_0}^{z_1} \frac{Sgn(\theta(z))}{c(z)} \left[1 - \cos^2\theta(z_0) \left[\frac{c(z)}{c(z_0)} \right]^2 \right]^{-1/2} dz \tag{4.2.5}$$

where Sgn is the signum function, and $\cos^2\theta(z_0)\left[\frac{c(z)}{c(z_0)}\right]^2 < 1$ is implicitely assumed for all z. If the medium is isovelocity, i.e. for all z $c(z) = c(z_0)$, Equation (4.2.5) reduces to the plane wavefront result :

$$\phi = \frac{2\pi f \sin\theta(z_0)}{c(z_0)} (z_1 - z_0) \tag{4.2.6}$$

Equation (4.2.5) provides the variation of phase in the vertical and is identical to a ray representation of the field. Following [Ahluwalia1977], the pressure field from ray theory is given by

$$p(r, z) = \exp(jk_0 S(r, z)) \sum_{m=0}^{\infty} (jk_0)^m A_m(r, z) \tag{4.2.7}$$

The summation term corresponds to the amplitude and $k_o S(r, z)$ gives the phase variations in space. k_0 is the reference wavenumber and $S(r, z)$ often is being called the eikonal [Brekhovskikh1982]. The amplitude and the eikonal are solutions of the Helmholtz equation. For horizontally stratified ocean, the $S(r, z)$ can be expressed as [Ahluwalia1977, pp 82-83]

$$S(r,z) = a\,r + \int_{z_0}^{z\,(>z_0)} \left[n^2 - a^2\right]^{1/2} dz \tag{4.2.8}$$

$$S(r,z) = a\,r + \int_{z\,(<z_0)}^{z_0} \left[n^2 - a^2\right]^{1/2} dz \tag{4.2.9}$$

where z_0 is the reference depth taken at the sound axis. n is the refraction index given by $n = \frac{c(z_0)}{c(z)} \leq 1$, and a is a constant equal to $n(z_0)\sin\alpha$ where α is the take-off angle in spherical polar coordinate (that is $\alpha = \frac{\pi}{2} - \theta$). Then Equation (4.2.9) is equivalent to Equation (4.2.5).

IV.2.2 Partial Insonification

The ability to generate a curved wavefront array manifold will allow us first to simulate a realistic field consisting of curved wavefronts, and second will constitute a set of replica vectors for use with the high resolution structures.

The final estimate of the angular spectrum greatly depends on the selected reference point, that is the depth to which the angular spectrum corresponds. In the following, the reference is chosen at the center of the array aperture. The results of Section IV.2.1 are used to compute the phase entering into the steering vectors stacked in the array manifold matrix. The array manifold matrix has complex columns that correspond to physical angles from -90^o to 90^o and lines that correspond to the different sensors of the array. The sensors are numbered from top to bottom. The i^{th} sensor or the i^{th} line in the matrix is associated with a sound velocity c_i. If $c_i > c_0$, where c_0 is the reference sound velocity (sound velocity at the center of the array), a ray with angle θ_0 with respect to the horizontal at the center may not propagate to the sensor depending on θ_0. The condition for physical existence of a ray at the i^{th} sensor is

$$\theta_0 \geq \cos^{-1}\frac{c_0}{c_i} \tag{4.2.10}$$

If Equation (4.2.10) is not verified, the ray has turned over, and the steering vector complex exponential is replaced by zero. Beyond the turning point, there is a shadow zone where the solution of the wave equation, under the WKB approximation, is exponentially decaying [Boyles1984, p 210]. Here, the model adopted assumes that there is no insonification past the turning point. Figure IV.3 shows the array manifold stacked steering matrix for a particular sound velocity profile with respect to a receiving line array.

IV.2.3 Phase Difference between Curved and Plane Wavefronts

The relative importance of wavefront curvature needs to be assessed. This can be done by comparing the phase of a curved wavefront to that of a plane wavefront, with the reference at the center of the array in both cases.

A simulation is performed on a 64 element array with 25 m spacing in the water column with a sound velocity of 1481 m/s at the top of the array. The sound velocity linearly increases across the array to 1515 m/s at the bottom of the array. The frequency is 20 Hz. The phase of the plane wavefronts is computed using Equation (4.2.6) with the sound velocity at the center of the array, 1498 m/s, as reference sound speed.

The differences of phase for each sensor position when insonified by arrival angles between -90^{o} and 90^{o} are overlaid on Figure IV.4. The phase change across the entire array for the endfire arrival is on the order of 66 radians. One therefore notes that the difference of phase varies as much as 10 % of this maximum phase. Figure IV.4 also indicates that only a few steering vectors yield a large phase difference between the curved and plane cases. The low angles actually are the only ones subject to these large deviations, and this effect still exists when the array aperture is reduced. A 16 sensor aperture from sensor number 24 to 40 will experience relatively important phase variations at low angles.

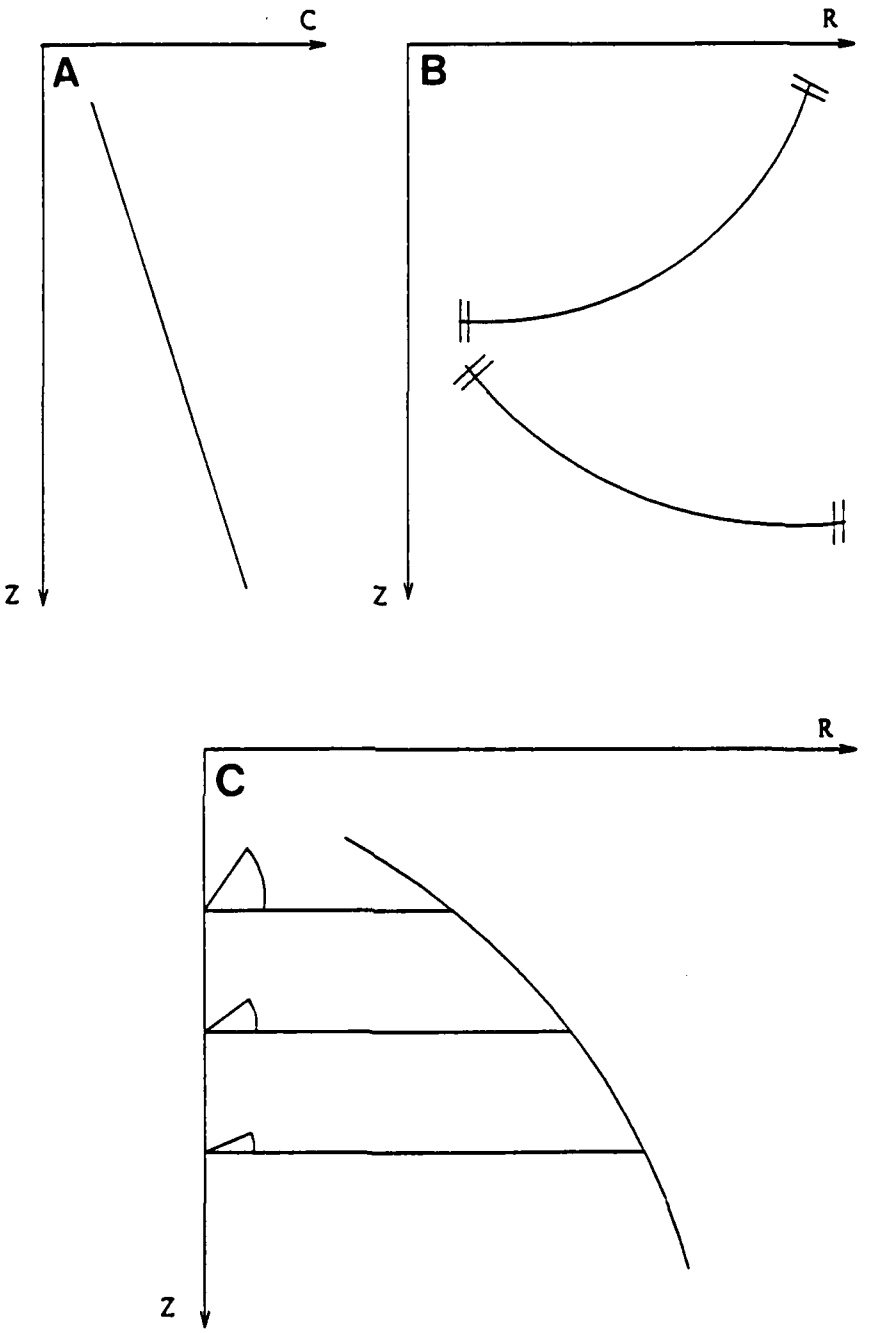

Figure IV.1: Effects of refraction on ray propagation. Panel A: sound velocity profile, Panel B: ray bending, Panel C: Variations of the arrival angle in the vertical and wave-front curvature.

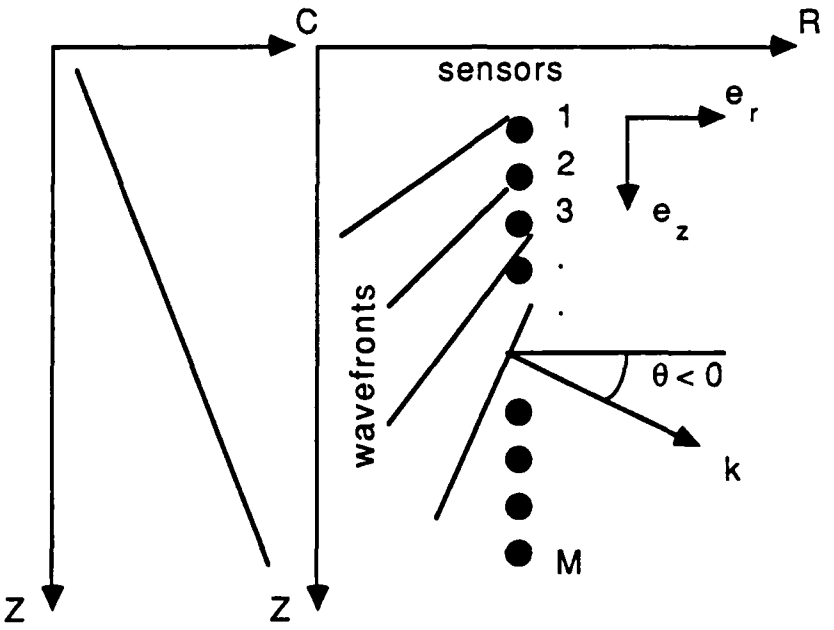

Figure IV.2: Geometry of the problem.

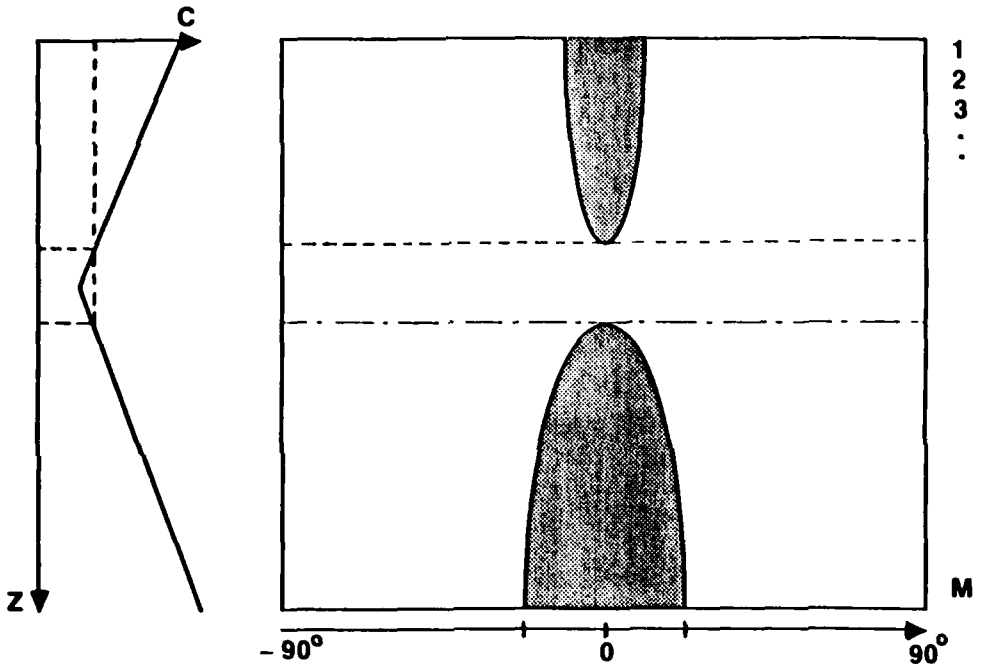

Figure IV.3: Array manifold stacked steering matrix for a particular sound velocity profile.

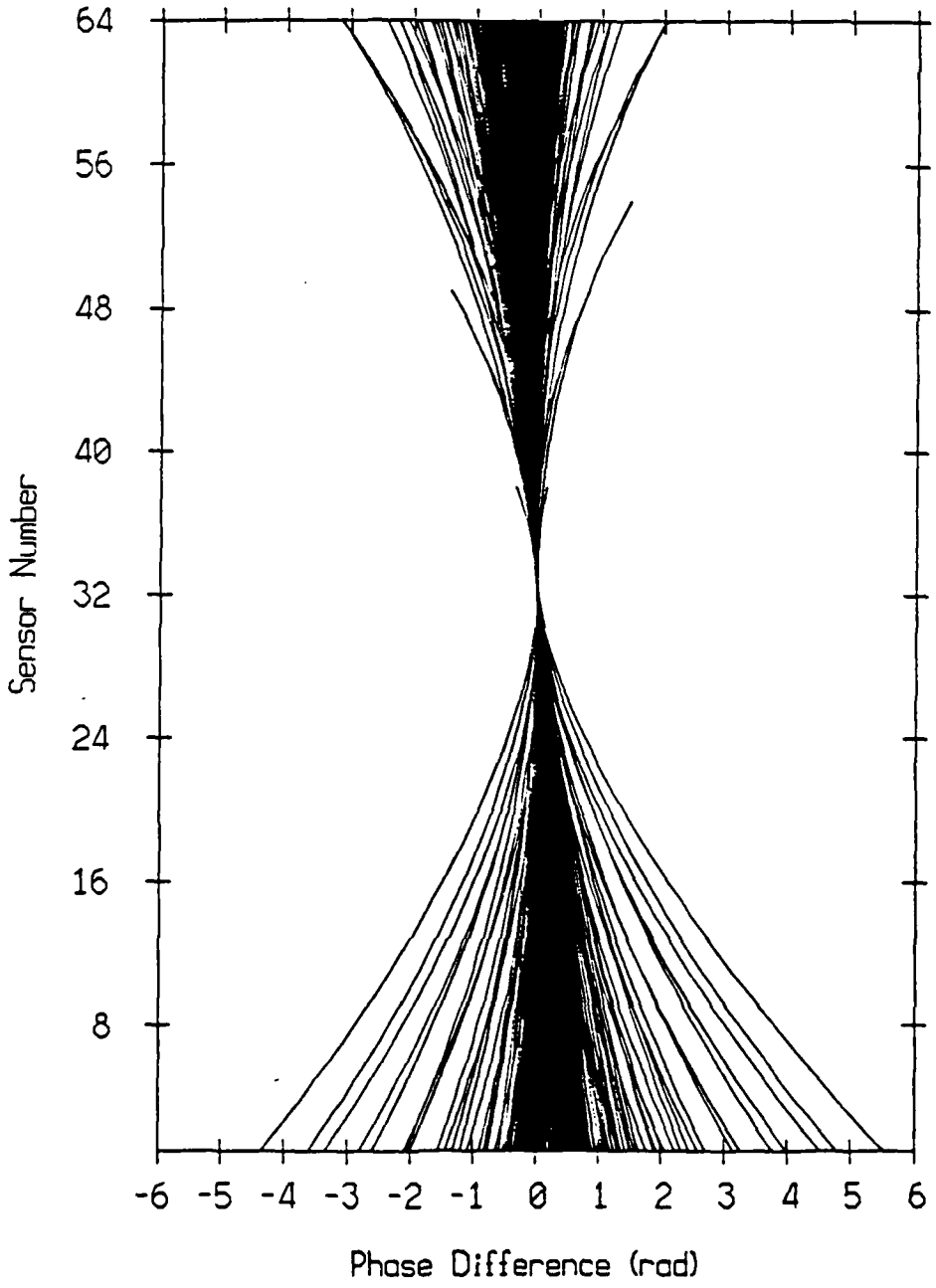

Figure IV.4: Overlaid plots of the phase difference between curved and plane wavefronts corresponding to angles with respect to the horizontal between $-90°$ and $90°$. The line array has 64 sensors (25 m interelement spacing) in a constant gradient sound velocity. The reference sound velocity at the center of the aperture is 1498 m/s.

IV.3 Plane Wave Beamformers in a Curved Wavefront Environment

IV.3.1 Performance of the Plane Wave Beamformers

The response of the beamformers to a curved wavefront field is of interest in order to assess the effects of the curvature on their performance.

The same 64 element array as in Section IV.2.4 is used in this simulation. The array operates at 20 Hz, and has a 25 m interelement spacing. The sound velocity has a constant gradient increasing from 1481 m/s at the top of the array to 1515 m/s at the bottom. The data at the input of the plane wave beamformer are curved wavefronts generated as discussed in the previous sections. A Kaiser-Bessel window with an α parameter of 1.5 weights the data across the array in order to yield a 38 dB side lobe rejection. Bearing responses for arrivals at $-40^\circ, -30^\circ, -20^\circ, -10^\circ, -5^\circ, -0.2^\circ, 0.2^\circ, 7^\circ, 10^\circ, 20^\circ$ $30^\circ, 40^\circ$ are plotted on Figure IV.5. These should be compared to the bearing responses for plane wavefront data which are plotted on Figure IV.6.

The bearing response of the conventional beamformer for curved data are similar to the one for plane data in case of high angles of arrival. Differences clearly appear for low angles of arrival since the peak indicating the curved arrival is smeared. The estimate suffers some loss for arrival angles between -10° and 10°, and some large angle bias for near horizontal arrivals (e.g. the 0.2° arrival yields a peak at 5° with a -3 dB loss). Furthermore the side lobe level is raised at least of 20 dB in the curved wavefront case with respect to the plane wave case.

As indicated in Chapter II, the MVDR beamformer has a high sensitivity to mismatch compared to the conventional processor [Seglison1970, McDonough1971]. The plane wave MVDR bearing responses are plotted on Figure IV.7 for curved data and on Figure IV.8 for plane data. With curved wavefront data, one notes that the MVDR processor suffers a considerable loss due to mismatch. In addition, the bearing response

for arrival angles between – 10° and 10° are smeared and biased in angle.

The bearing response results of the MUSIC algorithm are similar to those of the MVDR beamformer results as shown in Figure IV.9 (plane plane wave MUSIC processing curved wavefront data) and Figure IV.10 (plane wave MUSIC processing plane wavefront data).

In this particular case, one can conclude that the conventional beamformer somewhat suffers from an imperfect wavefront modeling. The deleterious effects occur where the curvature is the largest, that is for low angle arrivals. The effects of imperfect wavefront modeling are much larger for the MVDR and MUSIC algorithms. This loss due to mismatch cannot be afforded and curved wavefront replica vectors should be used.

IV.3.2 Influence of Aperture Length

The array discussed in Section IV.3.1 is 1575 m long (or approximately 21 wavelengths at 20 Hz) and the question of the dependence of curvature effects on aperture length can be raised. The same simulation is repeated for subarrays extracted from the 64 sensor array. These subarrays have same center as the large aperture array. The loss due to mismatch at the output of the conventional and the MVDR beamformers is plotted on Figure IV.11 for the different subarray lengths and for arrival angles between – 40° and 40°. The loss due to mismatch increases as the subarray length increases and as the arrival becomes close to the horizontal. While the curvature has only a mild effect on the output of the conventional processor, it has a strong effect on the MVDR results for any subarray length at low angles. Figure IV.11 clearly shows that curvature cannot be neglected even for fairly small apertures in the case of a high resolution beamformer.

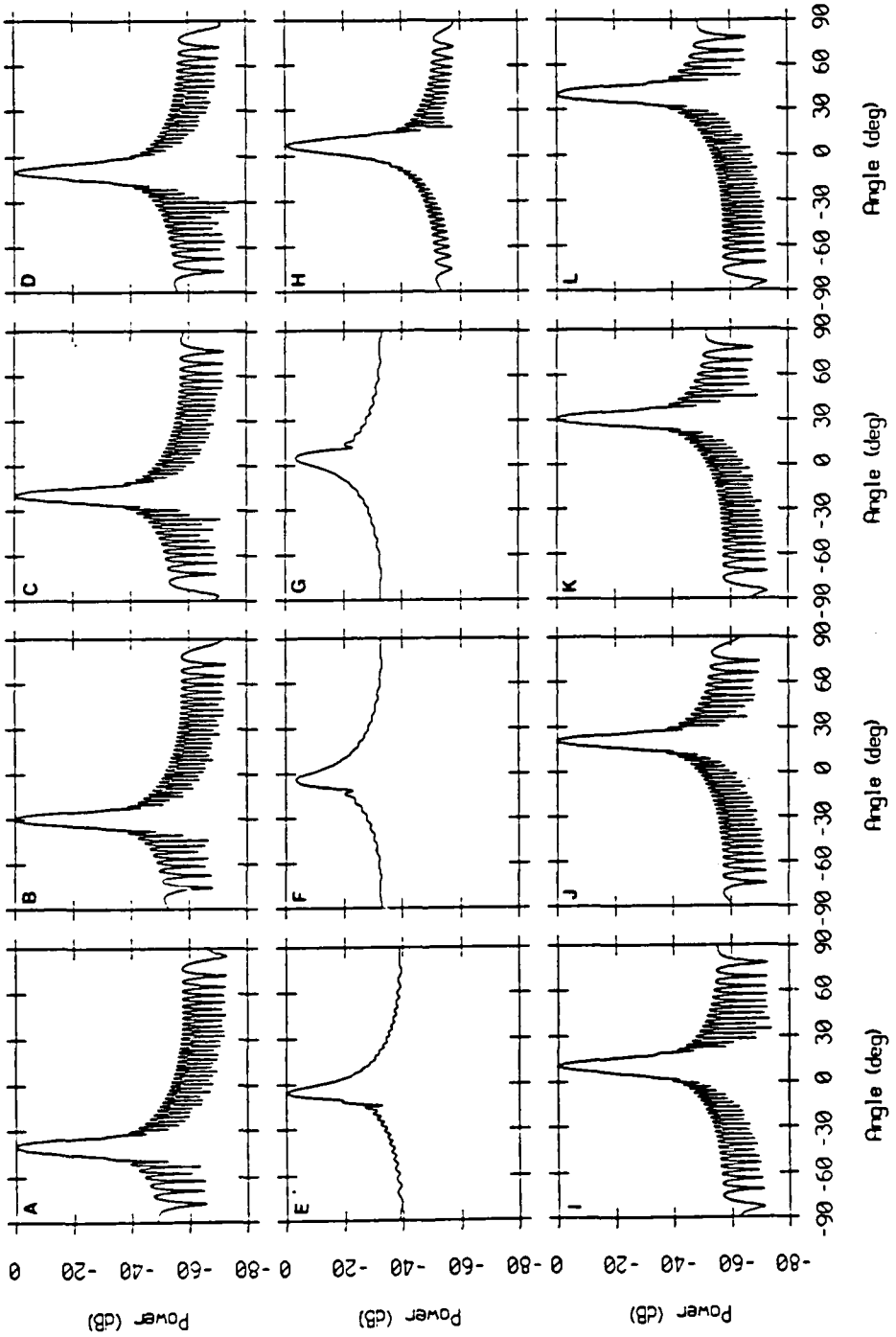

Figure IV.5: Bearing responses of the plane wave conventional processor with a Kaiser-Bessel Window with parameter $\alpha = 1.5$ in a curved wavefront field. Panels A, B, C, D, E, F, G, H, I, J, K, L correspond respectively to arrivals at $-40°$, $-30°$, $-20°$, $-10°$, $-5°$, $-0.2°$, $0.2°$, $7°$, $10°$, $20°$, $30°$, $40°$.

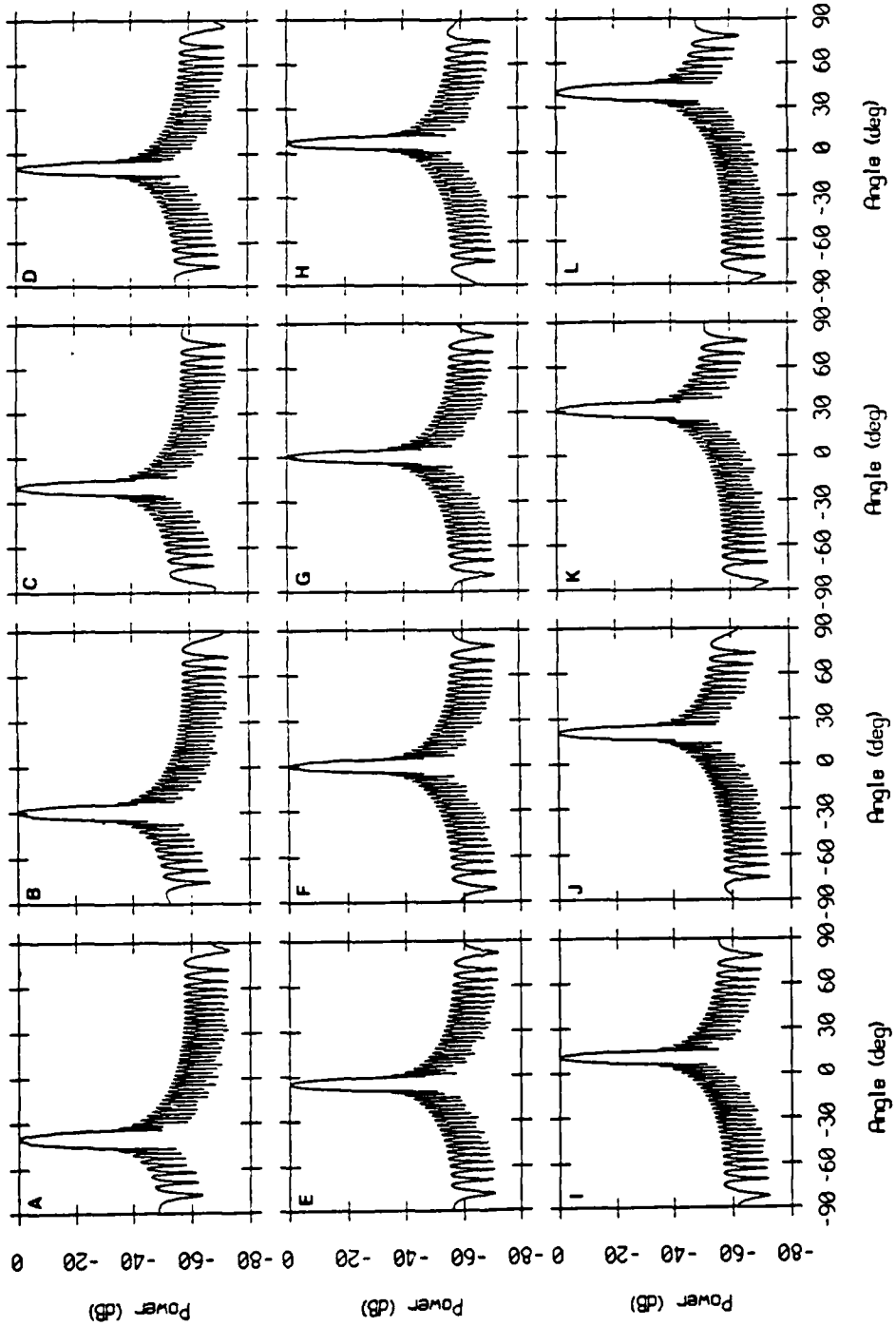

Figure IV.6: Bearing responses of the plane wave conventional processor with a Kaiser-Bessel Window with parameter $\alpha = 1.5$ in a plane wavefront field. Panels A, B, C, D, E, F, G, H, I, J, K, L correspond respectively to arrivals at $-40°, -30°, -20°, -10°, -5°, -0.2°, 0.2°, 7°, 10°, 20°, 30°, 40°$.

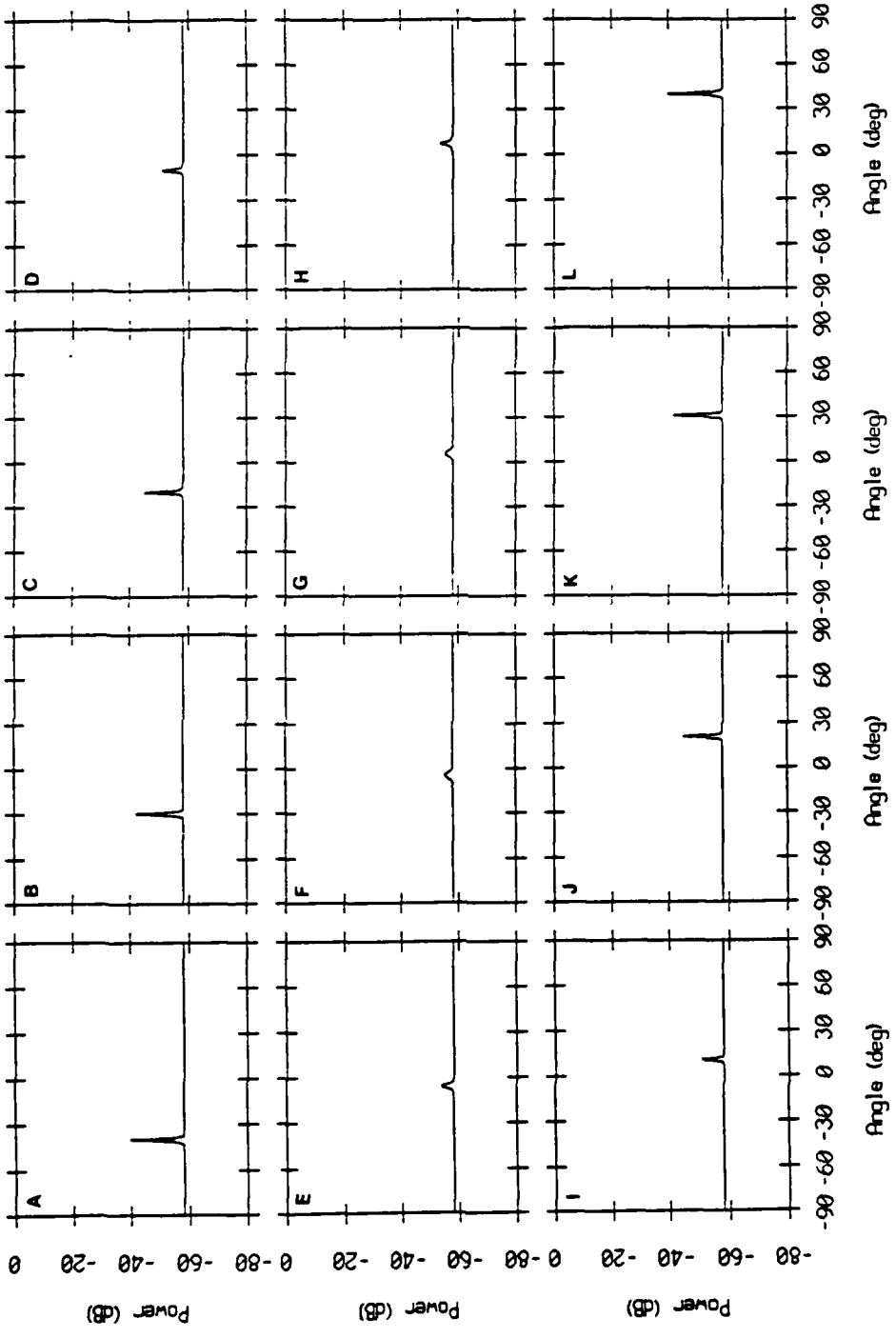

Figure IV.7: Bearing responses of the MVDR processor using plane wave replica vectors in a curved wavefront field. Panels A, B, C, D, E, F, G, H, I, J, K, L correspond respectively to arrivals at $-40°, -30°, -20°, -10°, -5°, -0.2°, 0.2°, 7°, 10°, 20°, 30°, 40°$.

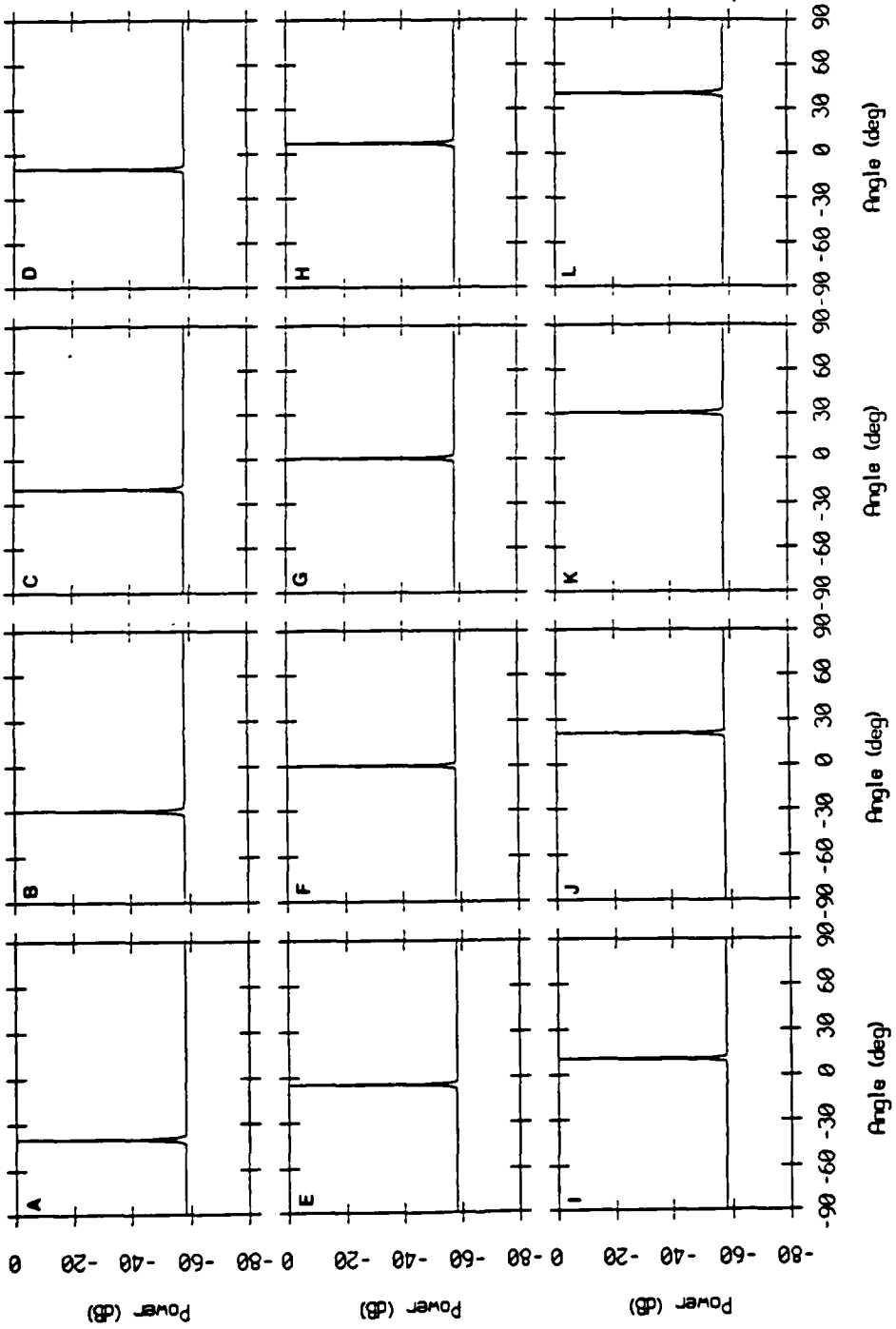

Figure IV.8: Bearing responses of the MVDR processor using plane wave replica vectors in a plane wavefront field. Panels A, B, C, D, E, F, G, H, I, J, K, L correspond respectively to arrivals at $-40°, -30°, -20°, -10°, -5°, -0.2°, 0.2°, 7°, 10°, 20°, 30°, 40°$.

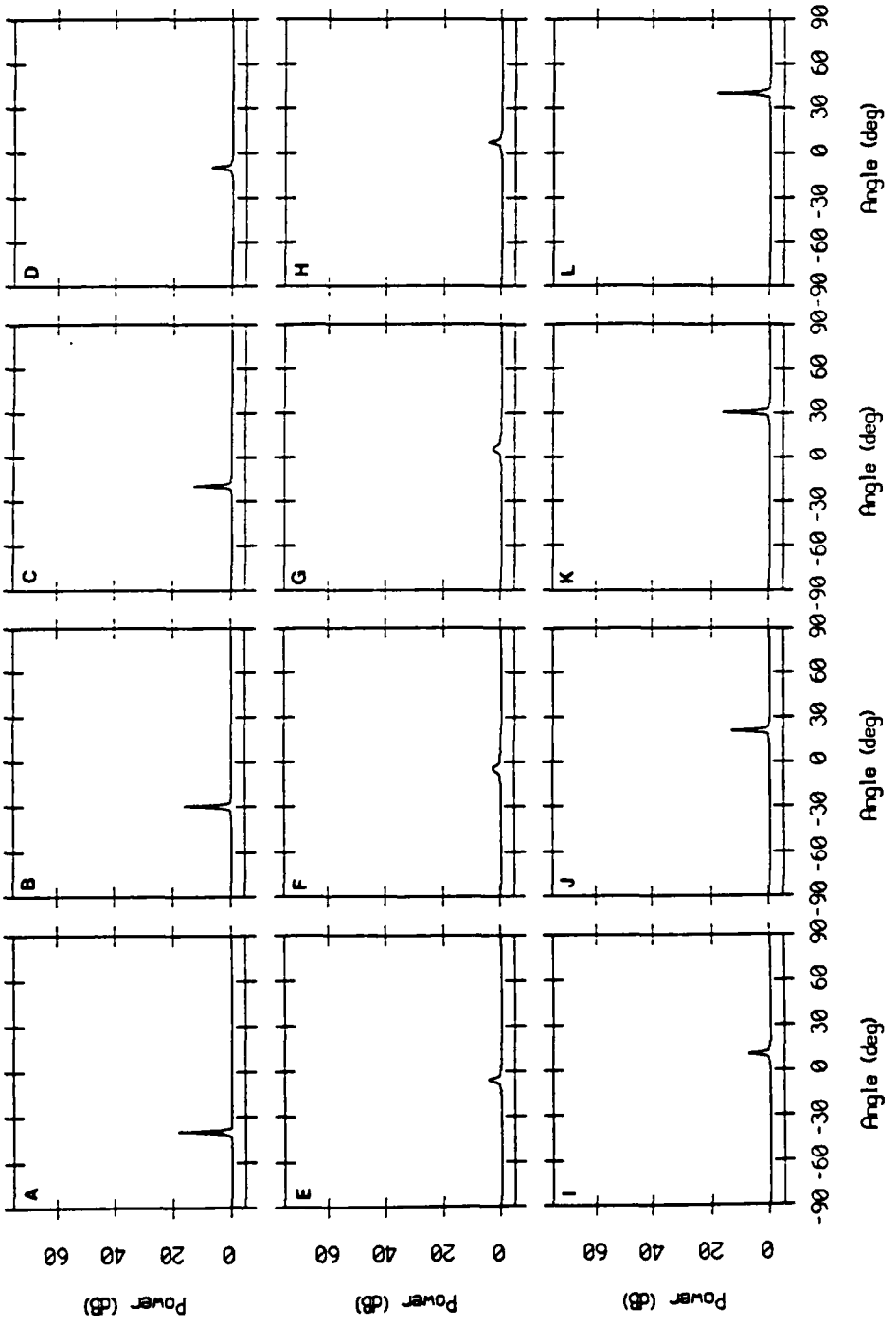

Figure IV.9: Bearing responses of the MUSIC processor using plane wave replica vectors in a curved wavefront field. Panels A, B, C, D, E, F, G, H, I, J, K, L correspond respectively to arrivals at $-40°, -30°, -20°, -10°, -5°, -0.2°, 0.2°, 7°, 10°, 20°, 30°, 40°$.

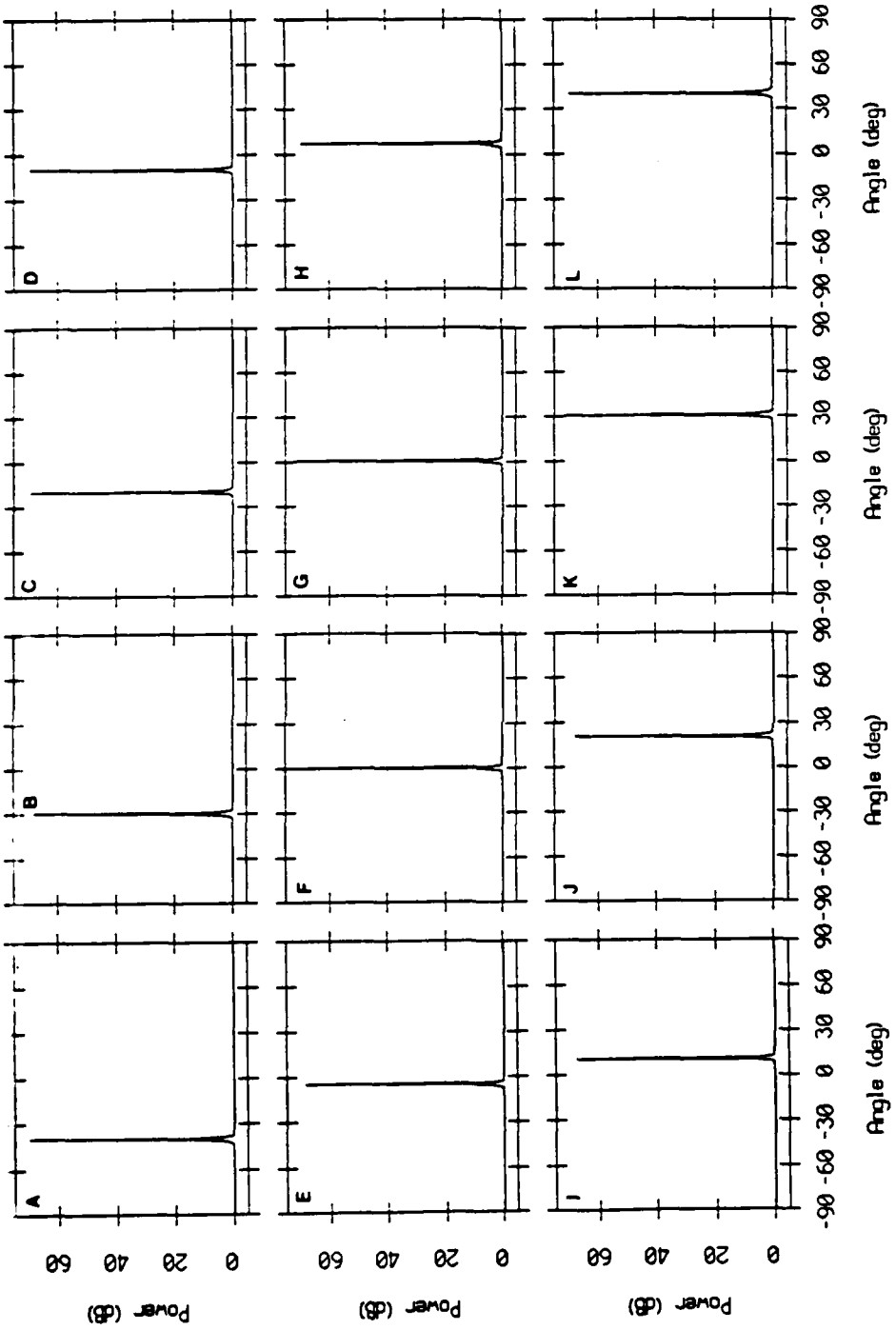

Figure IV.10: Bearing responses of the MUSIC processor using plane wave replica vectors in a plane wavefront field. Panels A, B, C, D, E, F, G, H, I, J, K, L correspond respectively to arrivals at $-40°, -30°, -20°, -10°, -5°, -0.2°, 0.2°, 7°, 10°, 20°, 30°, 40°$.

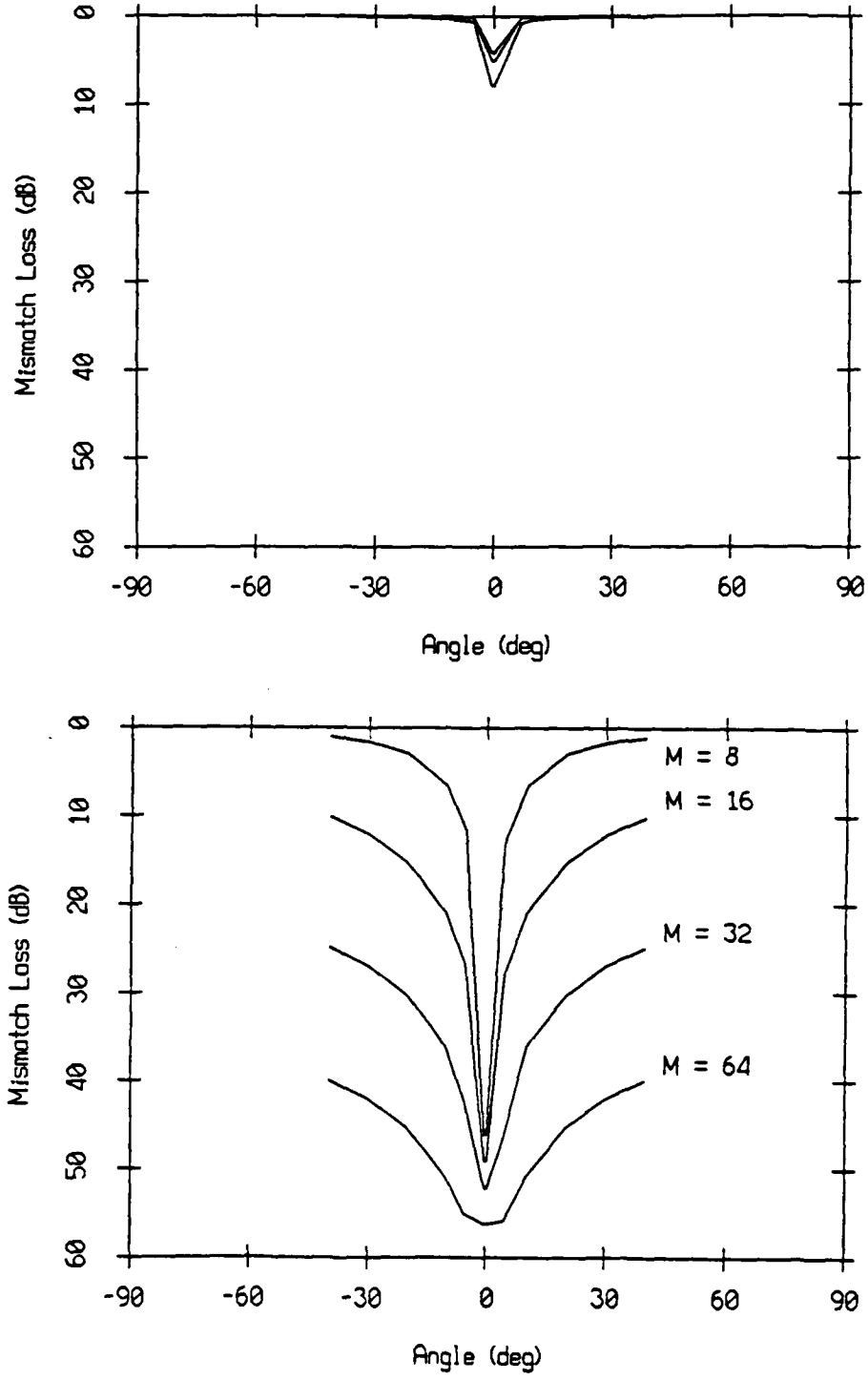

Figure IV.11: Loss due to mismatch for the conventional and MVDR beamformers using plane wave replica vectors under curved wavefront data for several array lengths (M is the number of sensors). Panel A: conventional processor, Panel B: MVDR processor.

IV.4 Curved Wavefront Beamforming

IV.4.1 Conventional Curved Wavefront Beamforming

In Chapter II, the beamforming operation was decomposed into two components, a processing structure and an array manifold. The results of the previous section indicate that the selection of the plane array manifold for an array in a curved wavefront environment is not appropriate, especially for high resolution methods and low angle of arrivals. Curved wavefront steering vectors should be used as replica vectors [Murphy87].

The Bartlett beamformer generally is used with a tapering window in order to provide good sidelobe rejection. The beampatterns of the untapered Bartlett beamformer steered to -40^o, -30^o, -20^o, -10^o, -5^o, -0.2^o, 0.2^o, 7^o, 10^o, 20^o, 30^o, and 40^o are plotted on Figure IV.11. The first sidelobes is around -15 dB, which is not acceptable. Windowing is necessary but not as simple as in the plane wave case, due to partial insonification of the array aperture. The window length has to be adjusted and applied to the insonified part of the array manifold stacked steering matrix. In Figure IV.13 are plotted the beam patterns when a Kaiser-Bessel window with an α parameter of 1.5 has been properly applied. The sidelobe rejection is equivalent to the plane wave case except at low angles where there is a large sidelobe around - 30 dB.

This high sidelobe indicates that the beamformer, steered in the 40^o direction, still receives energy from the near horizontal attenuated by 30 dB. This can be also observed in Figure IV.14 where bearing responses for the same angles are plotted. The side lobe floor is raised when the arrival angle approaches the horizontal. This sidelobe is due to the partial insonification of the aperture.

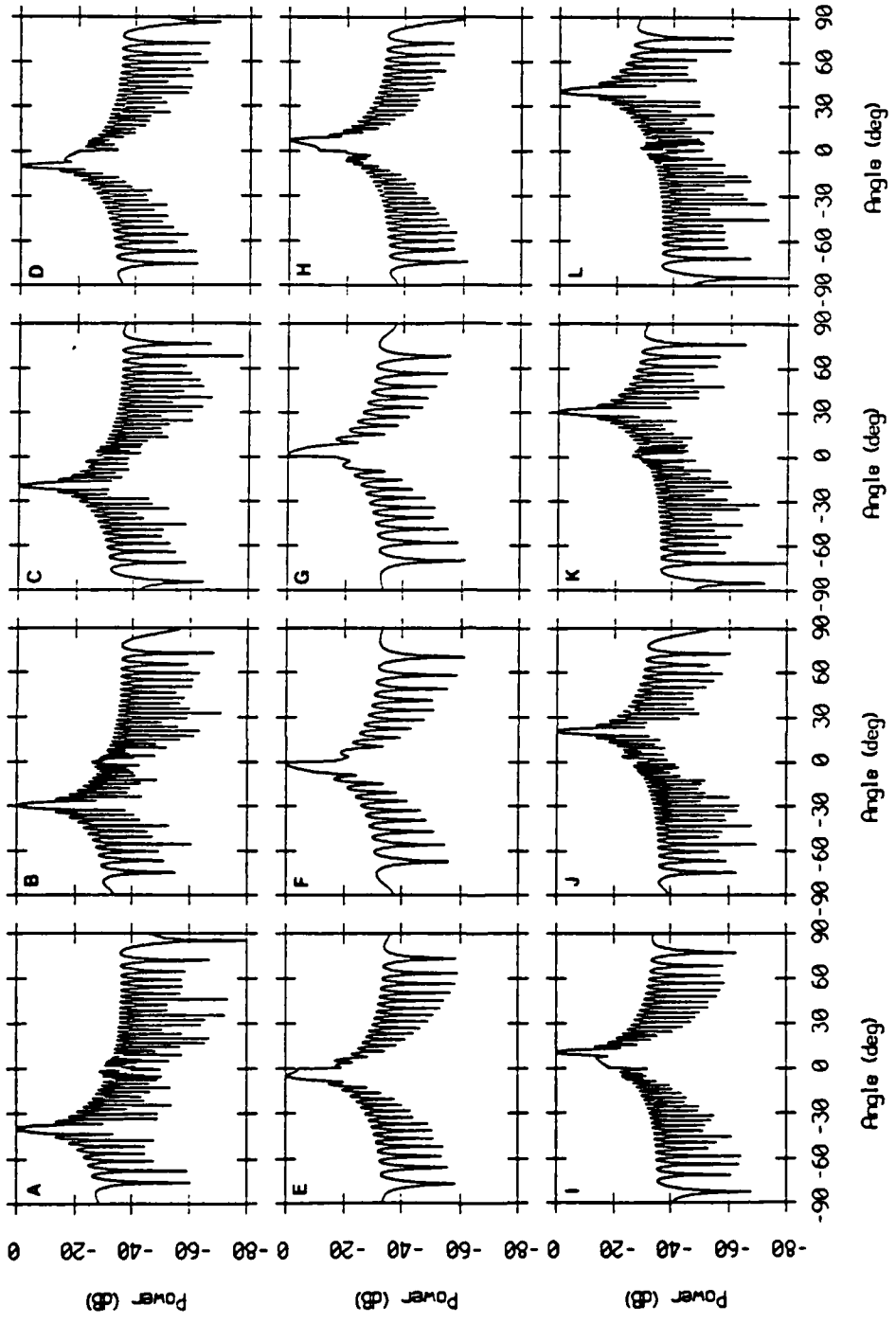

Figure IV.12: Beampatterns of the conventional beamformer using curved wavefront replica vectors under curved wavefront data. Panels A, B, C, D, E, F, G, H, I, J, K, L correspond to steering angles $\{-40°, -30°, -20°, -10°, -5°, -0.2°, 0.2°, 7°, 10°, 20°, 30°, 40°\}$.

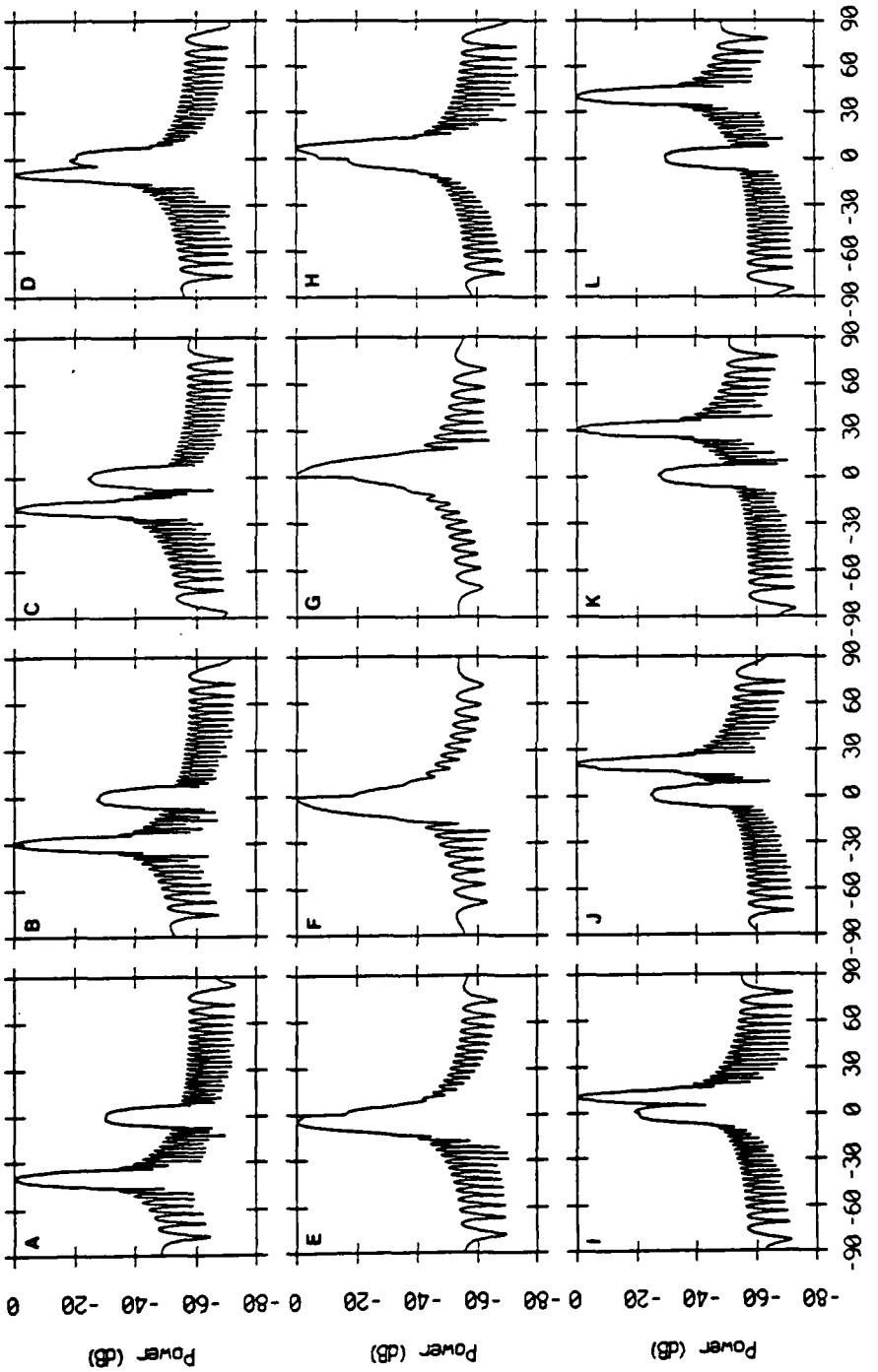

Figure IV.13: Beampatterns of the conventional beamformer using curved wavefront replica vectors with a Kaiser-Bessel window with $\alpha = 1.5$ under curved wavefront data. Panels A, B, C, D, E, F, G, H, I, J, K, L correspond to steering angles $\{-40°, -30°, -20°, -10°, -5°, -0.2°, 0.2°, 7°, 10°, 20°, 30°, 40°\}$.

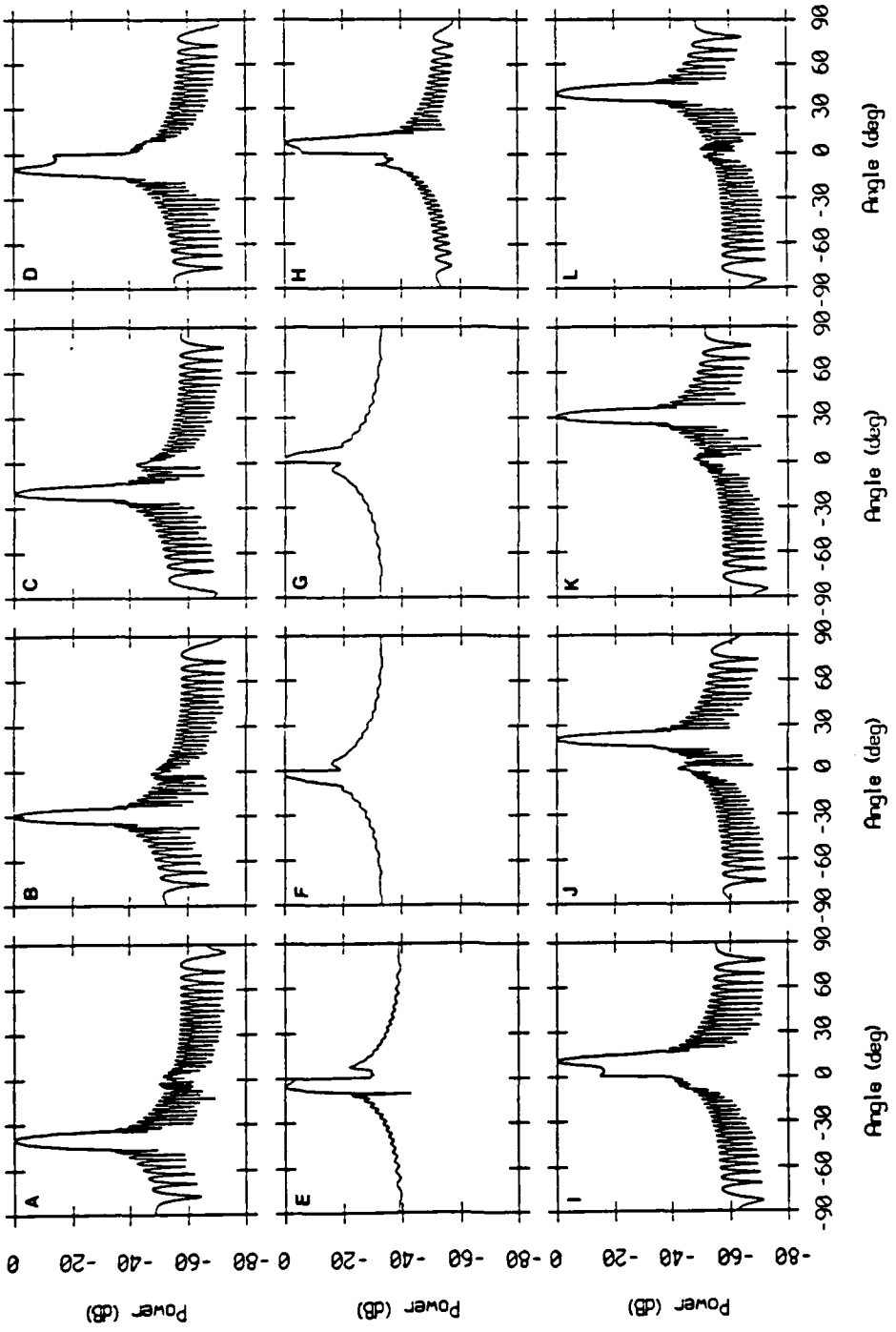

Figure IV.14: Bearing responses of the conventional beamformer using curved wavefront replica vectors with a Kaiser-Bessel window with $\alpha = 1.5$ under curved wavefront data. Panels A, B, C, D, E, F, G, H, I, J, K, L correspond to arrivals $\{-40°, -30°, -20°, -10°, -5°, -0.2°, 0.2°, 7°, 10°, 20°, 30°, 40°\}$.

IV.4.2 High Resolution Curved Wavefront Beamforming

IV.4.2.1 Effects of Curvature on the Array Covariance Matrix

To understand why the plane wave, high resolution beamformers do so poorly under curved wavefront data, the effects of curvature on the array covariance matrix are now investigated. Uncorrelated plane wavefront arrivals impinging on a line array with equispaced sensors lead to a Toeplitz Hermitian covariance matrix. When the arrivals have curved wavefronts, the corresponding phase variations from sensor to sensor are not constant as they are for plane waves. If $\mathbf{A}$ is a model signal direction matrix expressed as

$$\mathbf{A}^T = \left[e^{j\phi_1} e^{j\phi_2} \cdots e^{j\phi_M} \right] \tag{4.5.1}$$

its contribution to the array model covariance matrix, $\mathbf{A}\,\mathbf{A}^H$, is a matrix with first upper diagonal given by

$$\left[e^{j(\phi_1 - \phi_2)} e^{j(\phi_2 - \phi_3)} \cdots e^{j(\phi_{M-1} - \phi_M)} \right] \tag{4.5.2}$$

and because of curvature, one has for $i \neq j$

$$\phi_i - \phi_{i+1} \neq \phi_j - \phi_{j+1} \tag{4.5.3}$$

so that $\mathbf{A}\,\mathbf{A}^H$ is not Toeplitz and the model covariance matrix is not as well.

Figure IV.15 and Figure IV.16 illustrate the non-Toeplitz character of the covariance matrix in the case of a single arrival with a -10° angle with respect to the horizontal, and an uncorrelated arrival pair with -20° and -10° arrival angles. The scenario is the same as before with a 32 element array extracted from the large 64 sensor array of Section IV.2.4 and centered at the same depth. Curvature makes Figure IV.16 look significantly different from Figure III.3, its plane wave counterpart.

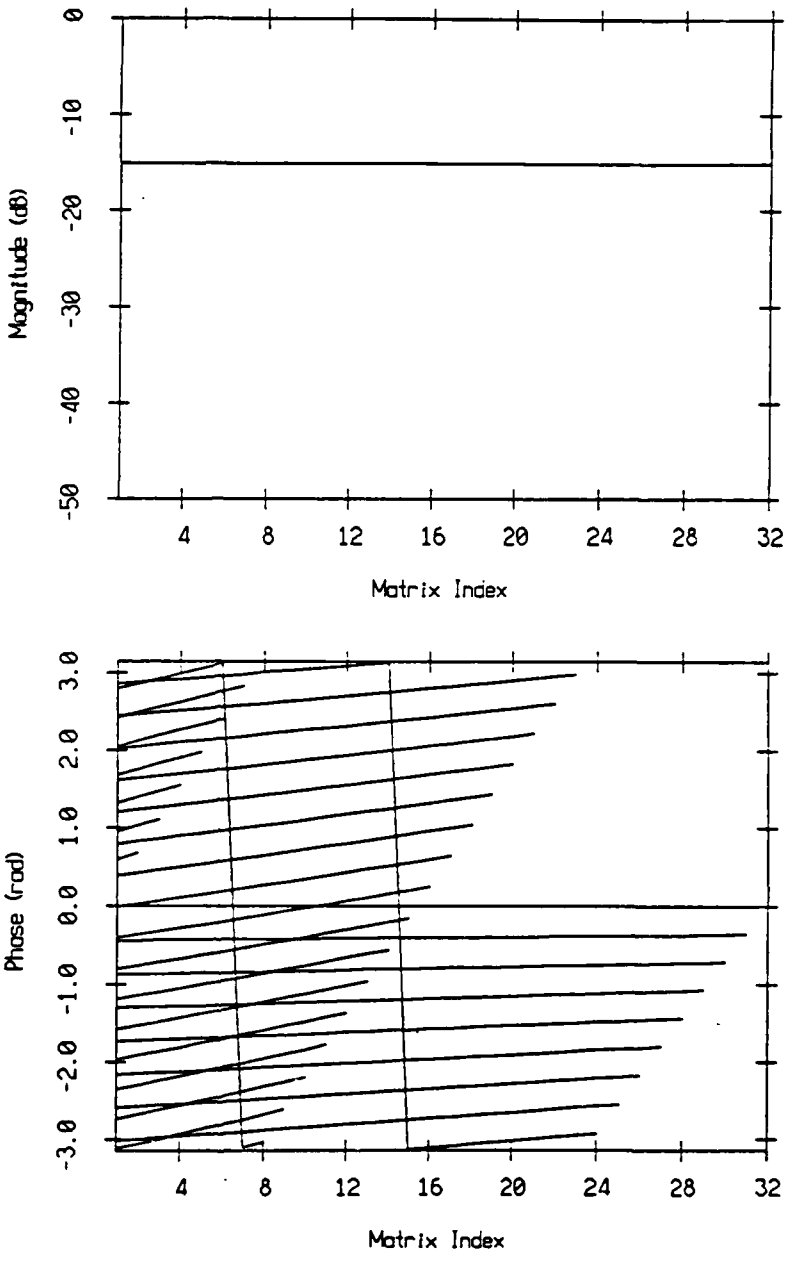

Figure IV.15: Upper diagonals of the 32 sensor array covariance matrix of a unit power curved wavefront arrival with -10° arrival angle. Matrix index corresponds to index on the diagonal. Each diagonal can be identified by its length.

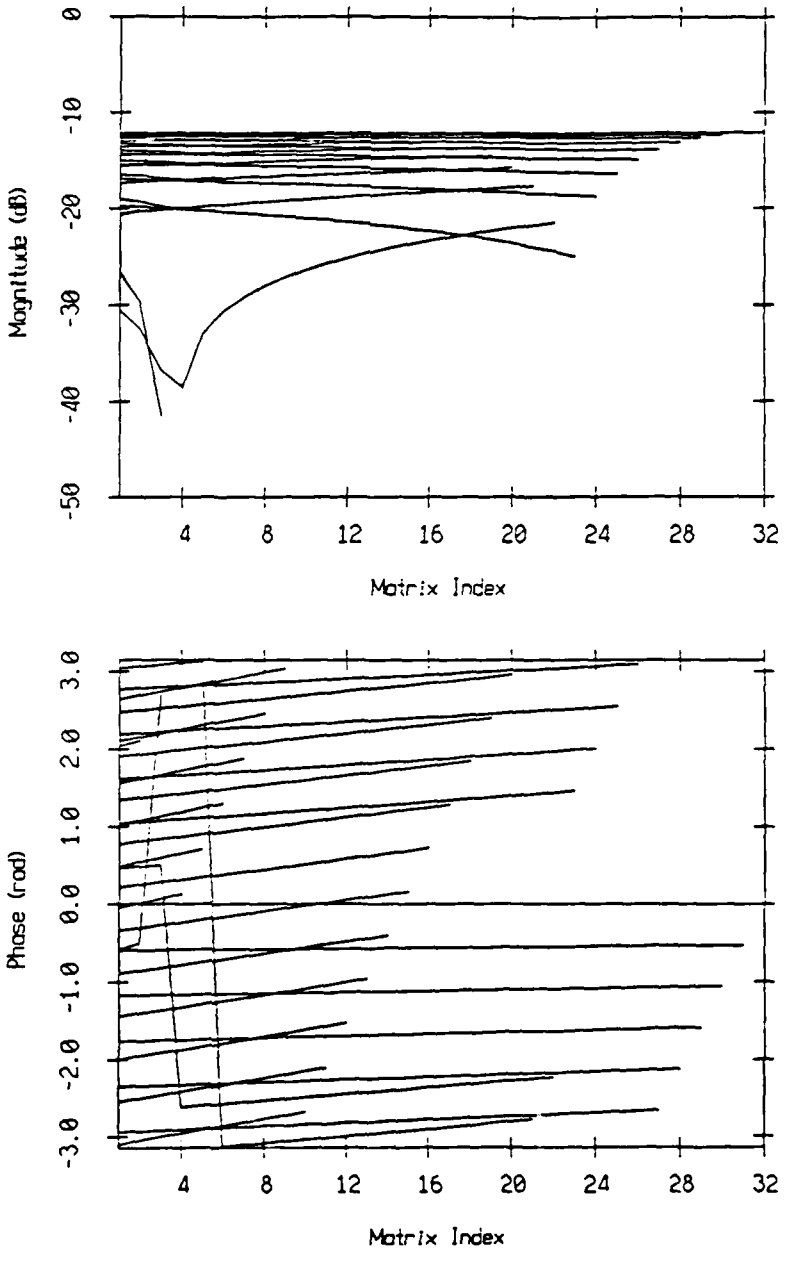

Figure IV.16: Upper diagonals of the 32 sensor array covariance matrix of two unit power uncorrelated curved wavefront arrivals with -20° and - 10° arrival angles. Each diagonal can be identified by its length.

IV.4.2.2 Curvature and Spatial Smoothing

Under correlated arrivals, the high resolution methods fail unless spatial or modified spatial smoothing is performed. It was shown in Chapter III that these preprocessing techniques specifically are designed for equispaced sensor arrays in a plane wavefront field. They use the special underlying structure of the covariance matrix: a Toeplitz structure.

In a curved wavefront environment, the direct application of these preprocessing schemes creates a twofold problem. One is the distortion introduced by the smoothing procedure, the underlying structure of the covariance is not Toeplitz and depends on the arrivals which are unknown a priori. The other is related to the actual decorrelation rate achieved by the smoothing procedure, thus directly influencing the performance of the high resolution beamformers.

IV.4.2.3 Limiting the Distortion Effects due to Smoothing

The study of distortion created by smoothing the original covariance matrix is based on the bearing response of the MVDR beamformer and the MUSIC processor for arrival angles at $\{ -40^o, -30^o, -20^o, -10^o, -5^o, -0.2^o, 0.2^o, 7^o, 10^o, 20^o, 30^o, 40^o \}$. The simulation is done under the same conditions as Section IV.3.1 with a smaller aperture of 32 sensors extracted from the large 64 sensor array with the same center.

After smoothing with a subarray length of s sensors, a natural choice for the set of replica vectors is the curved wavefront array manifold that corresponds to a s sensor array extracted from the large aperture with same center. The bearing responses of the MVDR beamformer after spatial smoothing with subarray lengths of 24 and 16 respectively, are plotted on Figure IV.17 and Figure IV.18. The bearing responses of the MUSIC algorithm for smoothing subsegment length of 24 and 16 respectively, are plotted on Figure IV.19 and Figure IV.20. One notes the loss due to mismatch for arrivals at low angle.

This loss is due to mismatch between the curved wavefront replica vector and the equivalent array signal vector after spatial smoothing. It is the result of the distortion due to smoothing. For each bearing characterized by a signal direction vector $\mathbf{A}$ and the corresponding covariance matrix $\mathbf{A}\,\mathbf{A}^H$, this mismatch loss can be minimized by choosing the replica vector $\mathbf{E}$ that maximizes the power at the output of the conventional processor

$$\mathbf{E}^H \left\{ T(\mathbf{A}\,\mathbf{A}^H) \right\} \mathbf{E} \tag{4.2.4}$$

where T denotes the transformation performed by smoothing on the covariance matrix. The best replica vector is given by the eigenvector of $T(\mathbf{A}\,\mathbf{A}^H)$ that has the largest eigenvalue. This replica vector will be referred to as the eigen steering vector. Because the distortion effects associated with the smoothing transformation are relatively small, the smoothed matrix is of rank 1 for all practical purposes. An eigenvalue/eigenvector decomposition of the smoothed version of the (32, 32) covariance matrix for both subarray lengths was performed for 256 steering vectors spanning the grazing angles from -90° to 90°. The eigenvalues are overlaid on Figure IV.21 for the subsegment lengths of 24 and 16 respectively. There is a single large eigenvalue of value one, the others decrease to the normalized fraction of noise used to stabilized the matrix.

Figure IV.22 and Figure IV.23 give the bearing responses for the MVDR beamformer after spatial smoothing with subsegment length of 24 and 16 using the eigen steering vectors. Figure IV.24 and Figure IV.25 give the bearing responses for the MUSIC algorithm after spatial smoothing with subsegment lengths equal to 24 and 16, using the eigen steering vectors. Loss due to mismatch is reduced to negligible values. Nevertheless, the use of the eigen steering vector cannot reduce the - 25 dB side lobe level at near horizontal angle in the case of the MVDR beamformer after smoothing with a subsegment length of 16.

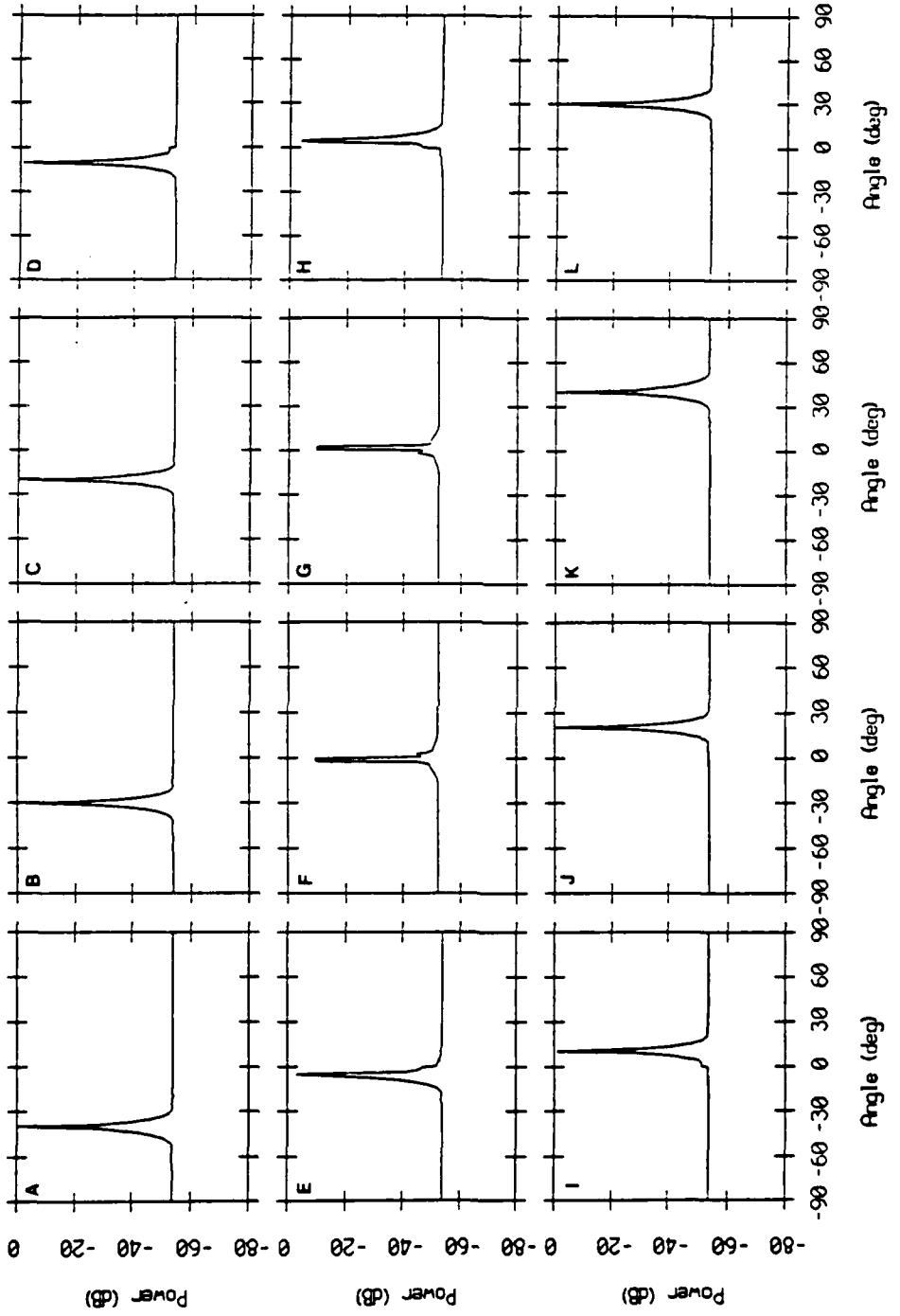

Figure IV.17: Bearing responses of the MVDR beamformer on a 32 element array after spatial smoothing with a subsegment length of 24 with curved wavefront replica vectors. The data are curved. Panels A, B, C, D, E, F, G, H, I, J, K, L correspond to arrivals $\{-40°, -30°, -20°, -10°, -5°, -0.2°, 0.2°, 7°, 10°, 20°, 30°, 40°\}$.

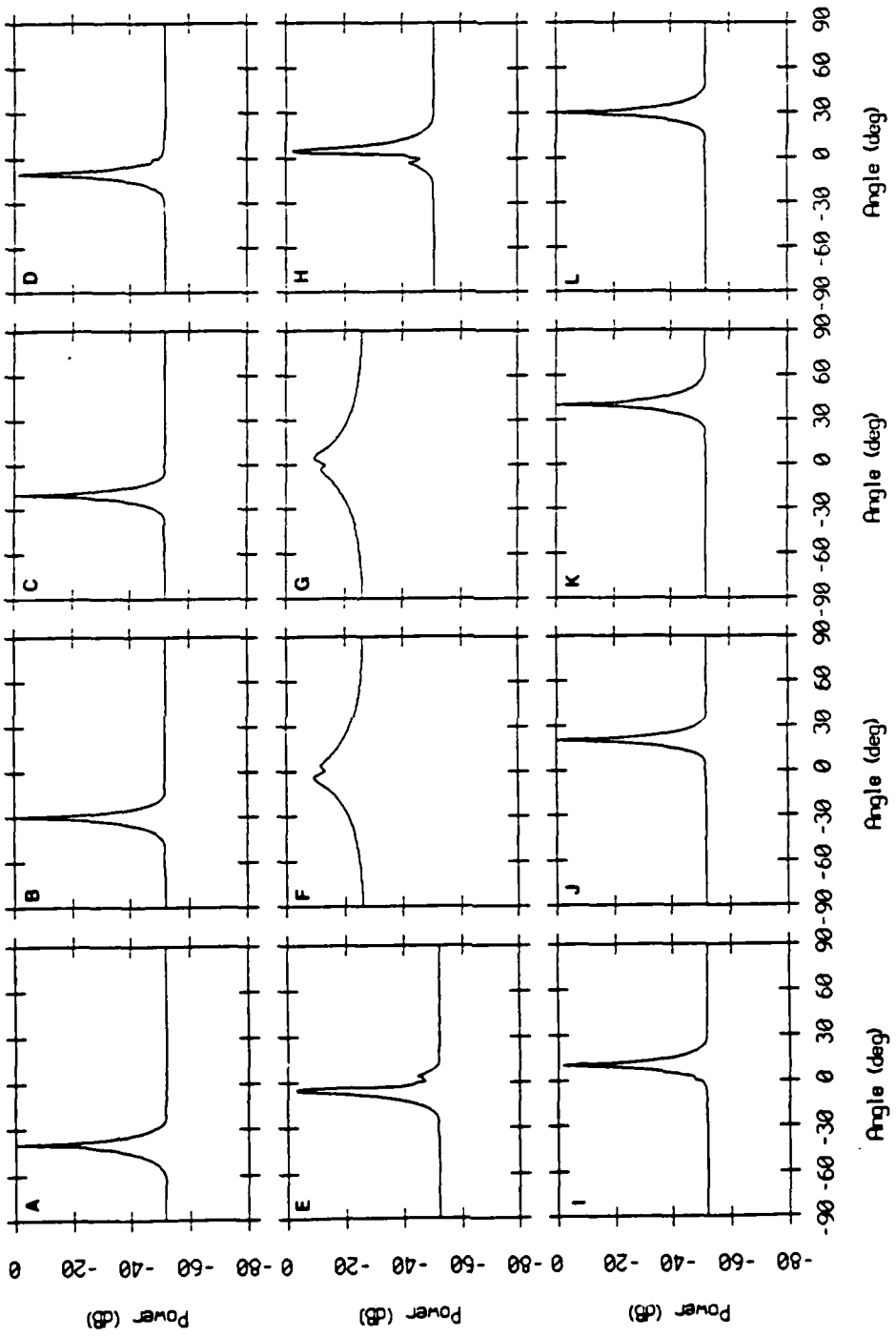

Figure IV.18: Bearing responses of the MVDR beamformer on a 32 element array after spatial smoothing with a subsegment length of 16 with curved wavefront replica vectors. The data are curved. Panels A, B, C, D, E, F, G, H, I, J, K, L correspond to arrivals $\{-40°, -30°, -20°, -10°, -5°, -0.2°, 0.2°, 7°, 10°, 20°, 30°, 40°\}$.

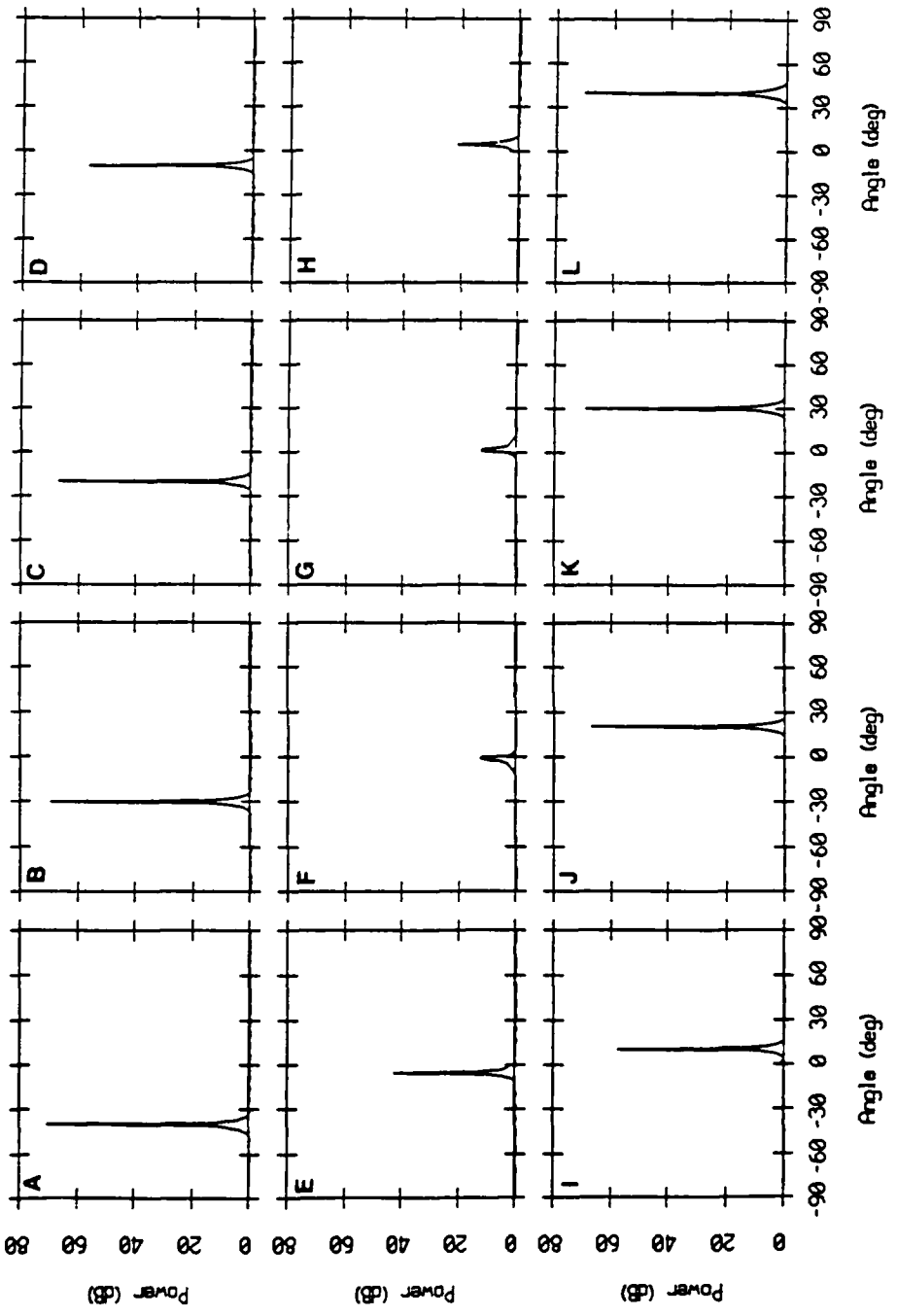

Figure IV.19: Bearing responses of the MUSIC beamformer on a 32 element array after spatial smoothing with a subsegment length of 24 with curved wavefront replica vectors. The data are curved. Panels A, B, C, D, E, F, G, H, I, J, K, L correspond to arrivals $(-40°, -30°, -20°, -10°, -5°, -0.2°, 0.2°, 7°, 10°, 20°, 30°, 40°)$.

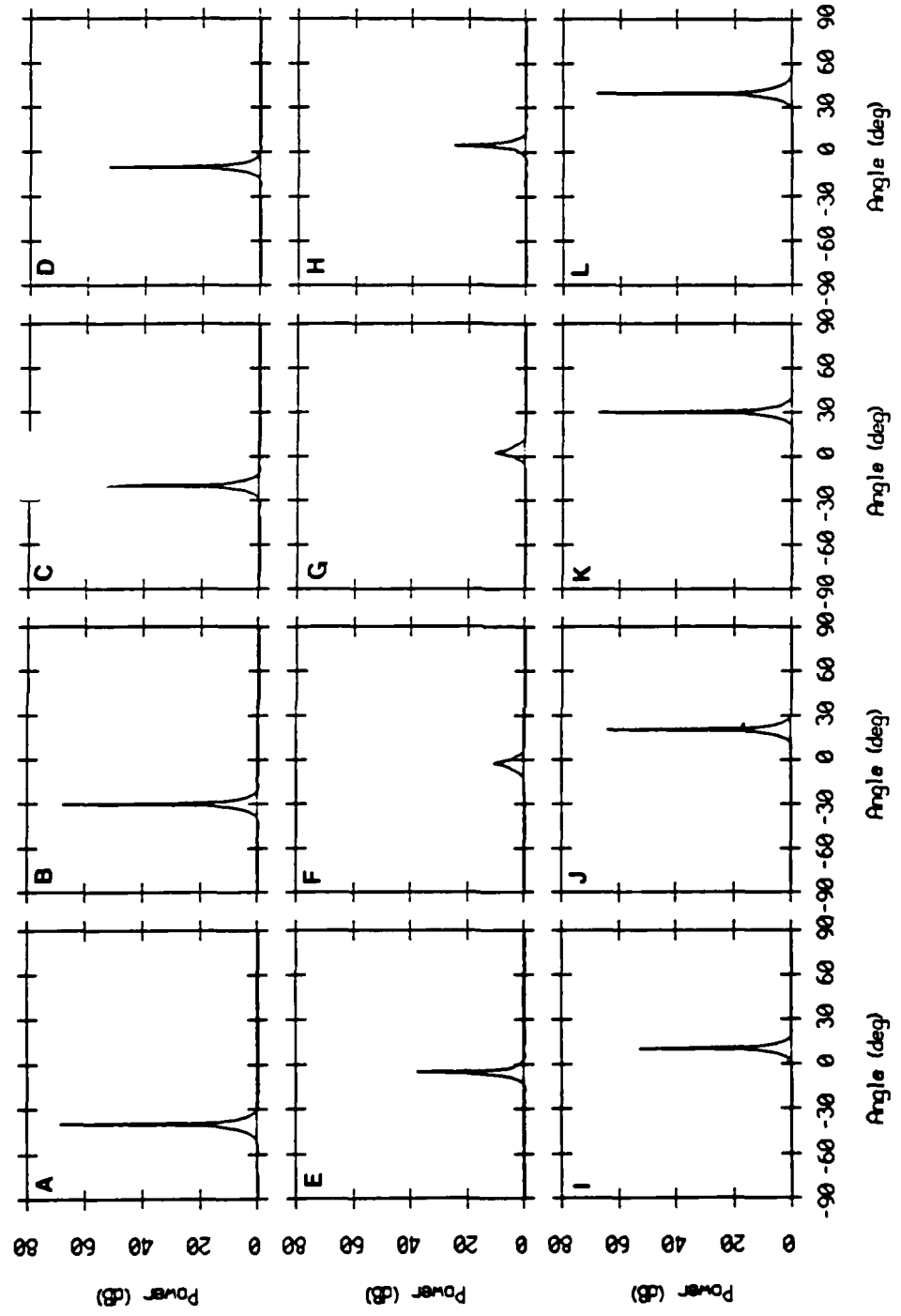

Figure IV.20: Bearing responses of the MUSIC beamformer on a 32 element array after spatial smoothing with a subsegment length of 16 with curved wavefront replica vectors. The data are curved. Panels A, B, C, D, E, F, G, H, I, J, K, L correspond to arrivals $\{-40°, -30°, -20°, -10°, -5°, -0.2°, 0.2°, 7°, 10°, 20°, 30°, 40°\}$.

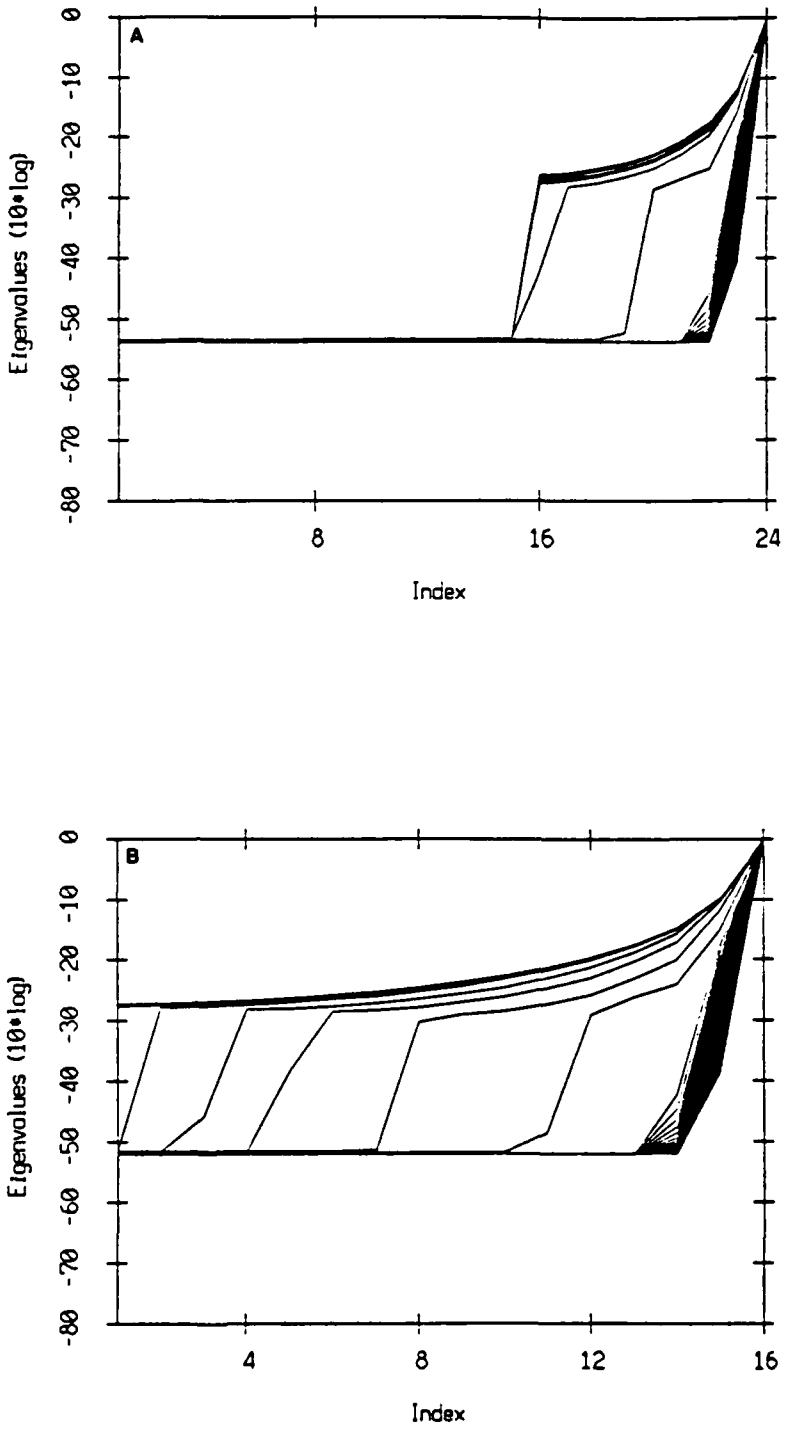

Figure IV.21: Overlaid eigenvalues of the spatially smoothed covariance matrix for all 256 curved wavefront steering vectors corresponding to arrival angles between -90° and 90°. Panel A correponds to a subarray length of 24, while Panel B to a length of 16.

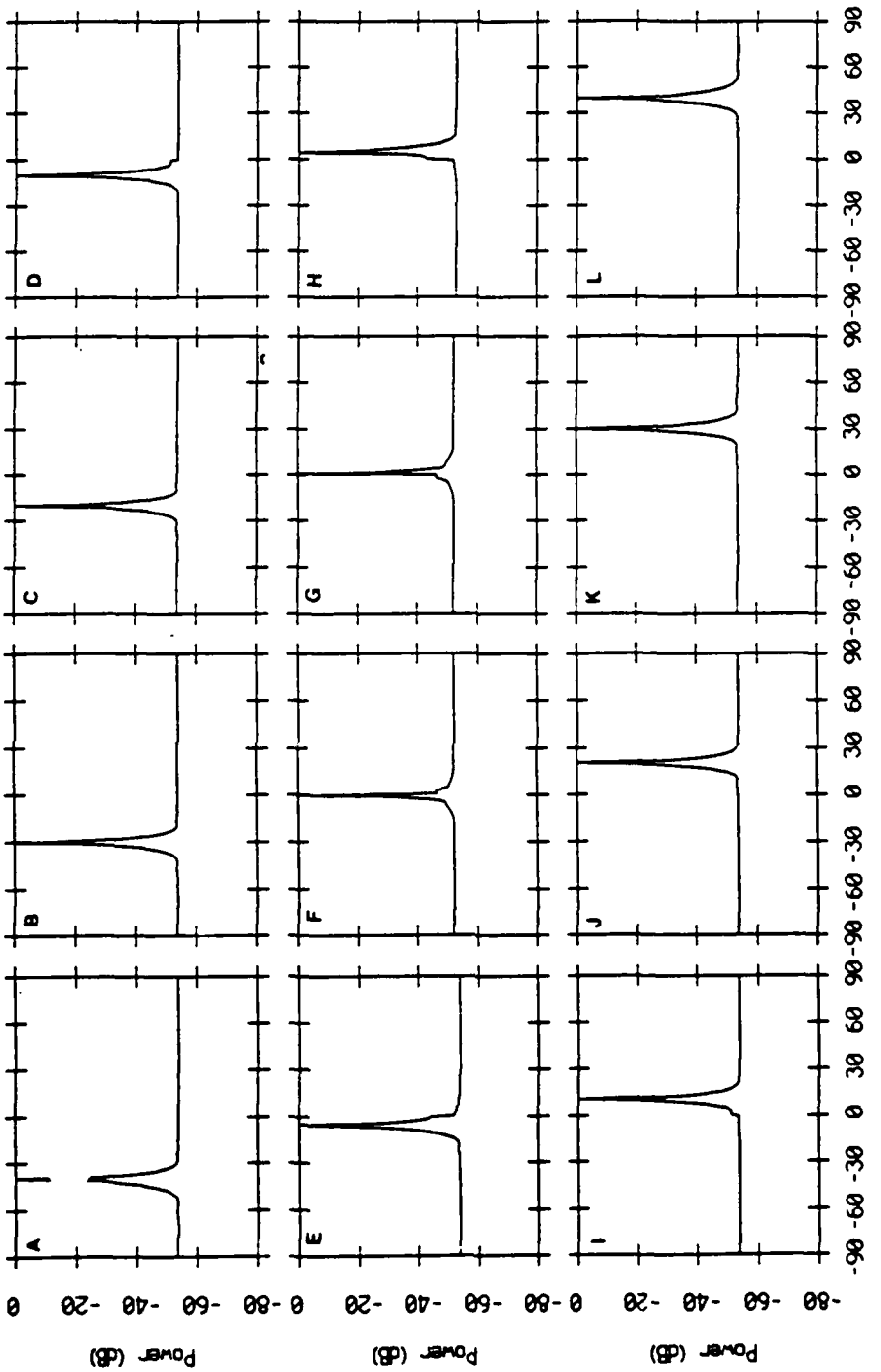

Figure IV.22: Bearing responses of the MVDR beamformer after spatial smoothing with 24 sensor subarrays using the eigensteering vectors. Panels A, B, C, D, E, F, G, H, I, J, K, L correspond to arrivals $\{-40°, -30°, -20°, -10°, -5°, -0.2°, 0.2°, 7°, 10°, 20°, 30°, 40°\}$.

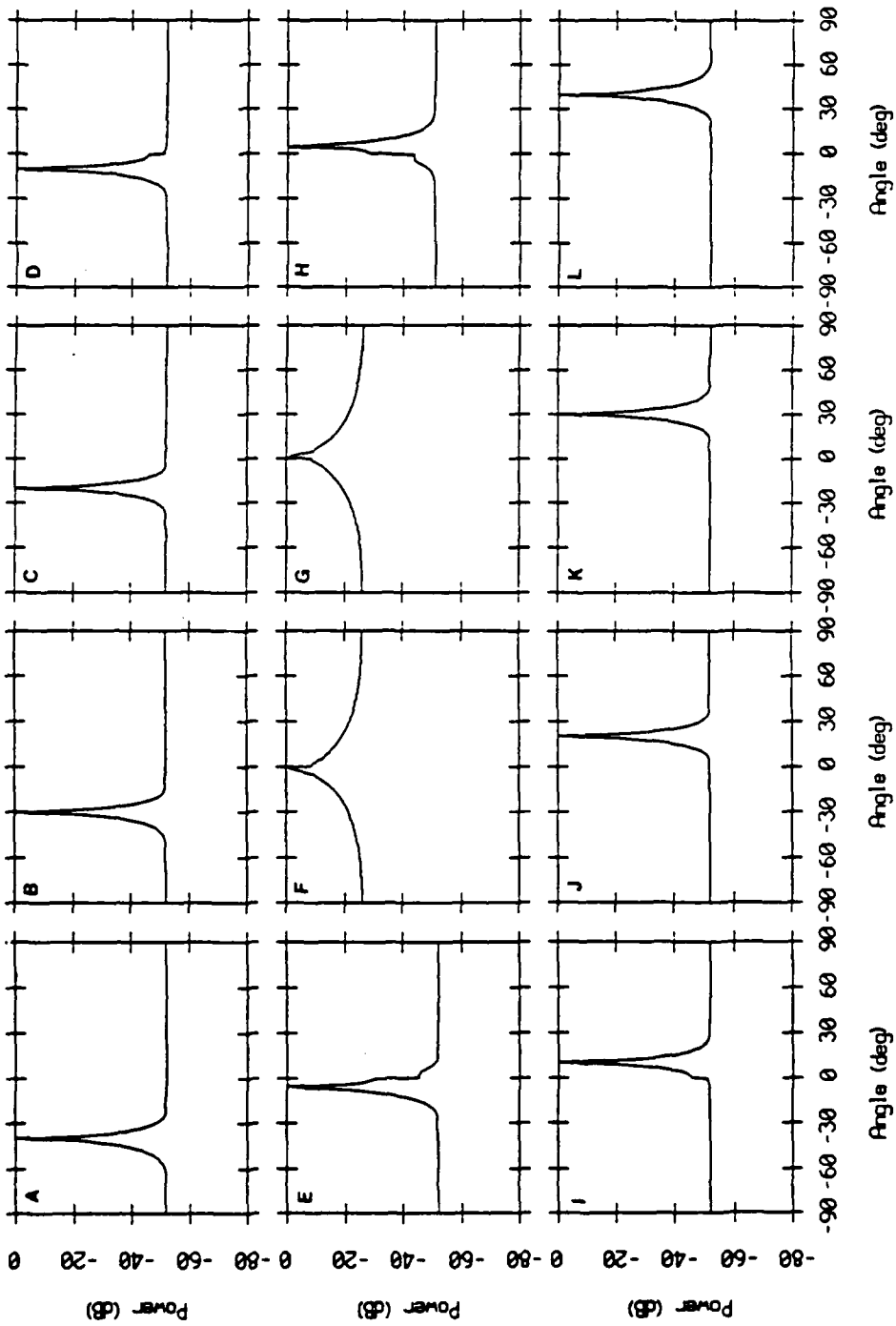

Figure IV.23: Bearing responses of the MVDR beamformer after spatial smoothing with 16 sensor subarrays using the eigensteering vectors. Panels A, B, C, D, E, F, G, H, I, J, K, L correspond to arrivals $\{-40°, -30°, -20°, -10°, -5°, -0.2°, 0.2°, 7°, 10°, 20°, 30°, 40°\}$.

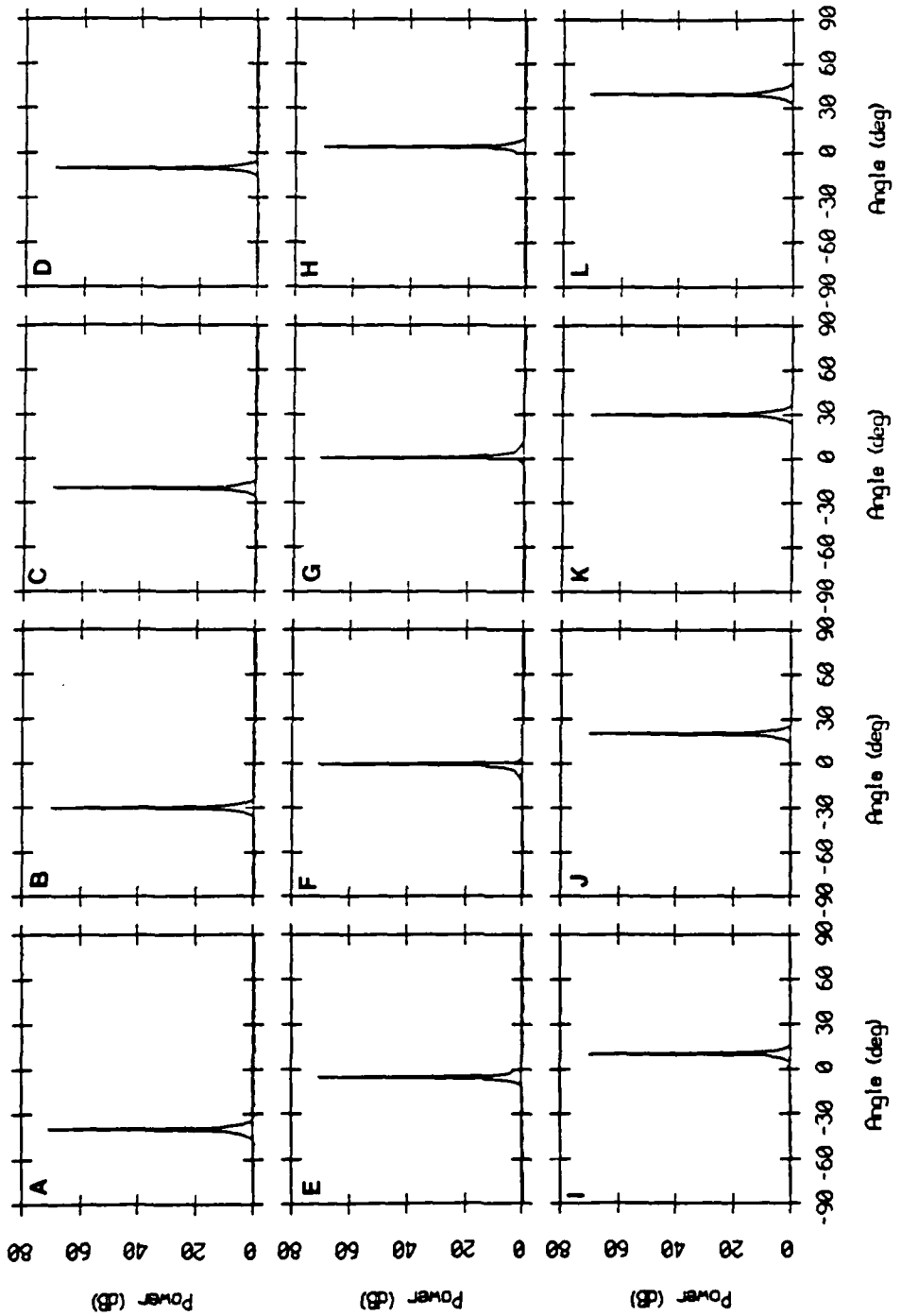

Figure IV.24: Bearing responses of the MUSIC processor after spatial smoothing with 24 sensor subarrays using the eigensteering vectors. Panels A, B, C, D, E, F, G, H, I, J, K, L correspond to arrivals ($-40°$, $-30°$, $-20°$, $-10°$, $-5°$, $-0.2°$, $0.2°$, $7°$, $10°$, $20°$, $30°$, $40°$).

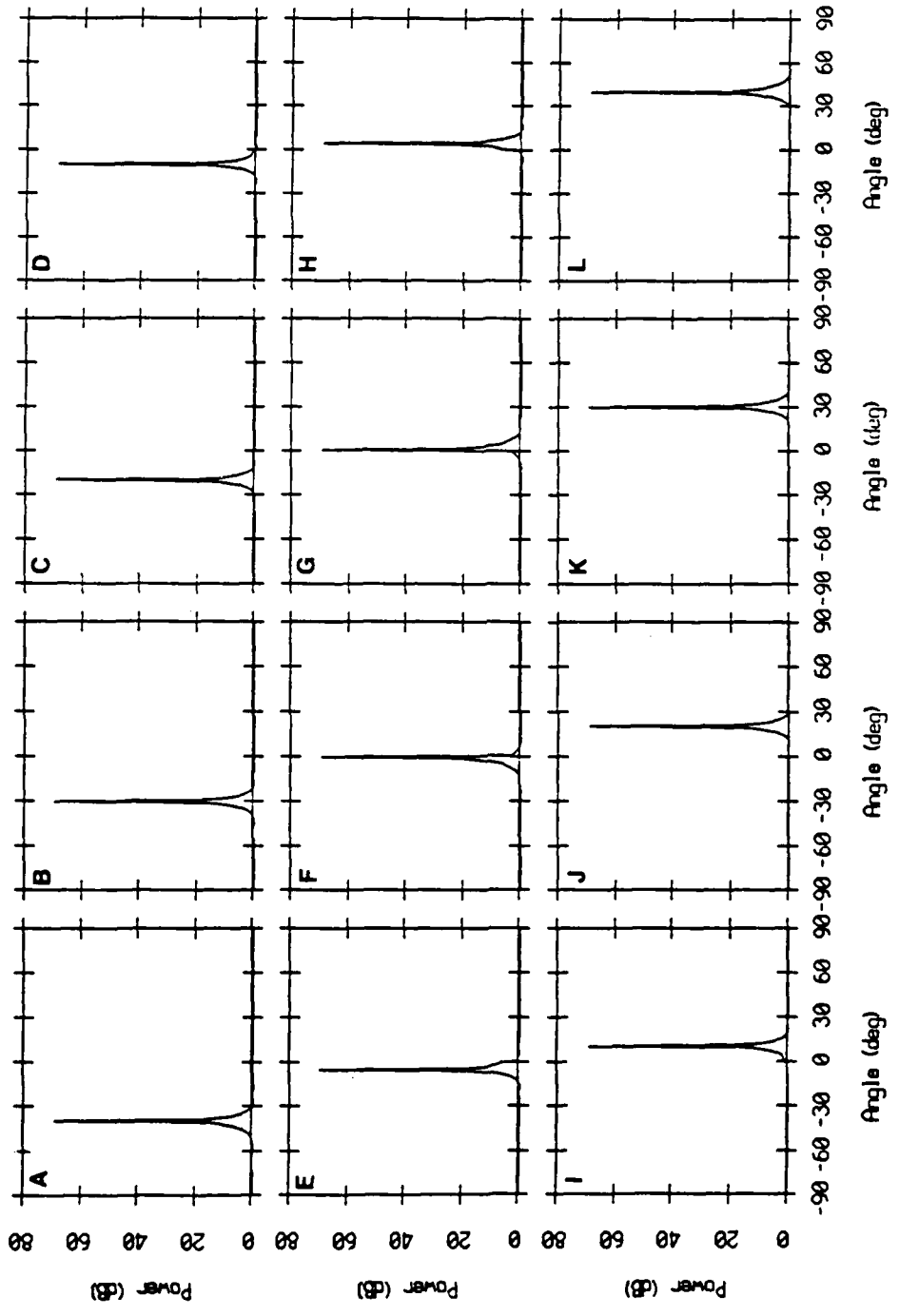

Figure IV.25: Bearing responses of the MUSIC processor after spatial smoothing with 16 sensor subarrays using the eigensteering vectors. Panels A, B, C, D, E, F, G, H, I, J, K, L correspond to arrivals $-40°, -30°, -20°, -10°, -5°, -0.2°, 0.2°, 7°, 10°, 20°, 30°, 40°$}.

IV.4.2.4 Performance of the MVDR Beamformer after Smoothing

In a plane wave environment, Chapter III showed that the performance of the MVDR beamformer after modified spatial smoothing is similar to the performance after spatial smoothing. The use of the modified covariance matrix in a curved wavefront environment is not easily justifiable since the symetry present in the plane wavefront problem is lost in a curved wavefront environment. Therefore, this study of performance will be only concerned with spatial smoothing.

In this simulation, the same 32 element array receives a pair of unit power fully correlated ($\rho = 1$) curved wavefront arrivals with arrival angles in the set { 0^o, 5^o, 10^o, 15^o, 20^o, 25^o, 30^o, 35^o, 40^o }. A background sensor noise of - 20 dB is also included. Spatial smoothing followed by the MVDR beamformer is performed using the eigen steering vectors that correspond to a particular smoothing scenario. The loss suffered by the arrivals is measured by taking the difference of the true underlying power (0 dB) and the power reported by the MVDR beamformer. The results summarized in Figure IV.26 and Figure IV.27. Figure IV.26 shows the influence of the arrival pair angular spacing on the loss due to coherence. Each angular separation corresponds to a number of combinations of arrivals (e.g. the 5^o pair spacing corresponds to the pairs (0^o , 5^o), (5^o , 10^o), ...). Figure IV.27 gives the same results in term of number of averages. This simulation correponds to the plane wave results summarized in Figure III.11 and Figure III.12 of Chapter III.

Panel A of Figure IV.26 indicates that without smoothing the MVDR suffers almost total signal cancellation as in the plane wave case. The other panels correspond to different subsegment lengths from 30 to 14 (the number of averages varies from 3 to 19). The beamformer fails to resolve the arrival pair (0^o, 5^o) for any subsegment length. When one of the arrivals is near horizontal, the power estimate suffers greater loss than for a pair with same angular separation but with higher arrival angle (Figure IV.27). A near horizontal arrival has the most curvature and partially insonifies the array (because

the sound velocity increases with the sensors, only the upper half of the array is insonified). One can note that with the exception of this case, the results are very similar to those for plane waves.

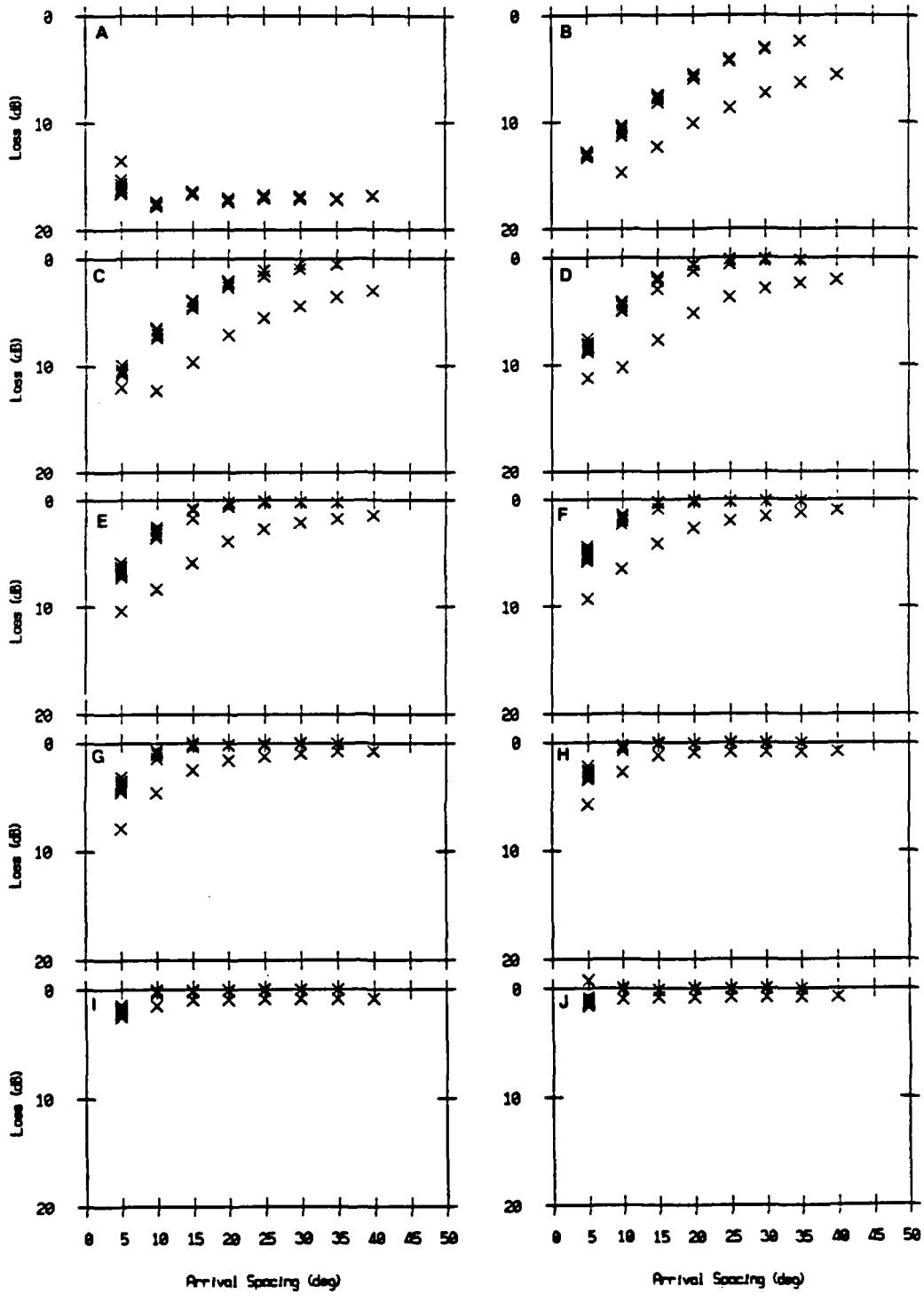

Figure IV.26: Loss at the output of the MVDR beamformer after spatial smoothing for a correlated pair with angular separation varying between 5° and 40°. The data are curved and the replica vectors are the eigensteering vectors. Panel A corresponds to no smoothing and Panels B, C, D, E, F, G, H, I, J correspond to smoothing subsegment lengths {30, 28, 26, 24, 22, 20, 18, 16, 14}.

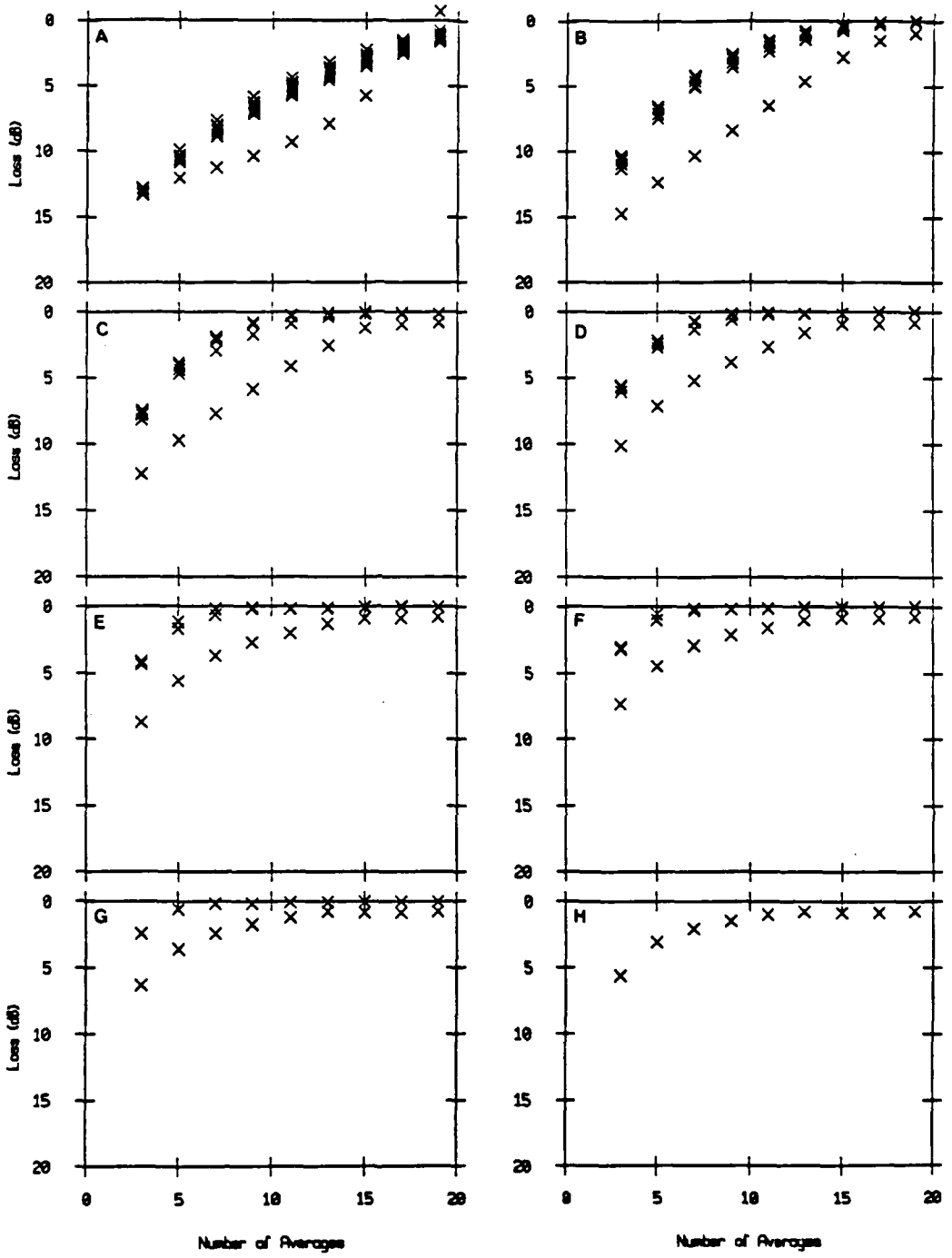

Figure IV.27: Variation of the loss at the output of the MVDR beamformer as a function of the number of averages in the spatial smoothing for a correlated pair with angular separation varying from 5° to 40°. The data are curved and the replica vectors are the eigensteering vectors. Panel A, B, C, D, E, F, G, H correspond to pair separations $\{5^\circ, 10^\circ, 15^\circ, 20^\circ, 25^\circ, 30^\circ, 35^\circ, 40^\circ\}$.

IV.5 Conclusions

The first part of this Chapter was devoted to deriving an expression for curved wavefront steering vectors. The simple geometric approach of ray theory provides a convenient way to generate a curved wavefront array manifold. The implemented integral equation of phase reflects the variation of sound speed with depth.

The importance of wavefront curvature has been assessed. It was shown that curvature is large for near horizontal arrivals, even for a relatively short aperture. On the other hand, arrivals with steep angles with respect to the horizontal are quite similar to plane wave arrivals. This result is observed on the bearing responses of the various beamformers using the plane wave array manifold with good results for steep angles with respect to the horizontal and poor results at near horizontal arrival angles. One also observes the great sensitivity to mismatch of the high and super resolution techniques with losses as large as 40 dB when curved wavefronts arrivals impinge on the array. To avoid loss due to mismatch, curved wavefront replica vectors should be used.

The direct application of spatial smoothing to decorrelate correlated curved wavefront arrivals causes some slight distortion, still yielding a loss due to mismatch even when using the curved wavefront array manifold. The loss due to mismatch can be avoided by taking the replica vectors that correponds to the steering vectors after the spatial smoothing transformation of the covariance matrix. By using these eigen steering vectors, loss due to mismatch is made negligible. The performance of the MVDR beamformer under correlated curved wavefront arrivals then was shown to be very similar to the plane wave case (plane wave data and plane wave replica vectors), except for near horizontal arrivals where performance degradation still occurs.

BIBLIOGRAPHY

Ahluwalia, D. S. and J. B. Keller, "Exact and Asymptotic Representation of the Sound Field in a Stratified Ocean," in *Wave Propagation and Underwater Acoustics*, ed. J. S. Papadakis, Lecture Notes in Physics, vol. 70, pp. 14-85, Springer Verlag, Berlin, 1977.

Anderson, V. C., "Vertical Noise Distribution," in *International Workshop on Low Frequency Propagation*, vol. 2, pp. 859-886, Woodshole, MA, October 1974.

Anderson, V. C., "Variation of Directionality of Noise with Depth in the North Pacific," *J. Acoust. Soc. Am.*, vol. 66, no. 5, pp. 1446-1452, 1979.

Baggeroer, A. B., "High Resolution Velocity/Depth Spectra Estimation for Seismic Profiling," *IEEE Inter. Conf. Engineering in the Environment OCEAN 74*, vol. 2, pp. 201-211, Halifax, Novia Scotia, 21-23 August 1974.

Baggeroer, A. B. and R. Falconer, "Refraction Profiles and Crustal Models of the Canada Basin," *J. Geophysical Research*, vol. 87, no. B7, pp. 5461-5476, 1982.

Barnard, T. E., "Two Maximum Entropy Beamforming Algorithms for Equally Spaced Line Array," *IEEE Trans. Acoust. Speech Signal Processing*, vol. 30, no. 2, pp. 175-189, 1982.

Bohme, J. F., "Array Signal Processing," in *Traitement du Signal / Signal Processing*, ed. J. L. Lacoume, T. S. Durrani and R. Stora, pp. 438-482, Elsevier, 1987.

Boyles, A. C., *Acoustic Waveguides, Applications to Oceanic Science,* John Wiley, N.Y., 1984.

Brekhovskikh, L. and Yu. Lysanov, *Fundamentals of Ocean Acoustics,* Springer Verlag, Berlin, 1982.

Burdic, W. S., *Underwater Acoustic System Analysis,* Prentice-Hall, Englewood Cliffs, N.J., 1984.

Burg, J. P., "Maximum Entropy Spectral Analysis," *Proc 37th Meeting of the Society of Exploration Geophysicists*, Oklahoma City, OK, 31 October 1967.

Cadzow, J. A., "A High Resolution Direction-of-Arrival Algorithm for Narrow-Band Coherent and Incoherent Sources," *IEEE Trans. Acoust. Speech Signal Processing*, vol. 36, no. 7, pp. 965-979, 1988.

Cantoni, A. and L. C. Gondara, "Resolving the Directions of Sources on a Correlated Field Incident on an Array," *J. Acoust. Soc. Am.*, vol. 67, no. 4, pp. 214-219, 1980.

Capon, J., "High Resolution Frequency-Wavenumber Spectrum Analysis," *Proc. IEEE*, vol. 57, pp. 1408-1418, 1969.

Capon, J. and N. R. Goodman, "Probability Distribution for Estimators of the Frequency Wavenumber Spectrum," *Proc. IEEE (Lett.)*, vol. 58, pp. 1785-1786, 1970.

Clarke, I. J., "High Discrimination Target Detection Algorithms And Estimation Of Parameters," *Nato Advanced Study Institute on Underwater Acoustic Data Processing*, Kingston, Ontario, Canada, 18 July to 29 July 1988.

Cox, H., "Resolving Power And Sensitivity to Mismatch Of Optimum Array Processors," *J. Acoust. Soc. Am.*, vol. 54, no. 3, pp. 771-785, 1973.

DeFatta, D., J. Lucas, and W. Hodgkiss, *Digital Signal Processing*, John Wiley, N.Y., 1988.

DeGraaf, S. R. and D. H. Johnson, "Capability Of Array Processing Algorithms To Estimate Source Bearings," *IEEE Trans. Acoust. Speech Signal Processing*, vol. 33, no. 6, pp. 1368-1379, 1985.

Dosso, S. E. and N. R. Chapman, "Measurement and Modelling of Downslope Acoustic Propagation Loss over a Continental Slope," *J. Acoust. Soc. Am.*, vol. 81, no. 2, pp. 258-268, 1987.

Gabriel, W. F., "Spectral Analysis and Adaptive Array Superresolution Techniques," *Proc. IEEE*, vol. 68, pp. 654-666, 1980.

Gabriel, W. F., "Using Spectral Estimation Techniques in Adaptive Processing Antenna Systems," *IEEE Trans. Ant. Prop.*, vol. 34, no. 3, pp. 291-300, 1986.

Griffiths, J. W. R. and J. E. Hudson, "An Introduction to Adaptive Processing in Passive Sonar System," in *Aspects of Signal Processing*, ed. G. Tacconi, vol. 1, pp. 299-308, Reidel, 1977.

Hsu, K. and A. B. Baggeroer, "Application of the Maximum Likelihood Method (MLM) for Sonic Logging," *Geophysics*, vol. 551, no. 3, pp. 780-787, 1986.

Johnson, D. J. and S. R. DeGraaf, "Improving the Resolution of Bearing in Passive Sonar Arrays by Eigenvalue Analysis," *IEEE Trans. Acoust. Speech Signal Processing*, vol. 30, no. 4, pp. 638-647, 1982.

Kanasewich, E. R., *Time Sequence Analysis in Geophysics*, University of Alberta Press, Edmonton, Alberta, 1975.

Kay, S. M., *Modern Spectral Estimation, Theory & Applications*, Prentice-Hall, N.J., 1988.

Kewley, D. J., "Using Eigenvalue Analysis to Identify Interference in Ambient Sea Noise Vertical Directionality Measurements," *J. Acoust. Soc. Am.*, vol. 75, no. 3, pp. 826-833, 1984.

Kumaresan, R. and D. W. Tufts, "Estimating the Angle of Arrival of Multiple Plane Waves," *IEEE Trans. Aerospace Electronics Syst.*, vol. 19, no. 1, pp. 134-139, 1983.

Lacoss, R. T., "Data Adaptive Spectral Analysis Methods," *Geophys.*, vol. 36, pp. 661-675, 1971.

Linebarger, D. A. and D. H. Johnson, "The Effect of Spatial Averaging on Coherence and Resolution," *Proc. ICASSP 1988*, vol. V, pp. 2865-2868, 1988.

Marple, S. L., *Digital Spectral Analysis with Applications,* Prentice-Hall, N.J., 1987.

McDonough, R. N., "Degraded Performance of Nonlinear Array Processors in the Presence of Data Modeling Errors," *J.Acoust. Soc. Am.*, vol. 51, no. 4, pp. 1186-1193, 1972.

Monzingo, R. A. and T. W. Miller, *Introduction to Adaptive Arrays,* John Wiley, N.Y., 1980.

Murphy, D. A. and D. R. DelBazo, "Multipath Processing for Improved Detection on a Long Vertical Array," in *Progress in Underwater Acoustics*, ed. H. M. Merklinger, pp. 765-772, Plenum Press, N.Y., 1987.

Naidu, P. S. and V. V. Krishna, "Improved Maximum Likelihood Spectrum For Direction Of Arrival (DOA) Estimation," *Proc. ICASSP 1988*, vol. V, pp. 2901-2904, 1988.

Nickel, U., "Angular Superresolution with Phased Array Radar: A Review of Algorithms and Operational Constraints," *IEE Proc. Part F*, vol. 134, no. 1, pp. 53-59, 1988.

Nickel, U., "Algebraic Formulation of the Kumaresan-Tufts Superresolution Method, Showing Relation to ME and MUSIC Methods," *IEE Proc. Part F*, vol. 135, no. 1, pp. 7-10, 1988.

Oltman-Shay, J. and R. T. Guza, "A Data-Adaptive Ocean Wave Directional Spectrum Estimation for Pitch and Roll Type Measurements," *J. Physical Oceanography*, vol. 14, pp. 1800-1810, 1984.

Oppenheim, A. V. and R. W. Schafer, *Digital Signal Processing,* Prentice-Hall, N.J., 1975.

Owsley, N. L., "Sonar Array Processing," in *Array Signal Processing*, ed. S. Haykin, pp. 115-193, Prentice-Hall, Englewood Cliffs, N.J., 1985.

Owsley, N. L., "Enhanced Minimum Variance Beamforming," *Nato Advanced Study Institute on Inderwater Acoustic Data Processing*, Kingston, Ontario, Canada, 18 July to 29 July 1988.

Priestley, M. B., *Spectral Analysis And Time Series,* 1, Academic, N.Y., 1981.

Reddy, V. U., A. Paulraj, and T. Kailath, "Performance Analysis of the Optimum Beamformer in the Presence of Correlated Sources and its Behaviour under Spatial Smoothing," *IEEE Trans. Acoust. Speech Signal Processing*, vol. 35, no. 7, pp. 927-936, 1987.

Schmidt, R. O., *A Signal Subspace Approach to Multiple Emitter Location and Spectral Estimation,* Ph.D. Dissertation, Stanford, CA, 1981.

Schmidt, R. O., "Multiple Emitter Location and Signal Parameter Estimation," *IEEE Trans. Ant. Prop.*, vol. 34, no. 3, pp. 276-280, 1986.

Seglison, C. D., "Comments on "High Resolution Frequency Wavenumber Spectrum Analysis"," *Proc. IEEE (Lett.)*, vol. 58, no. 6, pp. 947-949, 1970.

Sen, M. K., L. N. Frazer, S. Mallick, and N. R. Chapman, "Analysis of Multipaths Sound Propagation in the Ocean Near 49 N 128 W," *J. Acoust. Soc. Am.*, vol. 83, no. 2, pp. 588-597, 1988.

Shan, Tie-Jun and T. Kailath, "Adaptive Beamforming for Coherent Signals and Interference," *IEEE Trans. Acoust. Speech Signal Processing*, vol. 33, no. 3, pp. 527-536, 1985.

Shumway, R. H., *Applied Statistical Time Series Analysis,* Prentice-Hall, Englewood Cliffs, N.J., 1988.

Sotirin, B. J., F. V. Pavlicek, and J. A. Hildebrand, "Low-Frequency Digital Acoustic Array," in *Current Practices and New Technology in Ocean Engineering*, ed. G. K. Wolfe and P. Y. Chang, vol. 13, pp. 19-27, 1988.

Su, Y. L., T. J. Shan, and B. Widrow, "Parallel Spatial Processing: A Cure for Signal Cancellation in Adaptive Arrays," *IEEE Trans. Ant. Prop.*, vol. 34, no. 3, pp. 347-355, 1986.

Takao, K. and N. Nikuma, "An Adaptive Array Utilizing an Adaptive Spatial Averaging Technique for Multipaths Environment," *IEEE Trans. Ant. Prop.*, vol. 35, no. 12, pp. 1389-1396, 1987.

Urick, R. J., *Principles of Underwater Sound,* McGraw-Hill, New York, N.Y., 1983.

Van Veen, B. D. and K. M. Buckley, "Beamforming: A Versatile Approach to Spatial Filtering," *IEEE ASSP Magazine*, vol. 5, no. 2, pp. 4-24, 1988.

Wang, H. and M. Kaveh, "Coherent Signal-Subspace Processing for the Detection and Estimation of Angles of Arrival of Multiple Wide-Band Sources," *IEEE Trans. Acoust. Speech Signal Processing*, vol. 33, no. 4, pp. 823-831, 1985.

Wax, M., T. J. Shan, and T. Kailath, "Spatio-temporal Spectral Analysis by Eigenstructure Methods," *IEEE Trans. Acoust. Speech Signal Processing*, vol. 32, no. 4, pp. 817-827, 1984.

Wax, M. and T. Kailath, "Detection of Signals by the Information Theoretic Criteria," *IEEE Acoust. Speech Signal Processing*, vol. 33, no. 2, pp. 387-392, 1985.

White, W. D., "Angular Spectra in Radar Applications," *IEEE Trans. Aerosp. Electron. Syst.*, vol. 15, no. 6, pp. 895-899, 1979.

Widrow, B., K. M. Duvall, R. P. Gooch, and W. C. Newman, "Signal Cancellation Phenomena in Adaptive Antennas: Causes and Cures," *IEEE Trans. Ant. Prop.*, vol. 30, no. 3, pp. 469-478, 1982.

Williams, J. R., "Fast Beam-forming Algorithm," *J. Acoust. Soc. Am.*, vol. 44, no. 3, pp. 1454-1455, 1968.

Williams, R. T., S. Prasad, A. K. Mahalanabis, and L. H. Sibul, "An Improved Spatial Smoothing Technique for Bearing Estimation in a Multipaths Environement," *IEEE Trans. Acoust. Speech Signal Processing*, vol. 36, no. 4, pp. 425-432, 1988.

Zhu, J. X. and H. Wang, "Adaptive Beamforming for Correlated Signal and Interferences: A Frequency-Domain Smoothing Approach," *Proc. ICASSP 88*, vol. V, pp. 2757-2760, 1988.

Zoltowski, M. D., "On the Performance Analysis of the MVDR Beamformer in the Presence of Correlated Interference," *IEEE Trans. Acoust. Speech Signal Processing*, vol. 36, no. 6, pp. 945-947, 1988.